Gravitational waves in a new light: Novel stabilisation schemes for solid-state lasers

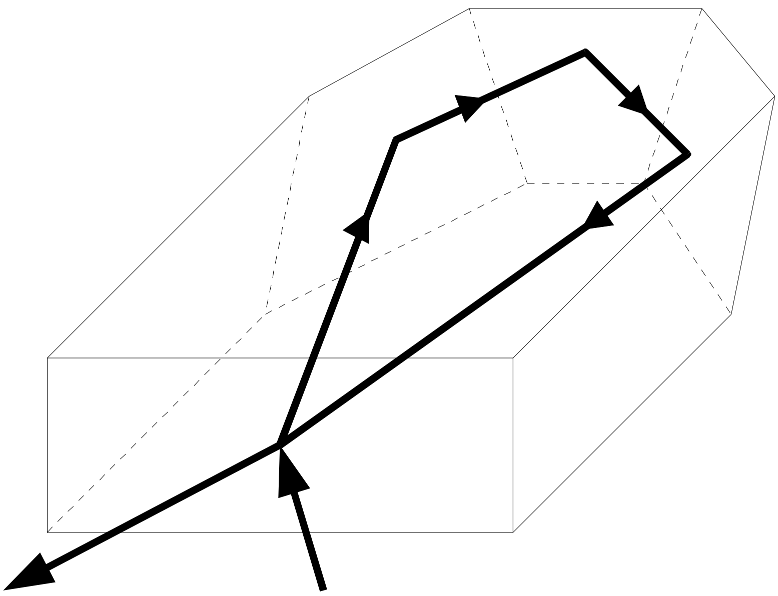

Vom Fachbereich Physik
der Universität Hannover
zur Erlangung des Grades
Doktorin der Naturwissenschaften
– Dr. rer. nat. –
genehmigte Dissertation

von
Dipl.-Phys. Michèle Heurs
geboren am 20. Februar 1975 in Hannover

2004

Zusammenfassung

Für viele Präzisionsexperimente – wie z.B. interferometrische Gravitationswellendetektoren – werden ultra-stabile Lichtquellen benötigt. Das intrinsisch bereits sehr stabile, injektionsgekoppelte Hochleistungs-Festkörperlasersystem, welches beim Gravitationswellendetektor GEO 600 zum Einsatz kommt, muß in seinen Observablen aktiv stabilisiert werden, um die ehrgeizigen Anforderungen zu erfüllen. Insbesondere muß die Frequenz und die Ausgangsleistung des Lasersystems im Frequenzband von 50 Hz bis 5 kHz auf ein Niveau von $\Delta f = 2 \cdot 10^{-4}\,\mathrm{Hz}/\sqrt{\mathrm{Hz}}$ im Frequenzrauschen (relativ zur Power Recycling Cavity) bzw. $\Delta P/P = 5 \cdot 10^{-8}/\sqrt{\mathrm{Hz}}$ im relativen Leistungsrauschen reduziert werden. Dieses sehr geringe Leistungsrauschen zu erreichen ist ein Schwerpunkt dieser Arbeit. Mittels einer im Rahmen dieser Arbeit entwickelten Regelelektronik für die Leistungsstabilisierung wird ein Leistungsrauschen des GEO-Lasersystems von $\Delta P/P = 2 \cdot 10^{-8}/\sqrt{\mathrm{Hz}}$ bei $f = 2\,\mathrm{kHz}$ mit einem Detektionsschema in Luft erzielt. Im Vakuum hinter einem räumlichen Modenfilter wird das Leistungsrauschen des baugleichen Labor-Lasersystems auf $\Delta P/P = 3 \cdot 10^{-8}/\sqrt{\mathrm{Hz}}$ im Frequenzbereich von $f = 100\,\mathrm{Hz}$ bis $f = 1\,\mathrm{kHz}$ reduziert.

Parasitäre Kopplungen zwischen Rauschquellen einer Laserobservablen in eine andere erschweren die Stabilisierungsaufgabe. Es ist somit ein Verständnis dieser Kopplungen vonnöten, wenn die fundamentalen Grenzen der Laserstabilisierung erreicht werden sollen. Diese Arbeit präsentiert daher im weiteren neuartige Stabilisierungskonzepte zur simultanen Unterdrückung von Leistungs- und Frequenzrauschen von Festkörperlasern. Für diese Untersuchungen wurde ein spezieller Laser entwickelt, der single-mode NPRO. Leistungsstabilisierung der single-mode Pumplaserdiode – als Pumplichtstabilisierung bezeichnet – führt zu einer Reduktion des NPRO Leistungsrauschens. Bereits dieses Ergebnis ist mit einem multi-mode gepumpten NPRO nicht erreichbar. Zusätzlich wird durch Pumplichtstabilisierung das Frequenzrauschen des single-mode NPROs im gleichen Maße wie das Leistungsrauschen unterdrückt, ohne direkte Detektion des Frequenzrauschens. Frequenzstabilisierung des single-mode NPROs mittels Rückkopplung auf den Pumpstrom der single-mode Pumplaserdiode – die Current Lock Technik – resultiert in einer simultanen Reduktion des NPRO Leistungsrauschens in der gleichen Größenordnung wie die Reduktion des Frequenzrauschens. Simultane Rauschunterdrückungen in der Größenordnung von 30 dB wurden mit beiden Techniken erreicht. Die Experimente und ihre Ergebnisse sind beispiellos in der Laserstabilisierung. Sie bieten vielversprechende Entwicklungsmöglichkeiten für die Laserstabilisierung der Gravitationswellendetektoren der nächsten Generationen.

Stichworte: diodengepumpte Festkörperlaser, Frequenz- und Leistungsstabilisierung, Current Lock, interferometrische Gravitationswellendetektoren

Abstract

Ultra-stable light sources are needed for many high precision experiments, such as interferometric gravitational wave detectors. The all-solid-state injection locked high power laser system implemented in the gravitational wave detector GEO 600, which is already intrinsically stable, must be actively stabilised in its observables to satisfy the ambitious requirements. In particular the frequency and the intensity of the Nd:YAG laser system must be stabilised to a level of $\Delta f = 2 \cdot 10^{-4}\,\mathrm{Hz}/\sqrt{\mathrm{Hz}}$ in frequency noise (relative to the power recycling cavity) respectively $\Delta P/P = 5 \cdot 10^{-8}/\sqrt{\mathrm{Hz}}$ in relative intensity noise, both in the frequency band from 50 Hz to 5 kHz. Achieving this level of intensity stability is one focus of this work. With an intensity stabilisation control electronics designed in the scope of this work an out-of-loop intensity noise of the GEO laser system of $\Delta P/P = 2 \cdot 10^{-8}/\sqrt{\mathrm{Hz}}$ at $f = 2\,\mathrm{kHz}$ is achieved with a detection scheme in air; in vacuum behind a spatial mode filter the out-of-loop intensity noise of the identical lab laser system is reduced to a level of $\Delta P/P = 3 \cdot 10^{-8}/\sqrt{\mathrm{Hz}}$ in the bandwidth from $f = 100\,\mathrm{Hz}$ to $f = 1\,\mathrm{kHz}$.

Parasitic coupling of noise from one laser observable into another complicates the task of laser stabilisation. An understanding of the couplings is therefore necessary if fundamental limits of laser noise are to be approached. In the further course of this work novel stabilisation schemes for simultaneous suppression of intensity and frequency noise in solid-state lasers are presented. For these investigations a special laser was designed, the single-mode NPRO. Intensity stabilisation of its single-mode laser diode pump source – pump light stabilisation – leads to a reduction of NPRO intensity noise, in itself a result not attainable with a conventional NPRO. Additionally, the frequency noise of the single-mode NPRO is suppressed to the same degree as the intensity noise, without direct detection of the frequency noise. Frequency stabilisation of the single-mode NPRO via feedback to the drive current of the single-mode pump laser diode – current lock – yields a simultaneous intensity noise reduction in the same order of magnitude as the frequency noise suppression. Simultaneous noise reductions in the 30 dB range were achieved with both techniques. The experiments and their results are unprecedented in the field of laser stabilisation. They are highly promising for the development of laser stabilisations for future generation gravitational wave detectors.

Keywords: Diode pumped solid-state lasers, frequency and intensity stabilisation, current lock, interferometric gravitational wave detectors

Contents

List of Figures

List of Tables

Nomenclature

Greek symbols

β	thermal expansion coefficient
$\Delta\omega_{\text{lock}}$	locking range
ΔT	temperature difference
η	quantum efficiency
η_{opt}	optical-optical slope efficiency
λ	wavelength
λ_{pump}	pump wavelength
ν	frequency
ϕ	phase
σ	population inversion
Θ	far field divergence of a Gaussian beam
θ	angle between beam and optical axis
Ω	modulation frequency
ω	angular frequency of the laser light

Roman symbols

d	core diameter of a fibre
d	size of an optical aperture
d	width of the active zone
$\vec{E}_0(t)$	initial laser light field
$\vec{E}(t)$	laser light field
E	energy
e	error point, $e = w - x$
E_1	energy of the lower laser level

E_2	energy of the upper laser level
E_g	energy of the bandgap
F	Fermi energy
F	finesse of an optical resonator
f	Fourier frequency
f	focal length
F_c	energy of the quasi-Fermi level of the conduction band
f_c	population probability for electrons in the conduction band
F_v	energy of the quasi-Fermi level of the valence band
f_v	population probability for electrons in the valence band
FSR	free spectral range
$\tilde{g}(\omega)$	regenerative gain
G	the control system or servo
$G(\omega)$	gain of the servo
$G(\omega)$	round-trip gain
h	Planck's constant
H	$H = \sum_i H_i$, plant
I	current
k	Boltzmann constant
LSD	linear spectral density
M^2	beam quality factor
M	modulation index
N_i	population of the i-th level
NA	numerical aperture
PZT	piezo-electric transducer
P	power
P_{laser}	laser power
P_{pump}	pump power

P_{thr}	laser threshold power
R	input-output mirror reflectivity
r	distance from the optical axis
$R(z)$	radius of curvature of a Gaussian beam at position z
s	$s = \text{i} \cdot \omega$, frequency in control theory
T	$T = p/\text{c}$, transit time for a cavity round-trip
T	thermodynamic temperature
t	time
w	set point of an observable of a control loop
w	waist size (radius)
$w(z)$	radius of a Gaussian beam at position z
x	actual value of an observable in a control loop
y	control variable
z	noise value
z	optical axis of a system
z_R	Rayleigh range of a Gaussian beam

1. Introduction

In 1608 Jan Lipperhey, an optician from the Netherlands, invented the optical telescope, consisting of two simple lenses. A year later Galileo Galilei built his first telescope, based on Lipperhey's design. With improved versions of this device he made some of the first observations of the skies, thereby founding the science of optical astronomy[1]. Since more than 70 years radio telescopes have given the World further insight on the history of the universe[2], letting us travel into its past. This kind of 'time travel' has its limits, though, since the universe only became transparent for electromagnetic waves (such as radio waves and light) 300,000 years after the Big Bang. Everything that happened before this point in time is barred from our view in the electromagnetic spectrum. If we want to gain knowledge on the infancy of the universe we need to open a new observational window.

When Albert Einstein predicted the existence of gravitational waves in 1916, he also uttered his belief that mankind would never be able to detect these faint echoes of energy density changes since the effects on mass distributions would be so minuscule. Gravitation is the fundamental interaction which can not yet be quantum mechanically described, and its Big Bang fingerprint would yield information on the very beginning of time. This fact is incentive for many scientists to join the ambitious hunt for gravitational wave detection and start the era of *gravitational wave astronomy*.

GEO 600 is one of currently four interferometric gravitational wave detector projects worldwide. The German-British project, located in Ruthe near Hanover, employs state-of-the-art technology in all areas to reach the sensitivity necessary for the detection of gravitational waves. The all-solid-state laser system used as the light source for GEO 600 plays a central role: Its stability in intensity, frequency and beam geometry is of fundamental relevance for the achievable sensitivity of the detector. Part of this thesis deals with the efforts invested in the stabilisation of the **injection locked high power laser system for GEO 600** (chapter 3).

The experiments conducted on the laser diode pumped Nd:YAG laser system for GEO 600 led to the discovery of coupling effects between the laser observables. Stabilisation of one observable might therefore lead to stability deterioration of another, seemingly unconnected, observable. Gravitational wave detectors of future generations (such as Advanced LIGO) pose even higher requirements on their light sources than the existing detectors. To reach these future specifications it is crucial to gain an understanding of the noise contributions and the achievable stabilisation limits in solid-state laser systems. To determine the possible couplings transfer functions from the known actuators to all relevant observables were measured (Quetschke 2003). In the course of these investigations a strong coupling was found between the laser diode pump current and the frequency of the Nd:YAG laser. This well defined transfer function makes the laser diode pump current a possible new

[1]Galilei's findings include the discovery of the moons of jupiter, the phases of venus and the realisation that the moon is not a perfect sphere, but covered with craters and mountains.

[2]In 1932 Karl Guthe Jansky discovered that the milky way emits electromagnetic waves in the radio band. This first observation of an extraterrestrial radio source was the birth of radio astronomy.

actuator for laser frequency, this new frequency stabilisation technique is labelled *current lock*. The effect of current lock on laser intensity noise was expected to be detrimental, but, contrary to expectations, current lock even resulted in a small but measurable reduction of intensity noise in a limited frequency band (Willke et al. 2000b). The reduction in intensity noise was much smaller than the degree of frequency stabilisation, though. The obviously existing coupling between laser intensity and laser frequency was therefore to be investigated with respect to the pump geometry. In this context the possibility of simultaneous stabilisation of both observables by actuation of only one was subject of intensive research. This thesis shows the experiments conducted on **new laser systems for fundamental physics** with different geometries to study the coupling effects between laser intensity and frequency (chapter 4). An emphasis is put on the results of these experiments and their analysis regarding the feasibility of simultaneous intensity and frequency stabilisation. This thesis describes the first-time simultaneous reduction of both laser intensity noise and laser frequency noise by the same degree by detection and actuation of merely one observable (Heurs et al. 2004; Heurs et al.). The possibilities opened by this novel stabilisation technique with its unprecedented results are of considerable significance for the stabilisation of future gravitational wave detector laser systems.

2. Laser stabilisation

The scope of this thesis encompasses different forms of laser stabilisation. One motivation is to provide and constantly improve the stabilised laser system for the interferometric gravitational wave detector GEO 600, the light source which forms the 'heart' of the Michelson interferometer. Not only must the laser system be stabilised, but experimental investigations are necessary to unveil the underlying causes for stabilisation limits.

All-solid-state laser systems (such as the Nd:YAG[1] lasers used in this work) are implemented in different fields of research and metrology. The reason for choosing a laser system of this kind is often the high achievable stability, besides compactness, modularity and longer lifetime compared to other laser systems. The existing and future interferometric gravitational wave detectors, though, pose the probably highest possible requirements regarding their light sources, compared to all other current research. These specifications call for sophisticated stabilisation schemes.

This chapter gives a short introduction on control theory (section 2.1) to build the understanding needed to deal with the general control problems in laser stabilisation (2.2). An overview on laser *intensity stabilisation* (section 2.3) and *frequency stabilisation* (section 2.4) techniques used on various Nd:YAG laser systems in our group is given. Here the noise sources in the laser are revealed and the methodology of laser frequency and intensity stabilisation is explained. Section 2.4 also explains the Pound-Drever-Hall-method (section 2.4.1) as well as the frequency stabilisation technique of *current lock* (section 2.4.2) developed in our group. Furthermore the technique of *injection locking* is described (section 2.6). Injection locking is used to realise the high stability high power laser system for the gravitational wave detector GEO 600 by coupling a high power laser with lesser stability to a relatively weak high-stability laser.

2.1. An inkling of control theory

This section introduces some basic ideas and terms of control theory. It establishes a common language which is useful when dealing with the control problems posed in the next chapters.

All stabilisation problems follow a similar 'plot' and can therefore basically be handled with a certain set of 'tools'. The individual stabilisation task will naturally vary and sometimes require more care, but the basic scheme is always the same. It is described in this section. The actual stabilisations realised in this work can then be found in the corresponding sections.

The very basics

A general control problem can be described as follows:

[1] Nd:YAG is an acronym for neodymium-doped yttrium-aluminum-garnet.

Consider a *system* H (which is not necessarily an electronic setup, but can also be mechanical, pneumatic, hydraulic etc.). H is called the *plant* and usually consists of several subsystems H_i.

The system is supposed to be stabilised in (for simplicity) one of its *observables*, i.e. the observable is to be held at some constant value, independent of disturbing influences. If the value of the observable is too big, then it has to be reduced and vice versa. This is accomplished by *negative feedback*. The opposite process (*positive feedback*) occurs when a signal which is already too large is further increased. Positive feedback at a certain frequency will lead to undesirable oscillations. Due to inevitable phase shifts it will always appear if the gain is too large and hence its prevention is one of the main concerns in servo design.

A *sensor* is needed to detect the observable. A *servo*, denoted by G, then delivers negative feedback to the system via an *actuator* which acts upon the observable and thereby changes its value.

The above described setup is illustrated in figure 2.1.

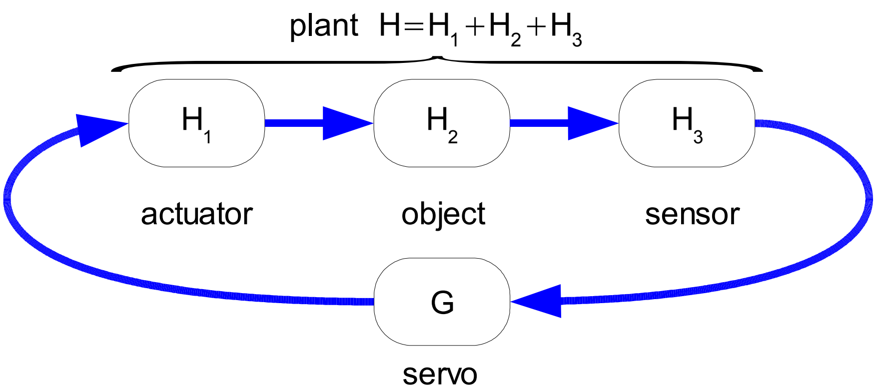

Figure 2.1: Schematic of a control loop. H_i: subsystems of the plant H, G: servo

Achieving *stability* of a control loop is a non-trivial task. Feedback which is applied with a slightly wrong phase causes oscillations in the system or even drives the system to an extremal (e.g. saturated) state, which is far from the stable state one wants to reach.

Let us consider the case where there are only small perturbations to the steady-state of the system. This is called the *linear small-signal regime*. It is convention in control theory to denote the angular frequency with the Laplace variable $s = \mathrm{i} \cdot \omega$. Any linear system's response at its output to a change of its input is expressed by the *transfer function* (denoted by for instance H). It is defined as the quotient of output signal U_{out} and input signal U_{in} and is a function of s:

$$H(s) = \frac{U_{\mathrm{out}}(s)}{U_{\mathrm{in}}(s)} \quad . \tag{2.1}$$

The transfer function is very important for the design of the control system. It can be plotted in different ways:

- *Nyquist plot*: The transfer function is visualised as a pointer in the complex field. The end of the pointer is the transfer function divided into real and imaginary part with the frequency as parameter. This type of plot is very common in control theory, but not widely used in our group.

- *Bode plot*: Amplitude and phase of the transfer function are plotted in two seperate graphs, with the frequency as the variable. In the following we will concentrate on the Bode plot, as this is the common method of plotting transfer functions in our group.

Amplitude $A(H)$ and phase $\phi(H)$ of the transfer function are defined as follows:

$$A(H) = \sqrt{(\Re(H))^2 + (\Im(H))^2}\,, \tag{2.2}$$

$$\phi(H) = \arctan\left(\frac{\Im(H)}{\Re(H)}\right) \quad . \tag{2.3}$$

The amplitude of the transfer function is plotted on a logarithmic scale:

$$\frac{A}{\mathrm{dB}} = 20 \cdot \log(A) \quad . \tag{2.4}$$

One advantage of the logarithmic representation is that the amplitude of compound transfer functions can simply be added. Furthermore, common factors of transfer functions, such as low-pass filters, poles, zeroes etc., take a characteristic form in the Bode diagram, which can easily be recognised. The amplitude of a transfer function is often referred to as *gain*.

As gain and phase are real and imaginary part of a transfer function (as can be seen in the Nyquist plot) they are coupled to one another. It is therefore not possible to, e.g. boost the gain and have no effect on the phase. This very important fact is based on the same mathematical relation as the Kramers-Kronig relations (Lipson et al. 1997) which yields the link between absorption and dispersion in optics.

Open loop gain, closed loop gain → servo design

From a control design point of view it is helpful to use schematics as in figure 2.1. The net gain of the complete open loop, the so-called *open loop gain*, can easily be calculated. It is the product of the transfer functions of the individual subsystems:

$$H_{\mathrm{OL}} = H_1 \cdot H_2 \cdot H_3 \cdot G \quad . \tag{2.5}$$

To determine the *closed loop gain* it is significant at which points in the loop the measurements are taken. Figure 2.2 illustrates the possibilities:

- *disturbance transfer function* =A/source. Point A shows how well the introduced disturbance (e.g. frequency sweep from the source) is reproduced with opposite sign (negative feedback) at the input of the addition point, so both cancel out at the output of the addition point and no disturbance of the loop remains.

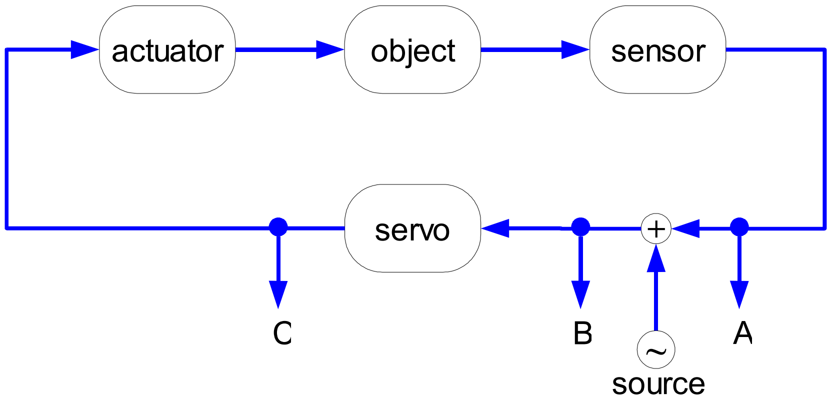

Figure 2.2: Schematic of a control loop with measurement points. A, B: points for measurement of transfer functions, A, C: points for measurement of noise spectrum, source: frequency sweep source (usually with fixed amplitude) for measurement of transfer functions.

- *disturbance suppression function* =B/source. At point B behind the addition point one sees to which degree the introduced disturbance is suppressed by the loop gain with active controls.

To investigate the influence of disturbances on the system consider figure 2.3:

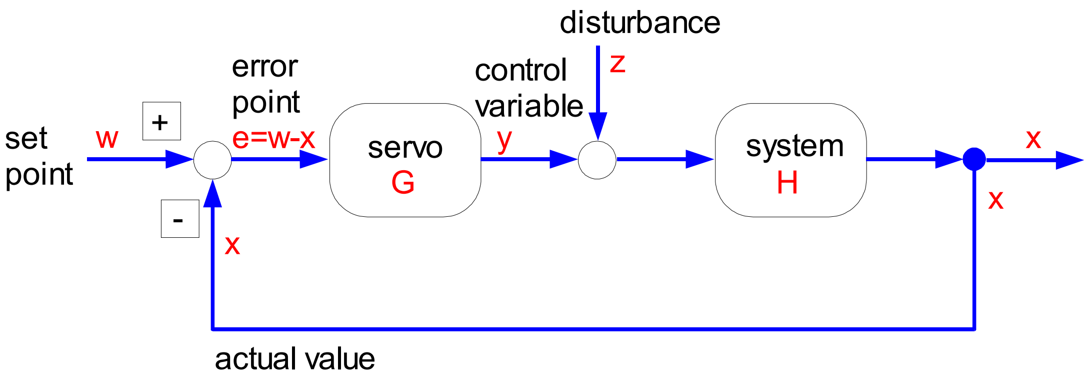

Figure 2.3: Schematic of a control loop with relevant points, where noise couples into the loop.

The *error point* is defined as the difference between set point w and actual value x of the observable. Therefore this is the signal which the loop tries to minimise. This is accomplished by the servo in closed loop for frequencies below *unity gain*. The unity gain frequency is the frequency where the open loop gain reaches unity, i.e. the amplitude of A equals the amplitude of B:

$$|H_{\mathrm{OL}}| = |A/B| = 0\,\mathrm{dB} = 1 \quad . \tag{2.6}$$

In practice this means that the desired observable is only stabilised up to this frequency; disturbances at frequencies higher than the unity gain frequency are not significantly attenuated by the servo.

For an analysis of the diagram in figure 2.3 the following assumptions are made, to comply with the most general case:

- the disturbance z is introduced at one point (in practice there are various noise contributions which couple in at different points)
- the set point value w does not vanish (to keep the analysis general)
- the negative sign of the feedback is applied just at the point where it is indicated (to stay concise in our analysis; in practice this can be anywhere in the loop)

The actual value x of the observable is made up of the weighted set point value w and the weighted disturbance z as follows:

$$x = (y + z) \cdot H \ , \tag{2.7}$$

$$y = e \cdot G = (w - x) \cdot G \ . \tag{2.8}$$

Substituting 2.8 in 2.7 yields

$$\begin{aligned} x &= [(w - x) \cdot G + z] \cdot H \ , \\ x &= [wG - xG + z] \cdot H \ , \\ x &= wGH - xGH + zH \ , \\ x(1 + GH) &= wGH + zH \ , \\ x &= \frac{GH}{1 + GH} \cdot w + \frac{H}{1 + GH} \cdot z \ . \end{aligned} \tag{2.9}$$

All these variables are frequency dependent, but the direct dependency was omitted for clarity. Without loss of generality H can be defined as unity.

Equation 2.9 means that the point before the servo is the most senstive for disturbances coupling into the loop (so-called *sensor noise*); it is transmitted without being attenuated if $G \gg 1$. This has to be avoided by all means. On the other hand, disturbances acting on the loop before or in the system (so-called *actuator noise*) are damped out for high servo gain $G \gg 1$.

Stability of the control loop is only given if the equation

$$\phi(\mathrm{TF})_{\mathrm{UG}} > -180^\circ \ . \tag{2.10}$$

holds at unity gain. When the phase at unity gain falls below -90° then the open loop transfer function exhibits a *servo bump*. Due to the implicit sign inversion a phase of 0° corresponds to negative feedback, -180° equals positive feedback. Therefore -90° marks the transistion from negative to positive feedback and a certain degree of oscillation is introduced into the loop at the unity gain frequency when the phase at this frequency lies between -90° and -180°. The difference between the phase at unity gain to -180° is called *phase margin*. By changing the gain of the loop unity gain can be shifted to other frequencies. The range in which the gain of the loop can be adjusted - whilst retaining sufficient phase margin - is called the *gain margin*. Figure 2.4 illustrates the connection.

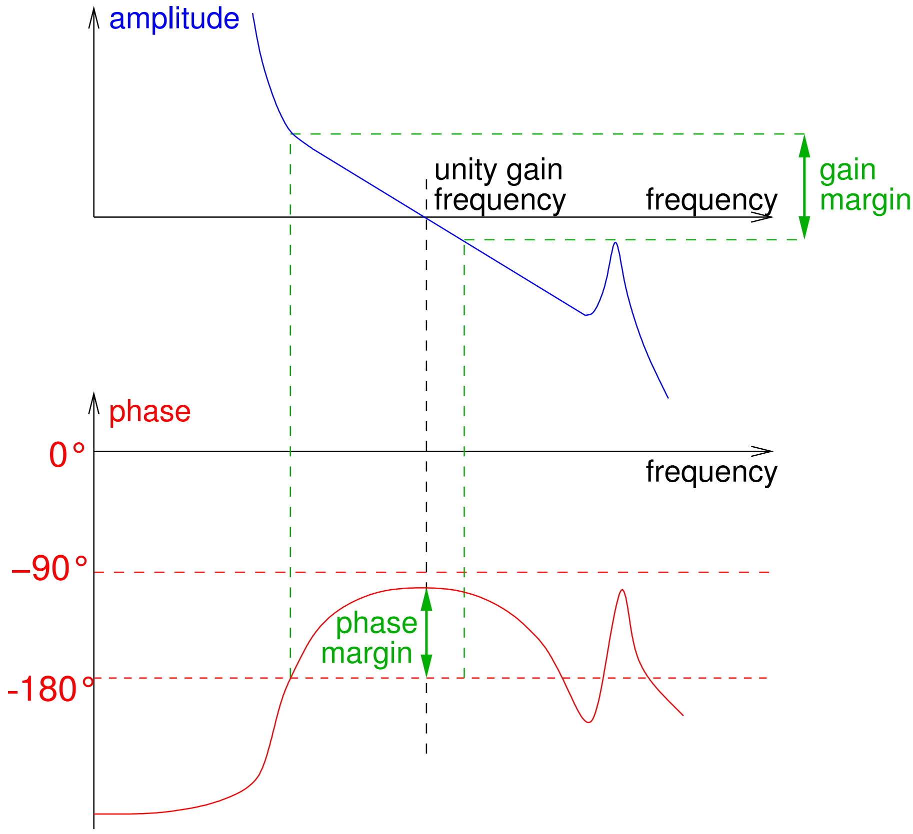

Figure 2.4: Illustration of phase margin and gain margin. Note that the gain margin in this example is limited at high frequencies not by the corresponding phase margin, but by the resonance visible in the amplitude plot. If unity gain was higher than this upper limit in the gain margin the system would exhibit two (at the peak of the resonance) respectively three crossings of unity gain due to the resonance, and probably start to oscillate at a frequency near the resonance peak.

2.2. General remarks on laser stabilisation

The techniques used for laser stabilisation vary, depending on the observable one wants to stabilise. Yet the general procedure in any stabilisation can be described as follows: The observable which is to be stabilised must be adequately detected, this calls for a suitable sensor (or *detector*). It is necessary to modify the detected signals by a servo to obtain an appropriate control signal, which is then fed back to the system via an actuator. These tools are described in detail in the following pages; photodiodes are treated in section 2.3, whereas the actuators are individually introduced in the corresponding sections.

The observables of a laser are

- laser intensity,
- laser frequency,
- laser beam geometry (including beam shape and beam jitter),
- polarisation.

This work primarily deals with the first two observables; the others are noted but not dealt with in the following sections. For information on laser beam geometry stabilisation the theses (Gossler 1999) (for mode filtering) and (Grote 2003) (for auto-alignment) are recommended. For simplicity a perfect Gaussian laser beam of lowest transverse order (as described in appendix D) is assumed.

A graphic example of control design

To demonstrate the principle of control loop design (introduced in section 2.1) in laser stabilisation the following example, illustrated in figure 2.5, is given:

A laser[2] is supposed to be frequency stabilised to an optical cavity; this is called *locking* the laser to the cavity. The laser, the cavity and all of the detection scheme together contribute the plant $H = H_1 + H_2 + \ldots + H_n$. The measured free running frequency noise (the observable) shows a $1/f$ behaviour. This is typical for the kinds of laser system treated in this work and can be seen in figure 2.6.

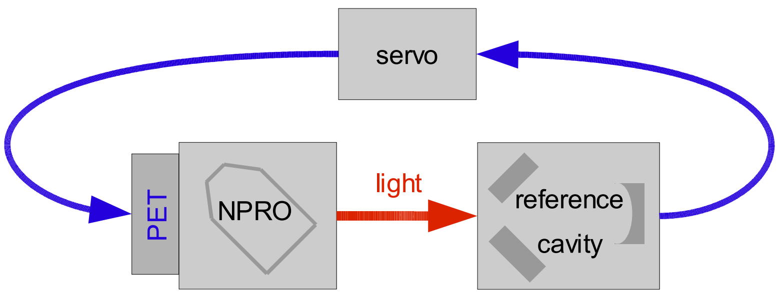

Figure 2.5: Exemplary control design: schematic of an experimental setup for stabilising the frequency of a laser ('NPRO') to an optical resonator ('reference cavity').

It might not be obvious at this point, but whenever frequency noise is measured, the result is always dominated by the noisier subsystem. In this case this is the laser. With the described experimental setup it is only possible to stabilise one subsystem (the laser OR the cavity) *relative* to the other (the cavity OR the laser). Both methods are analogous, but the resulting stabilised system will only be as stable as the subsystem to which the other subsystem was stabilised. If, as in this example, the laser frequency is to be stabilised to a resonator, then it is desirable that the intrinsic frequency noise of the resonator (the length

[2] we assume an NPRO design, see appendix A

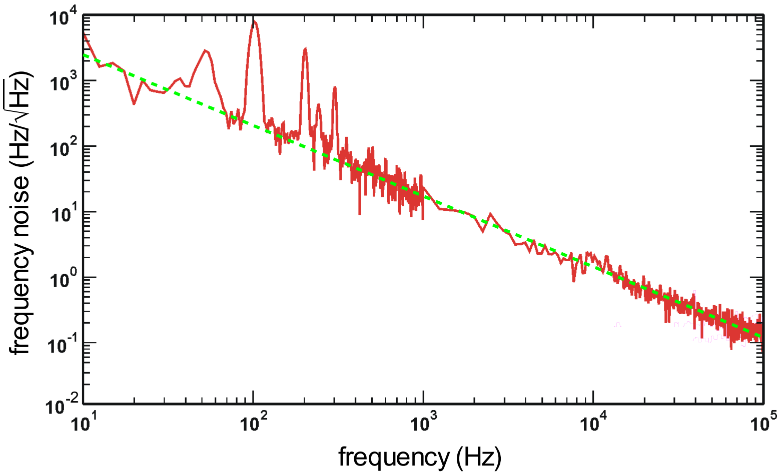

Figure 2.6: Exemplary control design: measured frequency noise (red, solid), 1/f-fit (green, dashed).

variations corresponding to the fluctuations of the cavity resonance frequency) be much smaller than that of the laser.

Let us assume the requirements are that the frequency noise shown in figure 2.6 is supposed to be reduced to a constant level of linear spectral density $LSD = 1\,\mathrm{Hz}/\sqrt{\mathrm{Hz}}$ in the frequency band from 10 Hz to 10 kHz. For this task the piezo-electric transducer contacted to the laser crystal is used to tune the frequency; in a different setup this could be any other actuator. The piezo-electric actuator has a flat transfer function with a coefficient of $\approx 10^6\,\mathrm{Hz/V}$ (Quetschke 2003), meaning that its response is frequency independent (up to its resonances at several 10 kHz). The photodetector likewise ideally has no frequency dependence (but a constant transimpedance amplifier gain of, say, $100\,\mathrm{V/A}$), as well as the rest of the detection and demodulation scheme, which is not further specified. The resulting transfer function of the plant is therefore flat with a constant value of $10^6 \cdot 100 = 10^8 \equiv 160\,\mathrm{dB}$.[3]

To be able to suppress the frequency noise of the laser according to the above specifications the system needs a frequency dependent *open loop gain* in the form that is shown in figure 2.7. This is exactly the transfer function that yields the desired frequency noise spectrum when the free running noise spectrum is divided by it. The open loop gain itself is the product of the gains of all subsystems in the loop: the plant and the servo. As the plant transfer function itself contributes a constant $10^8 \equiv 160\,\mathrm{dB}$, the servo transfer function only needs very little gain, but a characteristic of 1/f.

Figure 2.8 shows the projected result of the above designed frequency stabilisation: The frequency noise will be reduced to the desired level of $LSD = 1\,\mathrm{Hz}/\sqrt{\mathrm{Hz}}$ in the projected frequency band.

[3]For an introduction to the logarithmic scale (Bock 1994) is recommended.

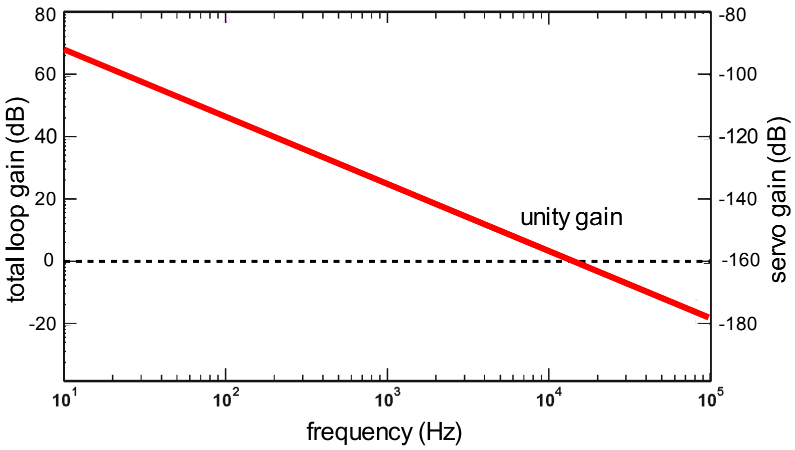

Figure 2.7: Exemplary control design: required open loop gain (left axis) and resulting servo transfer function (right axis).

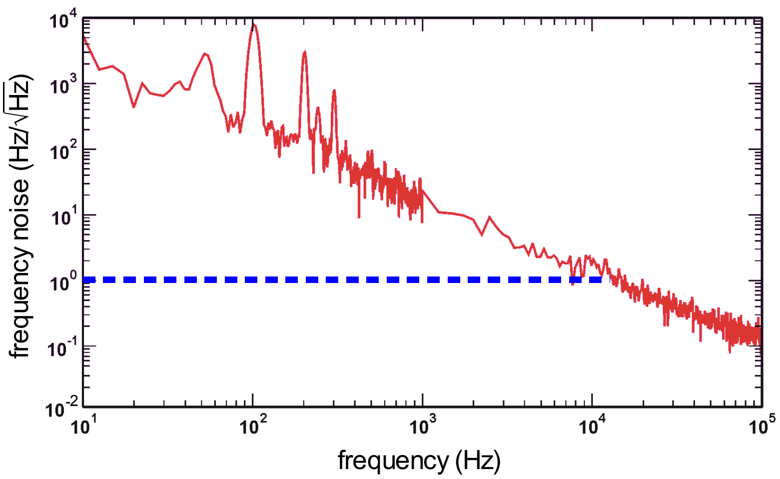

Figure 2.8: Exemplary control design: free running frequency noise (red, solid) and projected stabilised frequency noise level (blue, dashed) with the designed example loop gain.

2.3. Intensity stabilisation

The intensity is the most straightforward observable of a laser system. Nevertheless, laser intensity stabilisation is not a trivial task. This section describes the general methods and introduces the techniques employed in this work.

2.3.1. Photodiodes

Detection of laser intensity is not a mystery. Photodiodes, made of semiconductor materials, deliver a photo current when illuminated by light. This current is proportional to the light power and can be converted into a voltage by a transimpedance amplifier. The choice of photodiode depends on the wavelength of the light which is to be detected, on the expected light power and occasionally on the beam geometry. The diode pumped Nd:YAG lasers employed here emit light at a wavelength of $\lambda = 1064\,\mathrm{nm}$. Some semiconductor materials with absorption at this wavelength are indium-gallium-arsenide (InGaAs), germanium (Ge) and silicon (Si); typical responsivity spectra are shown in figure 2.9. As can be seen there the responsivities of the materials differ strongly at $\lambda = 1064\,\mathrm{nm}$.

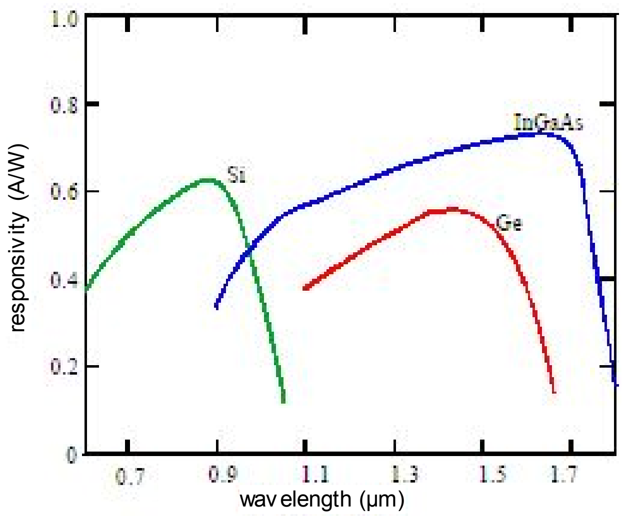

Figure 2.9: Typical responsivities of indium-gallium-arsenide (InGaAs), germanium (Ge) and silicon (Si) photodiode materials. Picture courtesy of the Institute of Photonics, Strathclyde, UK.

Chosing an appropriate photodiode now depends on what the stabilisation task is:

- If only very little light power is available or losses are detrimental, it is essential to chose a material with a high quantum efficiency, such as InGaAs. Squeezing experiments are a prime example for this (Franzen 2004; Vahlbruch 2004), losses dramatically diminish the amount of squeezing achievable. If on the other hand there is ample power it is not necessary to go for high quantum efficiency.

- If the beam is very large and cannot be focused sufficiently (e.g. due to large divergence or optical setup) it is advisable to use a large area photodiode. As opposed to InGaAs photodiodes (which commonly have a diameter of $d \leq 3\,\text{mm}$) silicon photodiodes are available with very large diameters, but have a much lower quantum efficiency at $\lambda = 1064\,\text{nm}$ than the afore mentioned.

- The homogeneity of the photodiode material is of importance if the intensity noise of the laser must be accurately measured. A laser beam with Gaussian intensity distribution (see appendix D) jittering across the active surface of an inhomogeneous photodiode can obviously feign, or in a control loop even introduce, intensity noise. Homogeneities of different photodiodes are documented in for instance (Larason and Bruce 1998; Seifert 2002).

- The dark current of a photodiode is relevant when the detected intensities are low or, more importantly in this work, when the laser intensity variations are much smaller than the 'DC' intensity (i.e. when a large dynamic range is need in the detection). Photodiodes made of germanium unfortunately have high dark currents (typically $I_{\text{dark}} \approx 1\,\mu\text{A}$ for a device with 1 mm diameter (Judson Technologies 2000)), but also InGaAs photodiodes can show significant dark currents; it is typically $I_{\text{dark}} \approx 5\,\text{nA}$ for a 1 mm-device, but depending on the batch we found that this can vary by a factor of 10.

In general the choice of the photodiode will be a trade-off between the different parameters. For a more detailed treatment of photodiodes, their basic function principles and the photodetector circuits used in this work please see appendix C.

2.3.2. Actuators for intensity stabilisation

The intensity of a laser diode pumped Nd:YAG laser depends on several parameters (pump current, temperature of the laser crystal, temperature dependence of the output coupler, etc.). The most important by far is the *drive current* of the pump laser diodes, as the coefficient from pump current to output power of the laser is very large (typically $\approx 1\,\text{W/A}$) and shows a linear dependence in the working regime. The pump current is therefore a possible actuator for laser intensity.

Another possibility of tuning the output power of a laser system is to place an *acousto-optic modulator* in the beam path, which is then driven by a radio frequency source and diffracts a variable amount of light power into higher diffraction orders by photon-phonon coupling (Yariv 1989). By adequately driving the acousto-optic modulator the laser intensity in zero order can be modulated to desire. This makes the acousto-optic modulator another actuator for laser power.

Special care has to be taken when realising the electronics for pump current actuation. The pump laser diodes are semiconductor devices which are very sensitive to reverse voltages and in most cases also to transients. There are two possible types of setup: the current driver and the current bypass.

The *current driver* feeds excess current into the diode laser, increasing the drive current and thereby the output power. Depending on the laser system the excess current will be up to $I = 1\,\mathrm{A}$, sometimes more, but for most systems this provides ample dynamic range. Special operational amplifiers deliver sufficient current to fulfil this task, such as the EL2009 from Elantec or the HA5002 from Burr-Brown. The obvious drawback is the danger of applying a voltage of wrong polarity. This has to be evaded by all cost, which is easily done by a safety diode (e.g. a Schottky diode with $U_{\mathrm{reverse}} = 0.1\,\mathrm{V}$). If, however, the safety diode fails, then the current driver can be fatal.

A passive *current bypass* does not pose this problem. It consists of a (power) MOSFET transistor with the drain connected to the anode of the laser diode. The control signal is fed to the gate of the transistor, so that a current is only bypassed when a voltage is applied. To achieve positve and negative range for the actuator an offset voltage is applied to the gate which constantly bypasses a fixed current. The control signal then determines wether more or less current is deducted from the laser diode, thereby actuating the drive current.

For safety reasons current bypass end stages were implemented in all intensity stabilisations realised in this work. Examples of the electronic setup of a current bypass can be seen in appendix B.

2.3.3. Laser intensity stabilisation for the gravitational wave detectors worldwide

One of the most demanding requirements of interferometric gravitational wave detectors worldwide is the intensity stability of their laser light sources. Designs for next generation detectors call for relative intensity stabilities of $RIN \leq 10^{-9}/\sqrt{\mathrm{Hz}}$, a very challenging task indeed. Yet this stability is crucial for the operation of future gravitational wave detectors, as intensity fluctuation will produce fake gravitational wave signals (Saulson 1994).

Current detectors employ different intensity stabilisation schemes, which are named in the following:

- GEO 600: The intensity stabilisation of the injection locked laser system of GEO 600 is subject of chapter 3. Intensity noise suppression is achieved by actuation of the pump laser diode current with a current bypass.

- LIGO: The american LIGO-project makes use of a current driver design to stabilise the output power of their master oscillator power amplifier (MOPA) laser system (Abbott and the LIGO Science Collaboration 2004).

- TAMA: The Japanese project uses an injection locked system (Yang et al. 1996) which is intensity stabilised via actuation of an AOM.

- VIRGO: The French-Italian collaboration uses an injection locked laser system similar to that of GEO 600; VIRGO employs an intensity stabilisation which is similar to that of GEO 600, using current feedback to the slave laser pump diodes. Details can be found in (Bondu et al. 2002).

2.4. Frequency stabilisation

Frequency stabilisation of laser systems used in gravitational wave detectors is a crucial issue. The reason is that frequency fluctuations entering the (slightly asymmetric) interferometer arms produce the same effect a gravitational wave would have - the signal at the interferometer output port varies. Therefore frequency fluctuations are a prominent noise source and have to be suppressed; for GEO 600 the specifications call for a frequency stability of $LSD = 2 \cdot 10^{-4}\,\mathrm{Hz}/\sqrt{\mathrm{Hz}}$ with respect to the power recycling cavity in the frequency band of $10 - 100\,\mathrm{Hz}$, where the specifications are the most demanding (Zawischa et al. 2002).

Unlike intensity stabilisation, frequency stabilisation of a laser system always requires an optical reference. A laser can be frequency stabilised, but only relatively to another system. This reference system should exhibit higher intrinsic frequency stability than the laser; in particular it must be 'quiet' with respect to the system in which the light is later to be used[4]. The need for suitable frequency references further complicates the task of frequency stabilisation. High finesse optical cavities can be used as frequency discriminators, but also molecular references are commonly employed (Arie et al. 1992; Kirchner). To accomplish frequency noise reduction in this work different optical cavities are used as a frequency reference; they are described in section 4.4.2. A more detailed description of these cavities can be found in (Brozek 1999; Quetschke 2003).

In our group frequency stabilisation of a laser to an optical cavity is generally accomplished via the Pound-Drever-Hall method, a heterodyne sideband technique already used in the 1940's in the microwave range (Pound 1946). Section 2.4.1 gives an overview of this method.

To be able to frequency stabilise a laser its frequency must be tuned by means of an actuator. The well-known frequency actuators for lasers of an NPRO design, such as piezoelectric element and temperature, have significant drawbacks which are discussed in section 2.4.2. Searching for optimised stabilisation schemes the experiments in our group led to the discovery of a new actuator for NPRO frequency, the drive current of the pump laser diodes. This current lock technique is introduced in section 2.4.2.

2.4.1. Pound-Drever-Hall method

A common scheme used for frequency stabilisation of laser systems is the *Pound-Drever-Hall method*. This technique was originally developed in the 1940's for stabilisation of microwave oscillators. In the laser stabilisation context it is used as an optical heterodyne technique (Drever et al. 1983). To gain an intuitive understanding of the Pound-Drever-Hall technique its principle will be explained in the phasor picture.

A *phasor* is a vector, with its length corresponding to the amplitude of an electrical field and its angle denoting a phase relative to a specified initial phase. This phase $\phi = 0$ is the initial phase of the *carrier* of the electrical field, in this case the laser light field $\vec{E}_0(t)$. The light field $\vec{E}_0(t)$ is phase modulated with a *modulation frequency* Ω; this is usually accomplished by an electro-optic modulator. Phase and frequency modulation are respresented identically in the phasor picture, but differ in the time dependence of the *modulation in-*

[4]In the case of gravitational wave detection this is the interferometer.

dex M. The laser light frequency is denoted by ω. Equation 2.11 shows the mathematical representation of the phase modulated laser light field $\vec{E}(t)$.

$$\vec{E}(t) = \frac{1}{2}\vec{E}_0 e^{i\omega t + iMcos(\Omega t)} + c.c. \ . \tag{2.11}$$

Equation 2.11 can be expanded in Bessel functions (Bronstein and Semendjajew 1993)

$$\vec{E}(t) = \frac{1}{2}\vec{E}_0 \sum_{n=-\infty}^{+\infty} (i)^n \mathrm{J}_n(M) \cdot e^{in\Omega t} + c.c. \ . \tag{2.12}$$

For modulation indices $M \ll 1$ this expression can be approximated to

$$\begin{aligned} \vec{E}(t) &= \frac{1}{2}\vec{E}_0[J_0(M)e^{i\omega t} - iJ_{-1}(M)e^{i(\omega-\Omega)t} + iJ_1(M)e^{i(\omega+\Omega)t}] + O(J_2) + c.c. \ , \\ &\approx \frac{1}{2}\vec{E}_0[e^{i\omega t} - \frac{M}{2}e^{i(\omega-\Omega)t} + \frac{M}{2}e^{i(\omega+\Omega)t}] + c.c. \ . \end{aligned} \tag{2.13}$$

The term in ω is the *carrier* of the light field, whereas the terms in $\omega \pm \Omega$ are called *upper* respectively *lower sideband*.

Phase modulation, as well as frequency modulation, is not directly detectable by a photodetector. This is due to the fact that the square of the electrical field, the light power, stays constant during phase or frequency modulation, as shown in equation 2.14:

$$\begin{aligned} I(t) &= \left|\vec{E}(t)\right|^2 \ , \\ &= \left(\frac{1}{2}\vec{E}_0[e^{i\omega t} - \frac{M}{2}e^{i(\omega-\Omega)t} + \frac{M}{2}e^{i(\omega+\Omega)t}] + c.c.\right) \ , \\ &\quad \cdot \left(\frac{1}{2}\vec{E}_0[e^{i\omega t} - \frac{M}{2}e^{i(\omega-\Omega)t} + \frac{M}{2}e^{i(\omega+\Omega)t}] + c.c.\right) \ , \\ &= \vec{E}_0^2 \ . \end{aligned} \tag{2.14}$$

The two phase modulation sidebands cancel out when interacting with the carrier. This is visualised in the phasor picture in figure 2.10.

The sum of the first order sidebands (shown in red and blue) is a phasor oscillating with 2Ω, which stands orthogonally on the carrier. This approximation holds for small modulation indices $M \ll 1$. For an exact calculation, taking into account all sidebands of higher order, the resulting sideband phasor tip moves on a circle segment, leading to an exact visual interpretation.

The phasors of carrier and sidebands are added vectorially to obtain the resulting light field. The length of the resulting phasor (shown in green) does not change during one period of phase modulation $T = 2\pi/\Omega$. The sum of the sidebands merely causes the carrier phasor to 'wiggle' a little; this corresponds to the phase modulation of the light field. The intensity of the light - the square of the absolute value of the light field, corresponding to the length of the sum vector - does not change.

When phase modulated light impinges on a Fabry-Perot cavity, which is near resonant for the carrier, then a fraction of the carrier light enters the cavity. The sidebands, though, are

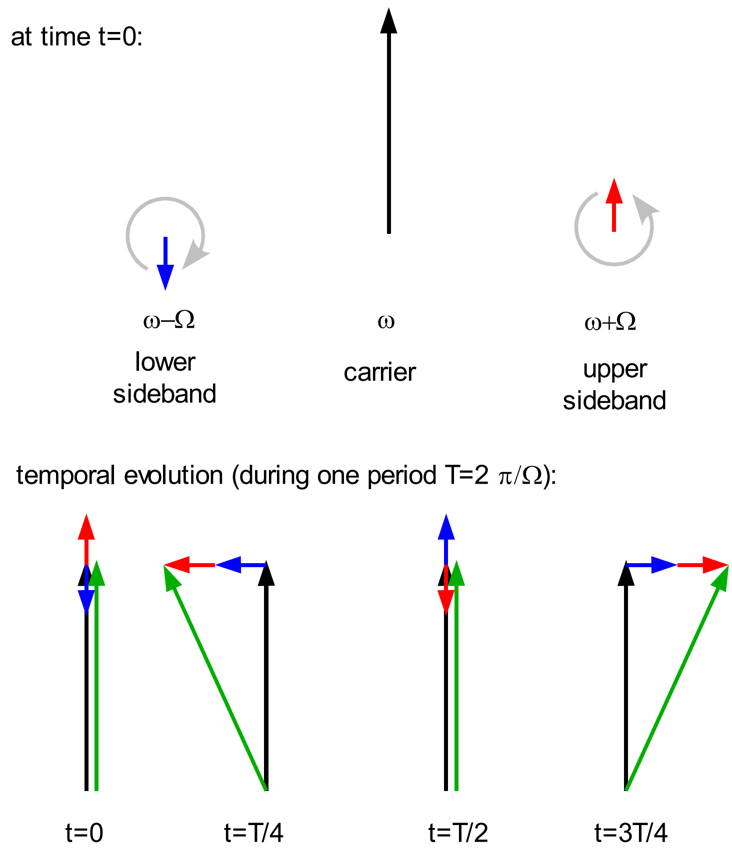

Figure 2.10: Phase modulation in the phasor picture, as seen from a coordinate system co-rotating with the the carrier at frequency ω. Legend: black - carrier, blue - lower sideband, red - upper sideband, green - resulting phasor (light field), grey - rotation orientation of a phasor.

directly reflected, as their frequencies ν do not fulfil the resonance condition $n \cdot c/2\nu = L$ of the Fabry-Perot interferometer[5].

By every round trip in the Fabry-Perot resonator the near resonant carrier experiences a phase shift. As the mirrors of the resonator have a finite reflectivity, a fraction of the carrier light leaves the resonator in every round trip. These phase shifted components of the carrier light field leaving the resonator interfere with the directly reflected sidebands and the fraction of the directly reflected carrier. Relative to the transmitted light the sum of the reflected components has a phase shift of π. The square of the total sum (the reflected light and the light leaking out of the resonator, shown in figure 2.11), the beat signal at the modulation frequency Ω, is detected with a photodetector.

[5]For the sake of an easier understanding we assume that the sideband spacing of the phase modulation is much larger than the linewidth of the Fabry-Perot cavity. If the linewidth is in the order of the sideband spacing, then the analysis becomes a little more complicated, but it still works.

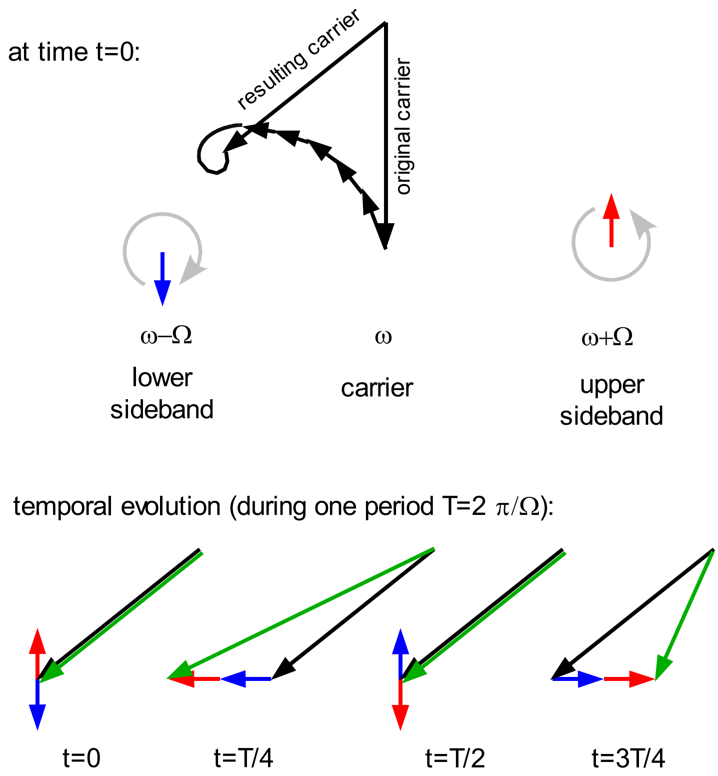

Figure 2.11: Sum light field in reflection of a Fabry-Perot cavity. Legend: black - carrier, blue - lower sideband, red - upper sideband, green - resulting phasor (light field), grey - rotation orientation of a phasor. Beating between the components leads to a change in the length of the resulting phasor, i.e. intensity modulation, which is detectable with a photodetector.

As can be seen in figure 2.11, the resulting carrier (made up of the directly reflected fraction and the components leaking out of the cavity with every round trip) experiences a phase shift. The interference of resulting carrier and directly reflected sidebands creates a sum phasor (shown in green), whose length varies with the modulation frequency Ω. The periodical length change corresponds to a change in light intensity with the oscillation frequency Ω, which can be detected with a photodiode.

The Pound-Drever-Hall method is a very sensitive technique to detect phase changes caused by an optical resonator. By transferring the detection frequency to the radio frequency regime (in the range of $\Omega \approx$ MHz) the high power noise floor at the actually interesting detection frequencies in the acoustic region is evaded.

2.4.2. Current Lock

Frequency stabilisation of NPROs routinely used to be conducted in our group by employing the commonly known actuators for laser frequency, piezo-electric transducer and crystal temperature. The Pound-Drever-Hall-technique (2.4.1) is used to stabilise the laser frequency either to an optical cavity or a molecular resonance[6] (Kirchner). Either way, the above actuators show coupling effects to other laser observables, which can be very disturbing. The parasitic couplings exhibited by all known NPRO actuators (for frequency, intensity and beam geometry) are investigated in (Quetschke 2003).

In the course of these coupling experiments the pump current of the NPRO pump laser diodes was examined as an actuator. Tuning the pump current of a laser diode obviously results in a change of the pump intensity, which has an effect on the NPRO intensity (Harb et al. 1997). Therefore the pump current of the pump laser diodes of an NPRO is well suited as an actuator for laser intensity (as described in section 2.3.2). During the experiments regarding the parasitic couplings, though, it was found that tuning the pump current of the pump laser diodes also results in a well-defined change of the emission frequency of the NPRO. This effect had been shown before (Day 1990), though actually using the pump current as an actuator for NPRO frequency was unprecendented[7].

The transfer function from drive current of the pump laser diodes to emission frequency of the NPRO was measured (Brozek 1999; Willke et al. 2000b; Quetschke 2003). The transfer function falls as 1/f for more than three frequency decades. At the resonant relaxation oscillation frequency a resonance structure is discernible. This well defined transfer function makes the pump current a possible actuator for NPRO frequency. The exact effect on the NPRO intensity, though, was yet to be determined. (Day 1990) comments on unwanted modulation of laser intensity when using the pump current as an actuator for laser frequency.

Frequency stabilisation of an NPRO by use of the pump current as an actuator is called *current lock*. Current lock of a conventional NPRO to an optical resonator was performed and an in-loop frequency noise reduction to a constant value of $LSD \leq 0.1\,\mathrm{Hz}/\sqrt{\mathrm{Hz}}$ up to unity gain at $f_{\mathrm{UG}} = 5 \cdot 10^4\,\mathrm{Hz}$ was achieved (Brozek 1999). The intensity noise of the NPRO was measured simultaneously to determine the effect of pump current actuation on the intensity. This measurement revealed a surprising fact: The intensity noise of an NPRO is not largely increased in current lock, but even reduced in a limited frequency band to a small degree of about 3 dB. Outside of this frequency band the intensity noise is larger than the free-running noise, though. Nevertheless this result gave rise to the experiments in chapter 4, spawning the hope that a simultaneous reduction of frequency *and* intensity noise of an NPRO might be possible by use of merely *one* actuator and active stabilisation of only *one* observable.

Even without the possibly useful coupling effect between frequency and intensity the pump current is a legitimate actuator for NPRO frequency, as it exhibits less disadvantages than other actuators. A comparison between the actuators is given in table 2.1.

---

[6] In this case the technique is not referred to as Pound-Drever-Hall-technique, but is called frequency modulation spectroscopy (FMS).

[7] The experiments by (Heilmann and Wandernoth 1992) used the pump current of additional 'heating' laser diodes as frequency actuators in twisted mode cavity lasers. The actuated laser diodes were not the laser pump source, though, since the emission wavelength of the heating laser diodes did not drive the laser transition. Their light therefore did not contribute to the inversion.

characteristics	PZT	crystal temp.	pump current
dynamic range	$\approx 500\,\text{MHz}$	$\approx$ GHz (modehops)	$\approx 50\,\text{MHz}$
bandwidth	$\approx 10\,\text{kHz}$	$\approx 1\,\text{Hz}$	see chap. 4
tuning coefficent	$2-3\,{}^{\text{MHz}}/_{\text{V}}$	$1\,{}^{\text{GHz}}/_{\text{K}}$	$\approx 1\,{}^{\text{MHz}}/_{\text{mA}}@10\,Hz, \propto 1/f$
cross coupling to	position	none (Quetschke 2003)	laser intensity
realisation	HV-amplifier	temp. controller	current bypass / driver

Table 2.1: Comparison of the actuators for the frequency of a solid-state laser.

2.5. The dreaded in-loop / out-of-loop problem

Stabilisation of laser observables is a straightforward procedure, which is described above for laser frequency (section 2.4) and intensity (section 2.3). As explained in section 2.1 one needs a suitable detector for the observable, an actuator to act upon the system and an adequate servo to supply loop gain. The detection of the now stabilised observable can then be done with the same detector that is used for stabilisation, or with an independent one. These are called the *in-loop* and *out-of-loop detector*, respectively. The noise spectrum detected with the in-loop detector is called an *in-loop measurement*, as it is measured with an element which is part of the control loop. Sensor noise, though, is the worst noise for a control loop, as it is not reduced even for high servo gain G (shown by the equations in section 2.1). An imperfect detector therefore introduces noise in the loop. The servo compensates for this *in* the loop, counter-introducing 'matching' noise to minimize the noise in the loop, mirrored in the in-loop measurement of the stabilised observable. Even though one might then see a significant reduction of noise in the in-loop measurement, relative to the 'outside world' the noise level is increased. The independent detection of this 'real' noise is done with the out-of-loop detector and is called an *out-of-loop measurement*. It reflects much more accurately the effect of the stabilisation on the observable. The need for high out-of-loop stability is easily understood: The light used in-loop for stabilisation is not available for any other purpose after the stabilisation, it is 'used up' and does not leave the system. The out-of-loop light, on the other hand, leaves the system and is supposed to be used for spectroscopy or other purposes later on, so it must be the main objective to achieve stabilisation of this light.

As an example let us consider the detection of intensity noise with active intensity stabilisation, and let us assume two photodetectors which are both inhomogeneous and differ strongly from one another. Then the in-loop measurement of the stabilised intensity noise will show a strong reduction of intensity noise, whereas the out-of-loop measurement might show an increase in intensity noise as opposed to the free-running level. This discrepancy is then directly due to the differences between the detectors; the absolute level of stability (relative to the measurement setup, which will use the stabilised light in some way) is determined by the noise of the in-loop detector.

It is therefore crucial to take the utmost care when designing the detection scheme of a stabilisation. Sensor noise must be minimised, but it can also be necessary to minimise the non-common beam paths between the in-loop and the out-of-loop detector (which need not be another detector, but might also be the point where the stabilised laser light is to be used). Air drafts causing vibrations of optical mounts, fluctuations of the index of refraction of air and other effects are disturbances which can cause an extreme discrepancy between in-loop and out-of-loop measurements. The latter is at a maximum as good as the former, but it is also the by far more relevant measurement.

2.6. Injection locking

Injection locking is a technique known since 1665, when Christian Huygens observed the pendulums of two neighbouring clocks whose motion miraculously seemed to be locked, when the clocks were hung not too far apart. He traced this coupling phenomenon back to mechanical vibrations transmitted through the wall on which the two clocks were hung. This was probably the first observation of the coupling of two oscillators by injection locking. The technique can be used for instance in laser systems, to lock a high power slave oscillator to a weak, monochromatic master oscillator, but it also works in almost any other self-sustained oscillatory system (Siegman 1986). The following explanations will concentrate on laser oscillators.

The technique of injection locking is used to generate the high power, ultra high stability laser system for GEO 600, which is described in more detail in chapter 3. As the various methods of laser stabilisation used in this work are treated in this chapter, also injection locking will be explained here.

A laser oscillator below threshold is essentially a regenerative amplifier (Siegman 1986). Under the assumption that the round-trip gain magnitude $G(\omega)$ (made up of laser gain, internal losses and finite mirror reflectivities) approaches unity (highly regenerative limit) the regenerative gain $\tilde{g}(\omega)$ near any one axial-mode frequency ω_0 can be written in a simplified form as

$$\tilde{g}(\omega) \approx \frac{1-R}{1-G+iGT(\omega-\omega_0)} \tag{2.15}$$

with $T = p/\mathrm{c}$ being the transit time for a cavity round-trip and R the input-output mirror reflectivity. In the steady-state oscillation condition the internal round-trip gain G clamps at unity. Any externally applied signal at ω_0 then drives the regenerative gain to infinity, meaning that it is hugely amplified. Away from the resonance frequency ω_0 the gain an injected signal experiences remains finite and limited, though; the amplification for a signal at $\omega \neq \omega_0$ is approximately given by

$$|\tilde{g}(\omega)|^2 \approx \frac{\gamma_e^2}{(\omega-\omega_0)^2} \quad . \tag{2.16}$$

γ_e is the energy decay rate and thereby the frequency bandwidth of the laser cavity due to external coupling (Siegman 1986). Due to energy conservation the intensity of the amplified output must be limited to the intensity of the free-running laser plus the intensity of the injected signal.

If the laser is already oscillating at its resonance frequency ω_0 with an output intensity of I_0 when a small external signal at $\omega_1 \neq \omega_0$ with intensity I_1 is injected, then the signal at ω_1 can be regeneratively amplified in the cavity, even in the presence of the much stronger laser oscillation at ω_0.

Let's assume that the intensity of the injected signal is kept constant at I_0, but its frequency ω_1 is varied. Then the amplified output intensity of the injected signal, $|\tilde{g}(\omega)|^2 I_1$, increases strongly when ω_1 approaches ω_0. As ω_1 comes closer to ω_0, the output intensity of the injected signal approaches the output intensity I_0 of the free-running oscillation at ω_0, which means that the injected signal begins to saturate the laser gain. At this point the free-running oscillation is suppressed. For frequencies ω_1 close enough to ω_0 the injected signal takes over the complete laser oscillation, thereby suppressing the free-running oscillation of the laser.

According to equation 2.15 the regenerative gain would continue to increase towards infinity when ω_1 reaches ω_0. The laser medium is not able to supply this (infinite) power, though, so that the power of the amplified injected signal is limited to approximately the free-running power plus the power of the initially injected signal.

The frequency range in which the injected signal dominates the laser oscillation and the free-running oscillation is suppressed is called *locking range*. As stated above it is defined as the frequency range in which the power of the amplified injected signal equals the power of the free-running signal:

$$|\tilde{g}(\omega)|^2 I_1 = \frac{\gamma_e^2}{(\omega - \omega_0)^2} I_1 \approx I_0 \ . \tag{2.17}$$

The amplified injected signal will therefore dominate and suppress the free-running oscillation in the frequency range determined by the equation

$$|\omega - \omega_0| \approx \gamma_e \sqrt{\frac{I_1}{I_0}} \approx \frac{\omega_0}{Q_e} \sqrt{\frac{I_1}{I_0}} \tag{2.18}$$

where γ_e (the energy decay rate) equals the 'external' or 'cold cavity bandwidth' ω_0/Q_e with Q_e as the quality factor of the external cavity. The full locking range is twice the frequency range defined by equation 2.18:

$$\Delta\omega_{lock} \approx \frac{2\omega_0}{Q_e} \sqrt{\frac{I_1}{I_0}} \ . \tag{2.19}$$

The description of the injection locking process is kept short at purpose. It merely is supposed to build an understanding of the dynamics involved. For a more rigorous analysis (Siegman 1986) is recommended. (Zawischa 2003) deals extensively with the injection locking of the GEO 600 laser system.

By the process of injection locking the slave laser inherits the superior frequency noise characteristics of the master laser. By frequency stabilisation of the master laser (treated in section 3.4) the frequency noise of the injection locked system is even further reduced to comply with the specifications for GEO 600.

3. An injection locked high power laser system for GEO 600

GEO 600 is an interferometric gravitational wave detector designed to detect the fleeting deformations of space time caused by passing gravitational waves. The various subsystems of GEO 600 all work together to reach the necessary detection sensitivity to achieve this ambitious goal. The performance of the light source for the Michelson interferometer therefore plays a fundamental part in this effort - the injection locked 12 W laser system stands at the very 'heart' of the gravitational wave detector.

High power laser emission can be realised with diverse laser systems, yet it is a solid-state laser system which is used in all currently operating gravitational wave detectors (Willke and the GEO 600 team 2004; Yang et al. 1996; Bondu et al. 2002; Abbott and the LIGO Science Collaboration 2004). Argon ion lasers, which were used in some gravitational wave detector prototypes, have the disadvantage of being large and expensive, though their emission wavelengths in the visible are advantageous as opposed to systems emitting in the near infrared, as their smaller wavelength increases the sensitivity of the detector (Saulson 1994). Fibre lasers and amplifiers, which are becoming increasingly popular (partly due to new developments such as large mode area and photonic crystal fibres), are still fighting the intensity limiting problems caused by stimulated Brillouin scattering and possible destruction of the fibre ends by contamination or misalignment at high output powers; besides the phase noise of fibre amplifiers is yet another problem (Tröbs et al. 2004). The all-solid-state laser systems used in the current generation of interferometric gravitational wave detectors are constructed modularly to offer easy maintenance; the pump sources are readily available, high power fibre-coupled laser diode arrays which can easily be exchanged. The noise characteristics of the monolithically or quasi-monolithically built lasers are intrinsically excellent and can be stabilised further by well-known techniques.

This chapter deals with the specifications for the laser system (section 3.1), its design and optical setup (section 3.2) as well as its stabilisation by injection locking (section 3.3) and frequency stabilisation (section 3.4). Special emphasis is put on the intensity stabilisation (section 3.5) which was designed and realised in the scope of this work.

The gravitational wave detectors of future generations will pose even higher requirements on their light sources than the currently operating detectors. Now is the time to work towards even stabler laser systems, investigating limiting noise sources and reaching for the stabilisation limits, to provide these future detectors with lasers which fulfil their ambitious specifications. Work towards this goal is found in chapter 4.

3.1. Specifications for the laser system

The gravitational wave detector GEO 600 calls for a laser system which runs continuously, stably and virtually maintenance free. The requirements posed on the laser system are amongst the highest in contemporary science, regarding frequency and intensity noise as well as beam quality. The laser system must show very good noise characteristics with excellent long term stability. Its reliability is a crucial issue, since the continuous run of GEO 600 depends on this quality of its light source. Necessary modifications must be completed in as short a time as possible, so a modular system is desirable: This allows for easy maintenance.

The laser system is designed for a nominal output power of $P_{\text{laser}} = 10\,\text{W}$. For GEO 600 the intensity noise requirements of the system lie at $RIN = 5 \cdot 10^{-8}/\sqrt{\text{Hz}}$ in the frequency band from 50 Hz to 5 kHz, which is the designated detection band for the gravitational wave detector; the frequency noise relative to the power recycling cavity of GEO 600 is required to be $LSD = 2 \cdot 10^{-4}\,\text{Hz}/\sqrt{\text{Hz}}$ in the detection band (Zawischa et al. 2002). As the power recycling cavity eigen mode of the Michelson interferometer is a Gaussian TEM_{00} mode the laser beam must be in the fundamental mode at least to a degree of 95 %.

Even though the free-running solid-state GEO 600 laser system exhibits relatively good noise characteristics, active stabilisation of the laser observables is necessary to achieve the above specifications. The stabilisation electronics were all designed and first implemented in a lab environment, as frequent modifications were necessary during the development. All this is done much more conveniently in normal lab surroundings as opposed to a real clean room environment such as at the detector site. It was necessary to test all possible parameters of the stabilised laser system before installation at the detector site to ensure optimal performance of the system over a long period of time. The reliability of the laser system was verified by long term monitoring of the laser output in the laser lab.

3.1.1. The conditions in the laser lab

The conditions in the laser lab differ from those at the site of GEO 600. Much of the GEO 600 optics is placed in ultra-high vacuum, for instance the suspended mode cleaners (section 3.1.2), which serve as a frequency reference at the site. The lab does not have this option, instead a rigid ultra-high finesse three-mirror ring cavity, described in section 4.4.2, was used as a reference for frequency stabilisation.

The laser lab was a relatively clean environment without fulfilling clean room specifications. Normal clothing was worn, but clean shoes were required. Clean floors were enforced by sticky mats and frequent cleaning of the lab. These efforts resulted in a strongly reduced amount of dust in the lab, which was very convenient as scattering and losses of light on contaminated optics was minimised.

The temperature of the laser lab was held constant to about $\Delta T = \pm 2^\circ$ C by air conditioning. This measure entailed fairly strong air currents which sometimes posed problems during measurements. For this reason the air conditioning was occasionally switched off during sensitive measurements for short periods of time.

Ground loops were a frequent menace in the laser lab. Due to the ongoing development of the lab electronics hum loops were unintentionally built. If a measurement was limited by saturation of electronic stages due to hum loops, then these loops were identified and opened. A quick method of evading ground problems was to use battery powered photodetectors or pre-amplifiers.

The actual setup of the lab laser sytem for GEO 600 is shown in section 3.2.3.

3.1.2. The conditions at the site of GEO 600

The laser system in GEO 600 is situated below ground level in the central building of the detector. This is the level where the vacuum tanks with all the suspended optics stand. The laser bench is located in one corner of the building, right beneath were the mode cleaner electronics racks stand on the gallery (on ground floor). Due to the construction of the building the work space above the laser bench is not quite man height, the surface of the optical table itself is only about 60 cm high.

The experimentation floor of GEO 600 is a clean room close to class 1000 conditions. This necessitates clean room clothing being worn all throughout the work on the laser system, including a full overall, boots, headgear and gloves. Difficult alignment work was often complicated by this apparel.

The temperature at the site is held constant at $T = 19°$ C to a variation of max. $\Delta T = \pm 1°$ C. This is achieved by an adequate air conditioning system. Before this system was installed in March 2003 a weaker air conditioning was not able to keep the temperature in the central building from reaching values higher than 25° C in summer, which resulted in strong thermal problems especially with the laser electronics, but also with other control electronics, such as the mode cleaner electronics.

Ground loops were also a problem at the detector site, but in 2002 a major part of the electronics was re-connected and the amount of hum loops reduced.

As mentioned above the suspended mode cleaners can be used as a frequency reference for the laser system. The two mode cleaners are three-mirror ring cavities wtih the mirrors suspended as double pendulums with steel wires. Above the resonance frequencies of the pendulums (as of $f \approx 50$ Hz) the mirrors hang freely and can be assumed as completely still, which makes them a perfect frequency reference. For more information on the mode cleaners in GEO 600 (Gossler 1999) and (Gossler 2004) are advised. The optical setup of the laser system at the gravitational wave detector GEO 600 is described in section 3.2.4, the stabilisation scheme in section 3.4.2.

3.2. Setup of the laser systems

The laser system for the gravitational wave detector GEO 600 consists of a high stability master laser and a high power slave laser with lesser stability performance. The two laser systems are coupled by injection locking, the principle of this technique is explained in section 2.6. Master laser and slave laser are introduced in the following sections 3.2.1 and 3.2.2.

The two laser systems (in the Hannover laser lab and at the site of GEO 600) are for the most part identical. The optical setup surrounding the laser systems varies, though, due to differences in the lab infrastructure. The two setups are therefore individually described in sections 3.2.3 and 3.2.4.

3.2.1. Master laser

The master laser of the injection locked laser system is a Nd:YAG non-planar ring oscillator (NPRO). It is a commercially available system (type Mephisto 800 ™ from InnoLight GmbH (InnoLight GmbH 2004)). The laser crystal is specially facetted to act as laser medium and resonator in one. The non-planar beam path is defined by total internal reflection of the laser beam in the medium. The monolithic design entails very high intrinsic frequency stability of the NPRO, which lies at $LSD \approx 1\,\mathrm{kHz}/\sqrt{\mathrm{Hz}}$ at $f = 1\,\mathrm{Hz}$ and falls as 1/f up to the resonant relaxation oscillations. The end-pumped geometry allows for mode-selective pumping, which results in very high beam quality of the emitted light ($M^2 \leq 1.1$). The two laser diode arrays used for pumping (here type SPL 2Y81 from Osram Semiconductors (Osram Opto Semiconductors 2003)) emit $P_{\mathrm{pump}} = 1\,\mathrm{W}$ each at a wavelength of $\lambda_{\mathrm{pump}} = 808\,\mathrm{nm}$. The 2 W of pump power result in nominally $P = 800\,\mathrm{mW}$ of laser emission at $\lambda = 1064\,\mathrm{nm}$, though higher output powers of $P = 1\,\mathrm{W}$ have been achieved with the same pump power, depending on the pump parameters. NPROs with lesser or higher output power are available for different applications.

Without further measures the described pumping scheme would lead to bidirectional laser emission. Unidirectional lasing is achieved by making use of the non-vanishing Verdet-constant of the Nd:YAG crystal: A permanent magnet is placed beneath the NPRO; the losses are then higher for one beam direction than for the other.

Commercial NPROs can optionally be equipped with a noise eater (see appendix A). This control electronics suppresses the resonant relaxation oscillations by typically 40 dB, but also the relative intensity noise for lower frequencies by up to 20 dB. The master laser for GEO 600 has a noise eater implemented.

Chapter 4 goes into more detail on laser diodes and intricacies of the NPRO pumping scheme. For further information on NPROs (function principle, pump geometry, beam path, operation parameters, unidirectionality of emission etc.) see appendix A, where the pump geometry and the non-planar beam path of an NPRO (figure A.2) are shown. As a visual supplement figure 3.1 shows a photograph of the beam path in an NPRO crystal. To gain an insight on the original works (Kane and Byer 1985; Freitag 1994) are recommended.

3.2.2. Slave laser

The slave laser of the GEO 600 laser system was built at the Laser Zentrum Hannover and is inspired by the monolithic design of the NPRO. It is a quasi-monolithic end-pumped Nd:YAG rod laser in a planar bowtie-configuration. Since its implementation in the laser lab in Hannover the design has undergone significant changes, which is why this section will treat the 'old' design (which is now obsolete, but was used for most of the measurements shown in this chapter) as well as the 'new' design (which has recently been installed at the lab and at the site of GEO 600 by modification of the old design). The changes merely concern the pumping scheme. The general resonator design, which was not changed, will therefore be treated here first, before the differences are described.

The slave laser resonator is made of Invar, an alloy consisting of 36 % of Nickel and 64 % of Iron. Invar has a very low thermal expansion coefficient of $\beta = 0.8 \cdot 10^{-6}\,\mathrm{K}^{-1}$ (in relative units) (Verlag Stahleisen mbH 1991). The monolithic design renders the laser less succeptible to environmental influences. The laser resonator mirrors are glued to the Invar spacer by epoxy glue, after the optical alignment is fixed by temporary nylon screws. A design without glueing the mirrors to the spacer can result in a gradual deterioration of the alignment over a period of weeks by creeping.

A piezo-electric element is contacted to one of the plane resonator mirrors and acts as an actuator for the slave laser cavity length for frequency tuning. The cavity roundtrip length

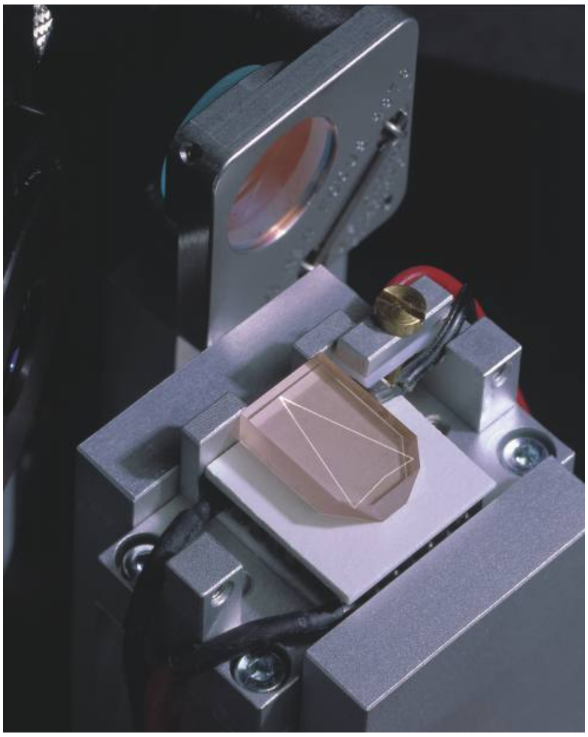

Figure 3.1: Photograph of the non-planar beam path in an NPRO (picture courtesy of Inno-Light GmbH).

is $L_{\mathrm{rt}} = 550.8\,\mathrm{mm}$, which results in a free spectral range of $FSR \approx 540\,\mathrm{MHz}$. The dynamic range of the piezo-electric transducer is approximately 700 MHz and therefore sufficient to scan over more than one free spectral range of the slave laser; the tuning bandwidth is limited by the piezo resonances, which typically lie at $f \approx 60\,\mathrm{kHz}$.

The two Nd:YAG laser rods are located in the crossed arms of the resonator, right behind the pump optics. The cylindrical rods have a diameter of 3 mm and are 6 mm long (Zawischa 2003). They are anti-reflex coated for $\lambda = 1064\,\mathrm{nm}$ and $\lambda = 808\,\mathrm{nm}$; the doping concentration is 1.1 %. The remaining 'free' plane mirror is the output port of the laser.

Two quartz Brewster plates in the beam path ensure that the output polarisation of the laser is mainly in the plane parallel to the table surface (in the so-called *p-polarisation*). The parasitic *s-polarisation* arising in the laser resonator due to thermally induced birefringence leaves the resonator due to reflection at the Brewster plates. In one round-trip a loss of approximately 40% is introduced for the s-polarisation. The laser output nevertheless has a small remaining content of approximately 1 % in the parasitic s-polarisation; this is eliminated by an external polarising beam splitter right after the output port.

The slave laser emits around $P_{\mathrm{laser}} = 12\,\mathrm{W}$ of output power at $\lambda = 1064\,\mathrm{nm}$ with a pump power of $P = 2 \cdot 17\,\mathrm{W}$ at $\lambda_{\mathrm{pump}} = 808\,\mathrm{nm}$. The laser beam is Gaussian with a beam quality factor of $\mathrm{M}^2 \leq 1.1$. The beam geometry is based on the resonator design, which entails two beam waists in the resonator. The small beam waist with $w_1 = 80\,\mu\mathrm{m}$ lies symmetrically between the two curved mirrors (between the Brewster plates); the output waist has a radius of $w_1 \approx 260\,\mu$m and is located symmetrically between the two plane mirrors.

A schematic of the optical design of the slave laser can be seen in figure 3.2.

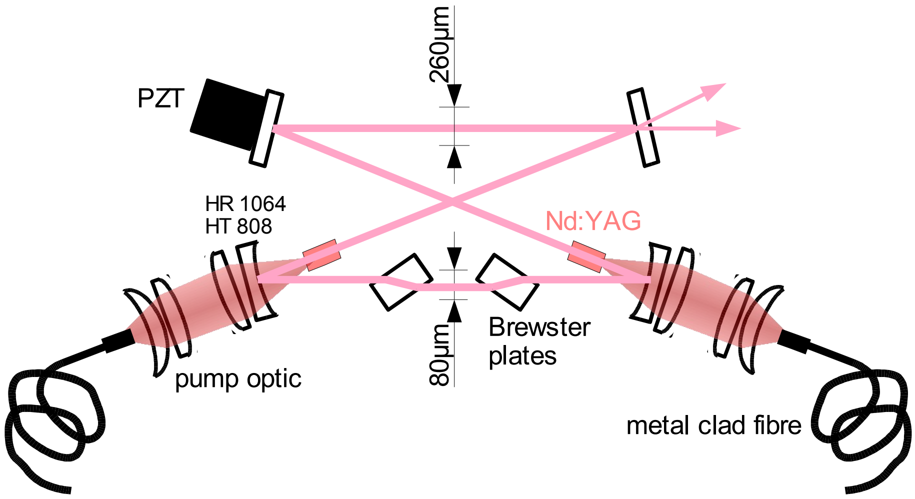

Figure 3.2: Schematic of the slave laser of the GEO 600 laser system.

Pumping scheme of the 'old' slave laser design

The slave laser is pumped by two high-power laser diode arrays from OptoPower / Spectra-Physics Semiconductor Lasers (type H01-D040-807FC respectively BFA1100-808-30-01). Each of these laser diode arrays nominally emits $P = 30\,\text{W}$ of laser light at $\lambda_{\text{pump}} = 808\,\text{nm}$. As the slave laser thermal design is optimised for lesser input power the laser diode arrays are driven at a pump current that leads to an emission of $P = 17\,\text{W}$ each, i.e. a total pump power of $P_{\text{pump}} = 34\,\text{W}$ at $\lambda_{\text{pump}} = 808\,\text{nm}$. By reducing the pump current the lifetime of the laser diode arrays is significantly increased.

The emitters of the pump modules are fibre-coupled by 19 individual thin fibres (numerical aperture NA=0.12) in a concentric setup. This leads to a pump spot intensity distribution with a cylindrical envelope, though in detail it consists of 19 individual pump spots with very high intensity, leading to 19 strongly pumped areas in the laser crystal. This does not pose a problem as long as the thermal processes in the crystal remain in the linear regime (Zawischa 2003). Failure of individual emitters leads to a highly inhomogeneous pump spot, though, which causes a degradation of laser intensity.

The resulting fibre bundle with a diameter of $d = 1.16\,\text{mm}$ has a robust metal jacketing. The light from the fibre-bundle is coupled into the slave laser resonator by an optical telescope as shown in figure 3.3.

Pumping scheme of the 'new' slave laser design

The pump laser diode arrays from OptoPower / Spectra-Physics Semiconductor Lasers have three major drawbacks: They are very expensive, failure of one array massively changes the pump profile, and they are meanwhile obsolete. For this reason an alternative pump source was sought, if possible with very little modifications necessary in the pumping scheme. For laser diode arrays by Dilas the mounting plate and heat sink for the laser diode

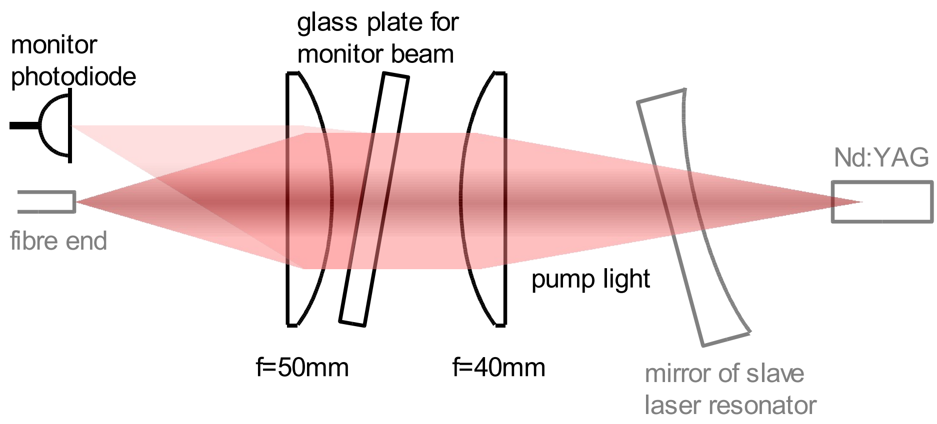

Figure 3.3: Optical telescope of the old slave laser pump optics.

packages could be adapted with moderate effort. The pumping scheme, however, had to be changed because the individual emitters of the Dilas laser diode array are fibre-coupled together in one large core diameter fibre ($d = 400\,\mu$m), which results in a different numerical aperture of the fibre (NA=0.22) as opposed to the old design. As changing the pump optics would have meant dismanteling the complete slave laser base plate and thereby losing the position of the laser on the optical table, the optics were exchanged using Owis tubes for mounting purposes. With this technique an extra lens could be incorporated in the design without the need to remove the laser box from the optical table for machining. The new pumping scheme is shown in figure 3.4. These modifications have two major disadvantages, though: For one the modified design with the Owis mounting tubes is mechanically not as stable as the old design due to the long lever arm. This is partly remedied by placing a post underneath the end of the tube as a support. Besides that, the tube cuts off the monitor beam coming from the glass plate, which therefore does not reach the monitor photodiode any more. For this reason the glass plate was omitted and the pump power can now not be monitored easily. In a redesign of the complete pump optic this problem can be solved.

The intensity profile behind the multi-mode fibre does not resemble the desired flat top pump profile, but has a strong radial dependency. This is remedied by twisting the metal jacketed fibre into two loops with a radius of curvature of $d = 40$ mm, which leads to mode scrambling and produces a nearly homogeneous pump intensity distribution across the diameter of the fibre.

For more detailed information on the design of the slave laser please refer to (Zawischa 2003).

3.2.3. The lab laser system

The injection locked 12 W laser system in the laser lab in Hannover serves two distinct purposes: It is a test and reference system for the laser system in GEO 600, where new stabilisation concepts are implemented and tested, but it is also a 'living donor' for any

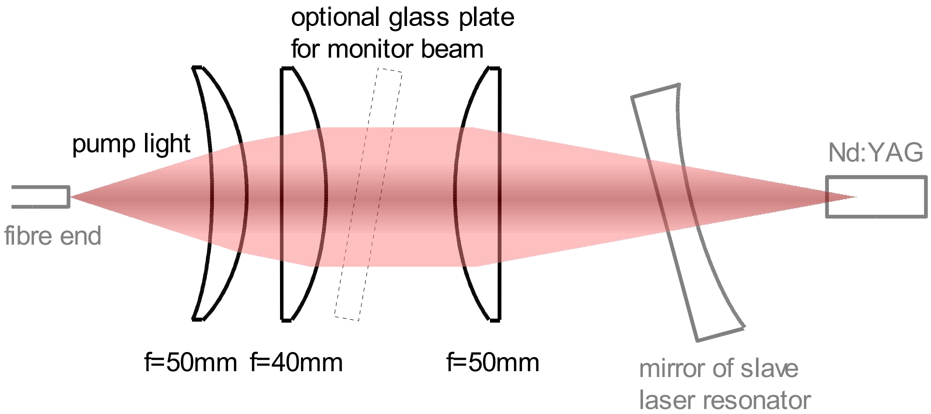

Figure 3.4: Optical telescope of the new slave laser pump optics. The optional glass plate is not implemented in the current slave lasers (neither in GEO 600 nor in the lab system).

parts that need to be replaced in the GEO 600 system. With these two functions it plays a very important role. The laser system in GEO 600 was first completed and then long-term tested over the stretch of a year before it was considered safe to be installed at the site of the gravitational wave detector.

A photograph of the optical setup of the 12 W lab laser system can be seen in figure 3.5. The light emitted by the master laser first passes a combination consisting of a quarter-wave plate and a half-wave plate: The quarter-wave plate eliminates any ellipticity of the polarisation of the laser beam, the half-wave plate turns the linear polarisation to the designated orientation. Then the master laser beam passes a broadband electro-optic modulator (an actuator for fast frequency tuning, which is not used in the following). The light power is then variably split up by a combination of half-wave plate and polarising beam splitter. A small fraction of the light ($P \approx 30\,\mathrm{mW}$) is sent to the reference cavity for frequency stabilisation (see section 3.4.1). The main beam passes a resonant electro-optic modulator, which imprints phase-modulation sidebands at $\Omega = 12\,\mathrm{MHz}$. This modulation is needed for injection locking of the system. Modematching lenses form the beam to comply with the slave laser resonator geometry, i.e. the Gaussian laser beam is transformed by lenses so that the imaged NPRO waist coincides with the slave laser resonator eigen mode. Optimal *modematching* is very important to obtain a stable injection lock of the system.

The NPRO beam enters the slave laser cavity through one of the plane mirrors, which also serves as the output port. The NPRO light circulates in the slave laser and is amplified by the gain of the active medium, as described in section 2.6, when the NPRO frequency lies in the locking range of the slave laser. According to equation 2.19 the locking range of the 12 W laser system is approximately $\Delta\omega_{\mathrm{lock}} \approx 1.6\,\mathrm{MHz}$. In this range the slave laser frequency is locked to the master laser frequency; the resulting 12 W beam leaves the resonator at the output port.

The first optic behind the slave laser is a high reflector for $\lambda = 1064\,\mathrm{nm}$, which serves as a beam steering mirror; it is used approximately under the specified angle of 45°. Any possibly remaining pump light is already eliminated in the slave laser box, as the output

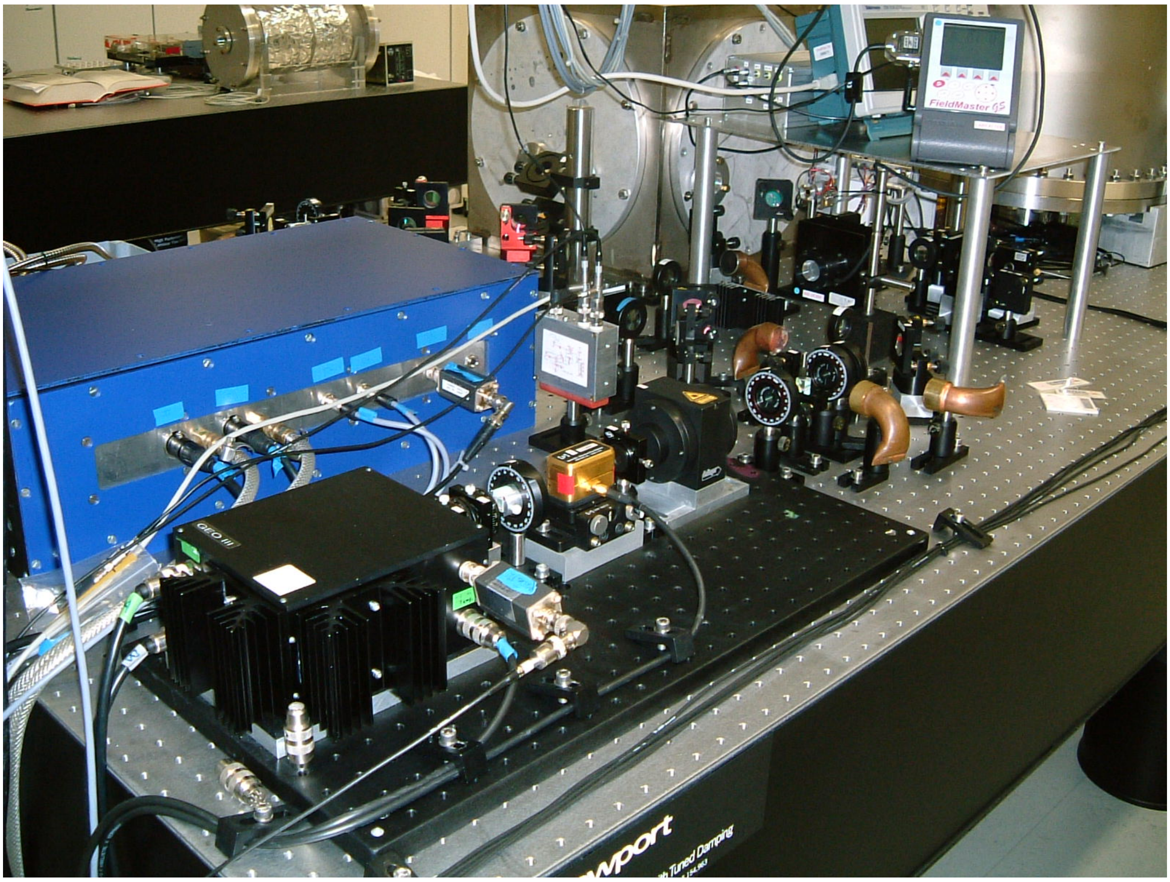

Figure 3.5: Photograph of the optical setup of the lab laser system.

windows are highly reflective for $\lambda = 808\,\text{nm}$. The small fraction of light at $\lambda = 1064\,\text{nm}$ which is transmitted by the beam steering mirror ($P < 10\,\text{mW}$) is used for the injection lock loop (see section 3.3).

The beam of the injection locked system then passes a first Glan-Laser-prism from Leysop, which eliminates any remaining parasitic s-polarisation of the beam with an extinction of up to 10^{-6} (strongly depending on the quality of the optical alignment). This parasitic polarisation is caused by uncompensated thermally induced birefringence in the slave laser and has a characteristic ‘clover leaf’ form. Its content in the injection locked beam is about 1 %.

The various following attenuation combinations consisting of half-wave plates and Glan-Laser-prisms are used to extract beams of varying intensities for diagnostics or stabilisation purposes. At last the (attenuated) high power laser beam is coupled into a pre-mode cleaner (see section 4.4.2) , which is located in a cubic vacuum tank. The pre-mode cleaner is used to fix the laser beam position firmly with respect to the table surface. As a consequence, any beam position or geometry fluctuations before the pre-mode cleaner are obviously transformed into intensity flutuations behind it. Right behind the pre-mode cleaner the light is split into two beams by a power beam splitter. The two beams individually hit a high power photodetector; one is used as an in-loop detector for intensity stabilisation (section 3.5), the other is the independent out-of-loop detector for intensity noise.

3.2.4. The laser system at the site of GEO 600

Much of the optical setup of the GEO 600 laser system at the site (of which a photograph is shown in figure 3.6) is equivalent to that in the laser lab. I will therefore focus on the differences:

As above, the master laser beam is corrected in ellipticity and polarisation orientation by a combination of quarter-wave plate and half-wave plate, before passing a broadband electro-optic modulator from New Focus for fast actuation. As the suspended mode cleaners are the best possible frequency reference for frequency stabilisation of the laser system for frequencies above 50 Hz, no reference cavity is needed, though one exists at the site (it was used before the setup of the mode cleaners). Due to the optical setup not the master laser beam is detected for frequency stabilisation (see section 3.4.2) , but instead a fraction of the complete injection locked beam. Feedback of the frequency stabilisation loop is applied to the master laser frequency actuators, though. This is legitimate, since the frequency noise budget of the laser system in injection lock is dominated by the master laser.

The attenuation optics at GEO 600 is the same as that of the lab system, as is the mode-matching optics with adapted parameters.

The intensity stabilisation of the laser system at GEO 600 is accomplished in two stages: The laser system is pre-stabilised before entering the suspended mode cleaners (this first active stage is described in detail in section 3.5.2). Then the laser intensity noise behind the second suspended mode cleaner is measured and the intensity is stabilised by feeding back a signal into the error point of the first power stabilization loop to obtain low intensity noise characteristics of the light entering the Michelson interferometer (this second intensity stabilisation loop is described in section 3.5.3).

For the first intensity stabilisation loop a pick-off beam of the injection locked laser is detected shortly before the beam enters the first suspended mode cleaner; the position of the in-loop and out-of-loop detector are indicated in figure 3.6.

3.3. Injection locking of the laser systems

Both high power lasers, the lab system as well as the system in GEO 600, are injection locked laser systems. The light of a high stability master laser is coupled into the cavity of a high power slave laser with less stringent stability requirements, in effect forming a high power, high stability system which emits unidirectionally. The technique of injection locking is described in section 2.6, a more rigorous analysis can be found in (Siegman 1986).

The lab laser system as well as the laser system in GEO 600 both employ the same injection locking electronics. The implemented version is documented in appendix B. Especially the autolock electronics is a major asset and leads to relocking times on the order of $t < 100\,\mathrm{ms}$.

The light from the master laser passes a resonant electro-optic modulator (from New Focus) which imprints phase modulation sidebands at $\Omega = 12\,\mathrm{MHz}$. It is then modematched into the slave laser cavity by a set of lenses. Intuitively injection locking can be understood

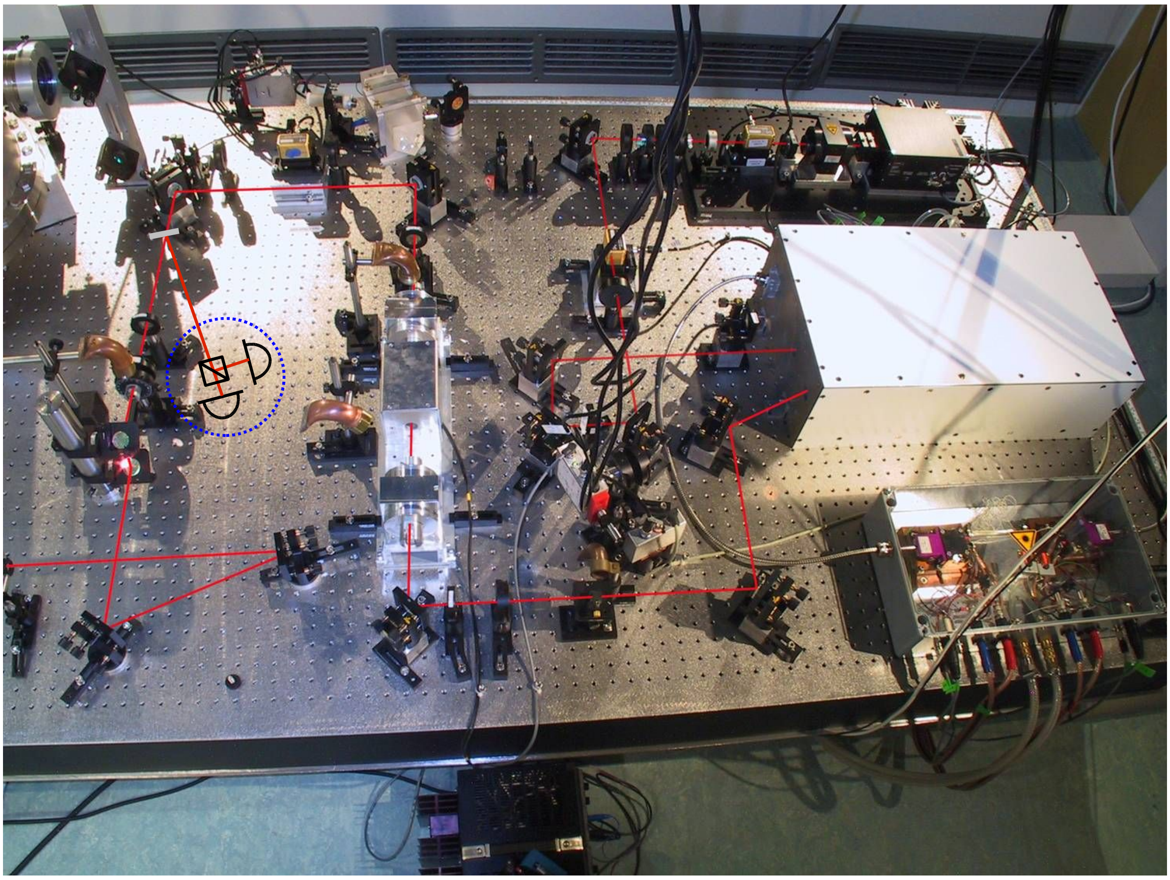

Figure 3.6: Photograph of the optical setup of the laser system at the site of GEO 600. The beam path is shown in red. The dashed blue circle indicates the position of the photodetectors for intensity stabilisation behind the wedged pick-off plate (in grey) shortly before the attenuated beam enters the first mode cleaner.

as a Pound-Drever-Hall-locking scheme used on a 'hot' (i.e. laser) cavity. The sidebands of the master laser light are directly reflected[1] from the slave laser and impinge on a photodetector together with the light leaking back out of the slave laser cavity. As the high output power of the system would destroy any photodiode in its direct light the injection locking photodetector stands behind the first high reflective beam steering mirror after the slave laser output coupler. The light transmitted through this mirror ($P \approx 10\,\mathrm{mW}$) is sufficient for a stable injection lock.

When the laser system is not injection locked the slave laser switches its emission direction with a typical frequency of 10 kHz (Zawischa 2003). Light from the slave laser going back to the master laser might cause damage to the master laser pump diodes, besides causing the noise eater electronics (appendix A) to oscillate. Therefore back reflexes into the master laser have to be avoided, which is accomplished by a Faraday isolator. Through

[1]The bandwidth of the cold slave laser cavity is $\Delta\omega_{\mathrm{cold}} \approx 10\,\mathrm{MHz}$. For the hot cavity the bandwidth is even smaller, therefore the phase-modulation sidebands are indeed directly reflected.

the technique of injection locking the superior frequency noise characteristics of the master laser are transferred to the slave laser. The intensity noise of the system, however, is dominated by the slave laser; therefore an active intensity stabilisation of the injection locked system is needed (see section 3.5).

3.4. Frequency stabilisation of the laser systems

The required frequency stability of the light source for GEO 600 lies at a level of $LSD = 2 \cdot 10^{-4}\,\mathrm{Hz}/\sqrt{\mathrm{Hz}}$ for detection frequencies from $f = 10\,\mathrm{Hz}$ to $f = 100\,\mathrm{Hz}$ (Willke et al. 2000a), whereas the unstabilised system shows frequency noise of $LSD \approx 1\,\mathrm{kHz}/\sqrt{\mathrm{Hz}}$ at $f = 1\,\mathrm{Hz}$ and has a spectrum which falls as 1/f. The spectrum is dominated by the free-running NPRO frequency noise, when the system is injection locked (as shown in section 2.6).

As mentioned above, frequency stabilisation of the injection locked 12 W laser system is realised differently for lab and GEO system, due to differences in the infrastructure. The frequency stabilisations of both systems are therefore treated individually, with an emphasis on the specially devised control electronics in the description of the lab laser system in section 3.4.1. The locking scheme to the system of suspended optical reference cavities in GEO 600 is described section 3.4.2. The frequency noise requirements are in both cases identical.

3.4.1. Frequency stabilisation of the master laser to the reference cavity by means of a multi-purpose control electronics in the laser lab

In the injection locked laser system the total frequency noise of the system is dominated by the frequency noise characteristics of the master laser, as explained in section 2.6. To fulfil the requirements of GEO 600 it is therefore necessary to stabilise the frequency of the (already inherently low noise) master laser. As the high power lab laser system can not use the suspended mode cleaners that serve as a frequency reference for the GEO laser system, a rigid ultra-high finesse reference cavity (section 4.4.2) is used instead. The master laser is frequency stabilised to the reference cavity by the Pound-Drever-Hall-technique (section 2.4.1). Feedback can be applied to the piezo-electric actuator contacted to the NPRO crystal for fast actuation and to the crystal temperature for slow drifts. Alternatively the current lock technique can be used by applying feedback to the drive current of the master laser pump diodes. A crossover network splits the feedback signal at $f \approx 500\,\mathrm{Hz}$ if the pump current is actuated; the low frequency signal goes to the master laser driver, the high frequency signal is fed to the noise eater electronics. The experimental setup for frequency stabilisation of the injection locked lab laser system can be seen in figure 3.7. The frequency stabilisation electronics ('Universalservo') designed in the scope of this thesis is shown in appendix B.

3.4.2. The frequency stabilisation scheme of the laser system in GEO 600

The mode cleaners in GEO 600 are ring resonators suspended as double pendulums (Gossler 2004). As their pendulum resonances lie below $f = 50\,\mathrm{Hz}$ they can be used as an excellent frequency reference for the frequency band above. The rigid reference cavity used in the laser lab is therefore not necessary for frequency stabilisation in GEO 600, the alternative

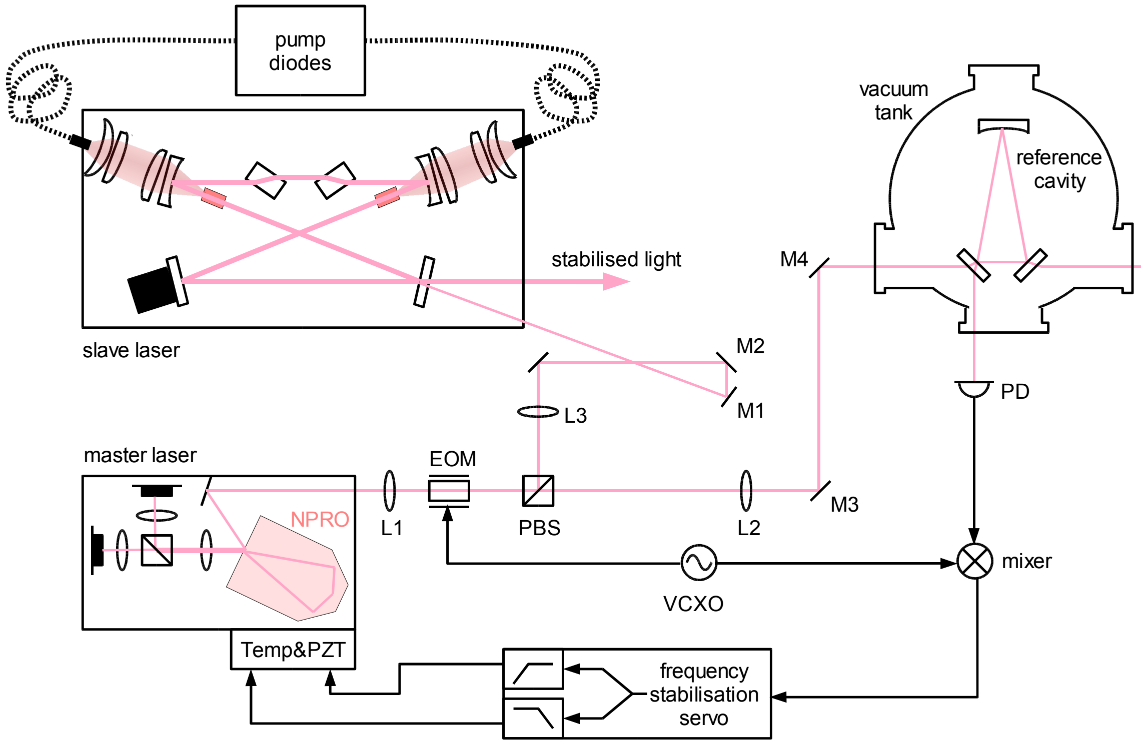

Figure 3.7: Experimental setup of the frequency stabilisation scheme for the injection locked lab laser system. Approx. $P = 30\,\text{mW}$ of NPRO light are modematched into the reference cavity in high vacuum ($p = 10^{-9}$ mbar). The major fraction of the NPRO light ($P \approx 500\,\text{mW}$) is coupled into the slave laser cavity for injection locking. The lenses L_i transform the NPRO beam parameters into those of the cavity eigen mode; optimal alignment of the laser modes is achieved by 'beamwalking' with the mirrors M1 and M2 (for the slave laser cavity) respectively M3 and M4 (for the reference cavity). The frequency stabilised light leaving the slave laser can be put to further use.

frequency stabilisation scheme is shown in figure 3.8: The laser system is injection locked as described in section 3.3. The light from the high power system enters the first mode cleaner (MC1); to achieve this the laser system must be made resonant with the suspended cavity by feedback to the actuators of the master laser[2]. The light then passes the second mode cleaner (MC2) by stabilising the frequency of the so-far locked system (laser system to MC1) to the resonance frequency of MC2. For this task feedback is applied to the length of MC1 (for frequencies below 50 Hz) respectively fed into the error point of the first loop (for frequencies above 50 Hz). The power recycling cavity with a length of 1200 m is then used as the actual frequency reference by locking the length of MC2 to it for frequencies below 50 Hz and actuating a fast broadband EOM for higher frequencies. The achieved frequency stability of the GEO 600 laser system is documented in (Freise 2003).

[2]In injection lock the frequency noise of the injection locked system is dominated by that of the master laser.

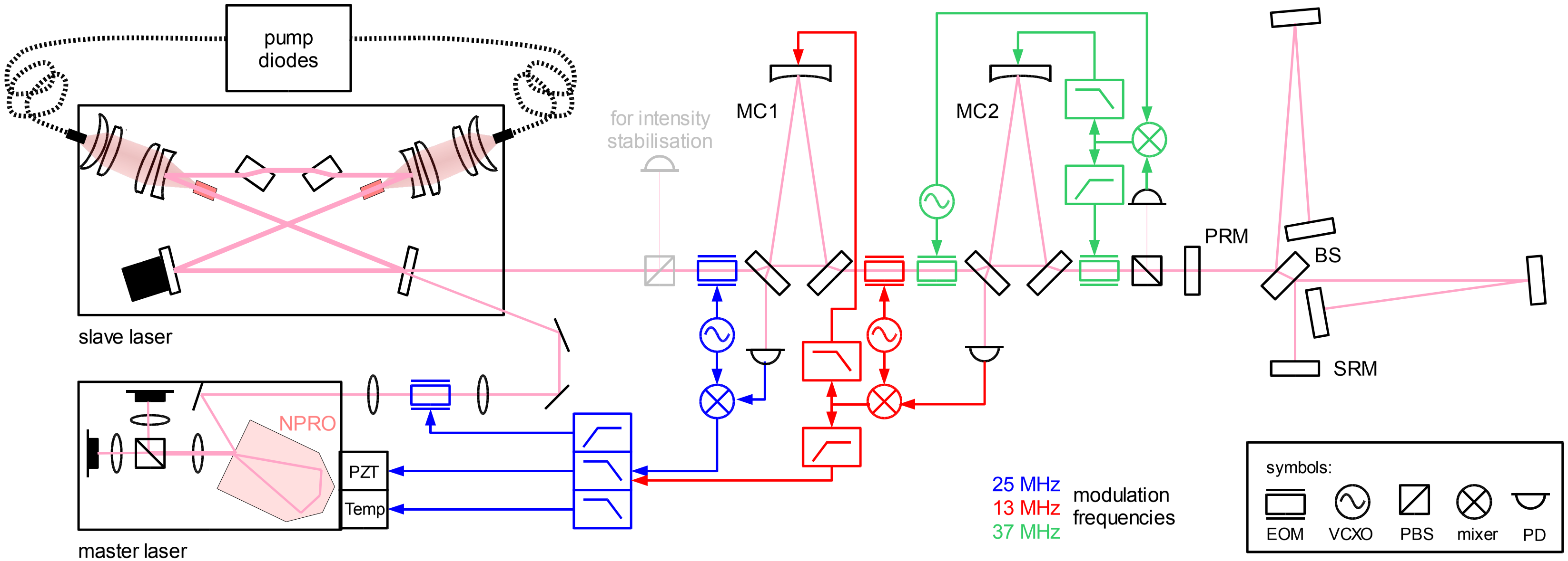

Figure 3.8: Experimental setup of the frequency stabilisation scheme for the injection locked laser system in GEO 600. The light of the injection locked system is coupled into the first mode cleaner (MC1). To make the system resonant with MC1 a feedback signal is applied to the NPRO piezo-electric transducer and temperature (for slow changes) and to a broadband EOM (for fast changes), shown in blue. To couple the light through MC2 the length of MC1 is stabilised to MC2 (for low frequencies by feedback to the the length control of MC1; for high frequencies feedback is applied to the actuators of the master laser, loop shown in red). The system is then stabilised to the power recycling cavity (green loop) by feedback to a broadband EOM for high frequency changes and to MC2 for low frequencies.

3.5. Intensity stabilisation of the laser systems

As mentioned in section 2.3.3 the sensitivity of interferometric gravitational wave detectors is limited by the shot noise of their light sources. Technical noise becomes an issue, though, if the intensity noise surpasses a certain limit (in the case of GEO 600 relative intensity noise of $RIN = 10^{-8}/\sqrt{\text{Hz}}$ is tolerable). The intensity noise then causes excess radiation pressure noise at the beam splitter. The existing first generation gravitational wave detectors reduce the intensity fluctuations by different techniques; the scheme employed in GEO 600 was realised in this work and is subject of this section.

GEO 600 consists of various subsystems which have to work together and function as an entity. Due to the need for this relative modularity of GEO 600 it is sensible to ask for a pre-stabilised laser output at a defined interface. In the case of the intensity noise level this point is directly in front of the first mode cleaner. At this point the required intensity stability of the injection locked laser system is $RIN = 10^{-5}/\sqrt{\text{Hz}}$ at $f = 10\,\text{Hz}$, $RIN = 10^{-6}/\sqrt{\text{Hz}}$ from $f = 100\,\text{Hz}$ to $f = 2\,\text{kHz}$ and may rise with f for higher frequencies (Brozek 1999). To satisfactorily reach the specifications at the input of the first mode cleaner an intensity noise level of $RIN = 10^{-7}/\sqrt{\text{Hz}}$ from $f = 1\,\text{Hz}$ to $f = 10\,\text{kHz}$ was aimed at. In April 2000 calculations showed that the necessary minimisation of radiation pressure noise at the beam splitter of the Michelson interferometer called for a relative intensity noise of $RIN = 10^{-8}/\sqrt{\text{Hz}}$ (Winkler 2002). To achieve this goal the first intensity stabilisation loop was designed, described in section 3.5.2. Beam geometry fluctuations of the beam entering the first mode cleaner, however, unfortunately lead to the introduction of intensity noise in the output of the mode cleaners. Still the interferometer needs light power with a very low intensity noise level, which is why a second intensity stabilisation loop stabilises the light intensity after the second mode cleaner. This is described in section 3.5.3.

3.5.1. Intensity noise characteristics of the slave laser

The frequency noise budget of the injection locked laser system is governed by the frequency noise characteristics of the master laser. The intensity noise, however, is determined by the slave laser, since it contributes the major part of the output power. The free-running slave laser shows an intensity noise spectrum as in figure 3.9. The intensity noise requirements for the laser system at the mode cleaner input are plotted in the intensity noise spectrum of figure 3.9.

The transfer function of the slave laser (from the drive current of the slave laser pump diodes to the slave laser output power) was measured and is shown in figure 3.10.

The designated intensity actuator for the slave laser is the drive current of one of its pump laser diodes. Direct actuation via a control input of the drive electronics is not possible due to its limited bandwidth. A modulation input, parallel to the current driver, was therefore constructed directly on the diode box. By means of this modulation input the drive current of slave laser pump diode A can be actuated.

3.5.2. First stage: Stabilising the laser intensity before the first mode cleaner

The first intensity stabilisation loop is supposed to reduce the intensity noise of the injection locked laser system to a level of $RIN = 10^{-8}/\sqrt{\text{Hz}}$ before the light enters the first mode

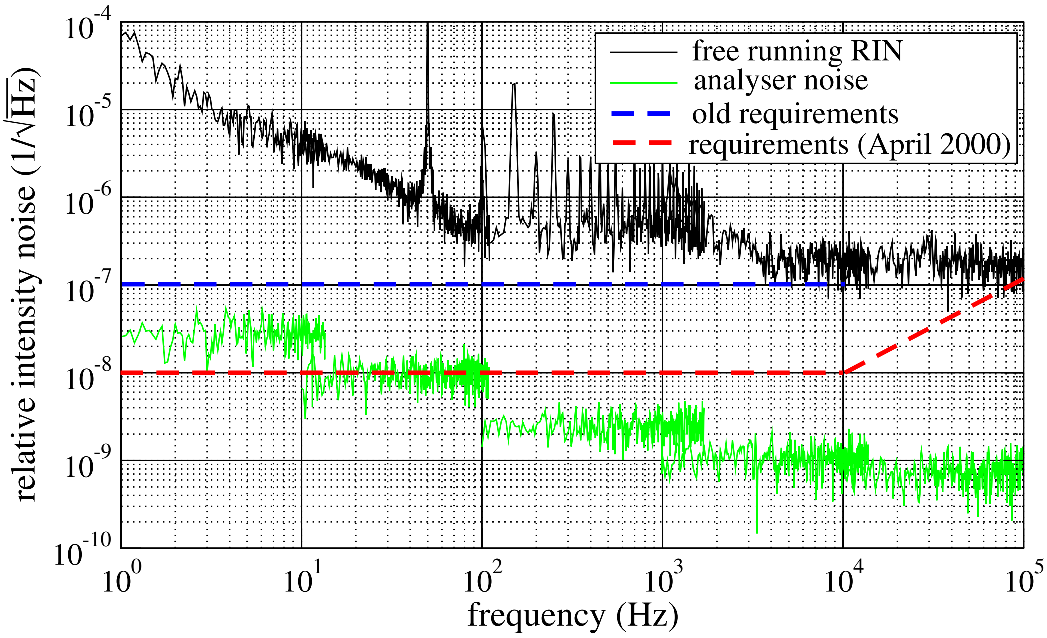

Figure 3.9: Intensity noise of the injection locked laser system (shown in black) without any intensity stabilisation. The blue dashed line shows the intensity noise requirements before April 2000, the red dashed line marks the current requirements for intensity stabilisation. Analyser noise is shown in green.

cleaner. For the lab laser system this is even the final requirement. To reach this level of intensity stability an open loop gain of the control electronics as shown in figure 3.11 is needed. The figure shows the actual measured open loop transfer function of the designed control electronics for the first intensity stabilisation loop.

The slave laser contributes its gain to the designed control loop. The required open loop gain of the designed intensity stabilisation control electronics is therefore determined by the difference between the free running intensity noise and the intensity noise requirements minus the gain contributed by the plant (the rest of the loop). Implementation of the designed intensity stabilisation results in an in-loop intensity noise reduction as shown in figure 3.12. The difference between free-running and in-loop intensity noise is determined by the open loop gain of the complete system.

The light of the injection locked laser system is detected after several attenuators behind the output port of the slave laser. This fraction of the light is divided into two beams of equal power by a power beam splitter. The in-loop and the out-of-loop photodetector are placed in transmission respectively reflection of the beam splitter, lenses are used for focussing and fine alignment. The non-common beam paths in free space between the photodetectors is thereby minimised. The measurement made with the out-of-loop photodetector is shown in figure 3.13.

There is a strong difference between the in-loop and the out-of-loop intensity noise measurement. The out-of-loop intensity noise reduction is obviously not limited by the gain of the control electronics (which is mirrored in the in-loop reduction). The intensity noise

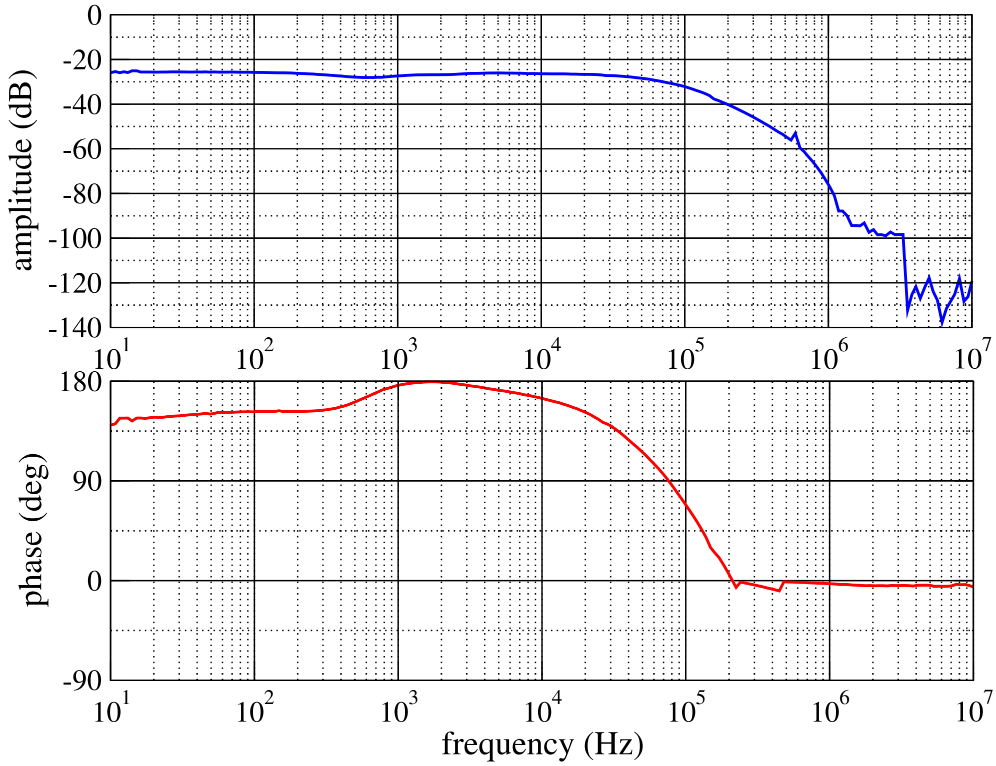

Figure 3.10: Transfer function from the drive current of the slave laser pump diodes to the slave laser output power. It shows a lowpass at approx. $f = 50\,\text{kHz}$ (which is due to the life time of the upper laser level) and a second lowpass at $f = 2\,\text{MHz}$ (caused by the limited bandwidth of the electronics).

rises as $1/f$ for frequencies below 100 Hz. This low frequency increase in intensity noise is an example of flicker noise. The discrepancy between the two measurements is primarily caused by the following mechanisms:

- Air currents in the non-common beam paths give rise to variations of the index of refraction of air and thereby cause different intensity variations in the two paths.
- The responsivities of the photodiodes are inhomogeneous, i.e. they vary spatially and differ from photodiode to photodiode. Intensity noise is therefore feigned when a pointing laser beam impinges on an inhomogeneous photodiode. If this is the in-loop photodiode, then the laser intensity is stabilised such as to minimise the intensity noise on this photodiode. But this means that noise is introduced in the loop, since a different photodiode (the out-of-loop photodiode) will now detect a higher level of intensity noise.

To minimise the effect of the non-common beam paths the detection scheme including the two photodetectors was placed in a vacuum tank ($p \approx 10^{-3}$ mbar). The same measurements were conducted and the results of the in-loop and the out-of-loop measurements can be seen in figure 3.14.

It is clearly visible that the discrepancy between in- and out-of-loop measurement is largely reduced, but does not vanish for detection frequencies below $f = 100\,\mathrm{Hz}$. Polarisation dependences of the power beam splitter and etalon effects in the photodiode window were eliminated as possible causes for this difference. In all likelyhood the discrepancy is caused by the dark noise in the photodiodes which shows a 1/f characteristic when illuminated with a white light source (He et al. 1990).

The achieved out-of-loop intensity stability fulfils the requirements given in section 3.5.1. For the intensity stabilisation in GEO 600 a second loop is needed to stabilise the light behind the second mode cleaner; this is described in the following section.

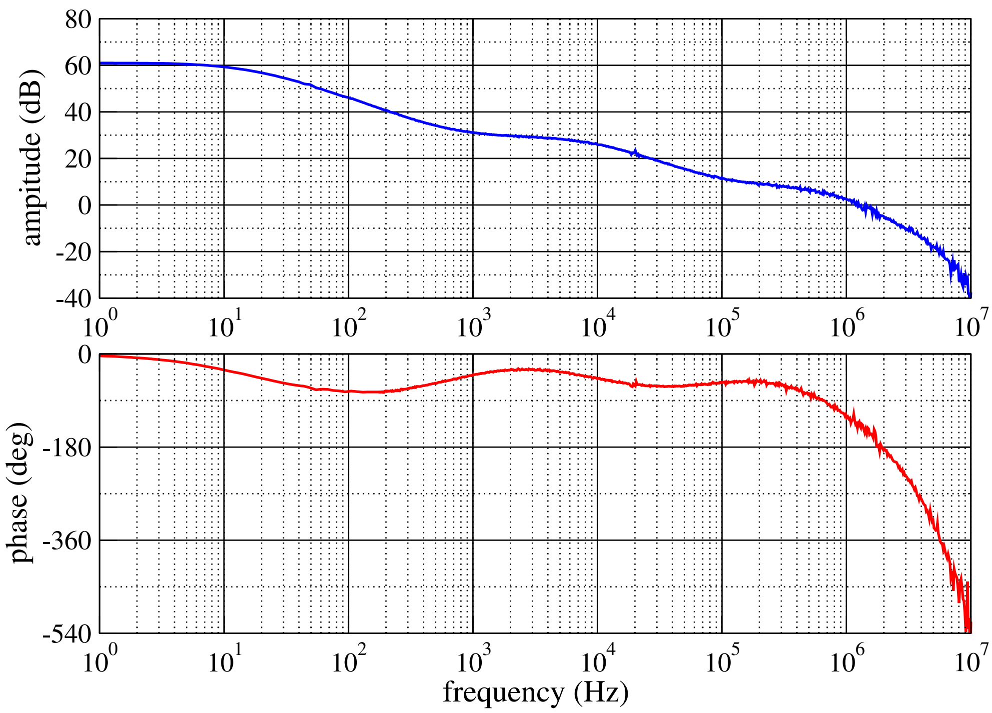

Figure 3.11: Open loop transfer function of the intensity stabilisation electronics (first loop) for the slave laser.

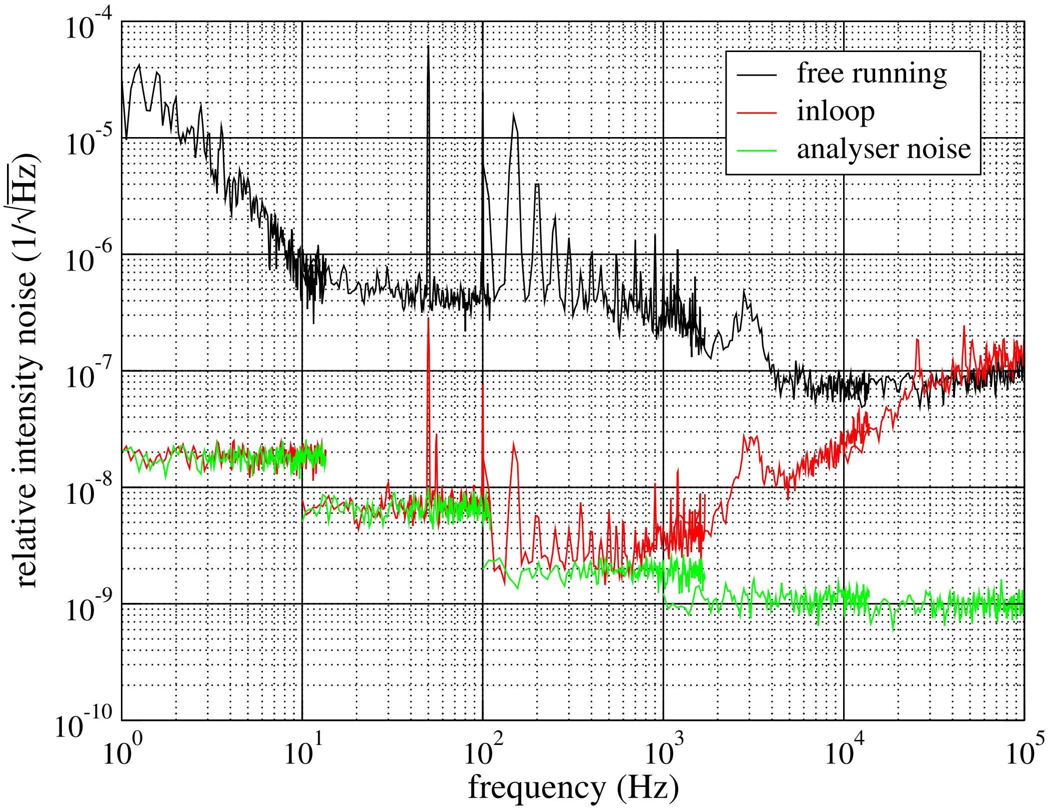

Figure 3.12: In-loop intensity noise (red, middle graph) of the injection locked laser system with active intensity stabilisation (first loop). The detection sensitivity is limited by the analyser noise (in green, lower graph). The free running intensity noise level is shown in black (upper graph).

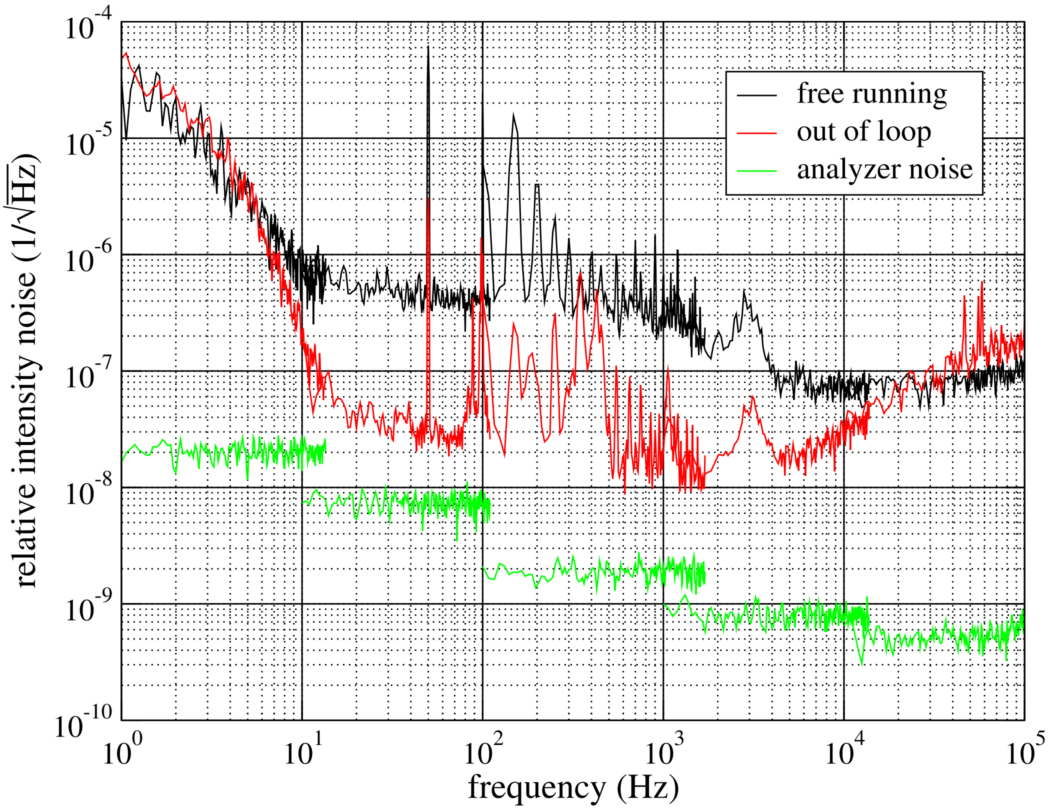

Figure 3.13: Out-of-loop intensity noise (red, middle graph) of the injection locked laser system with active intensity stabilisation (first loop). In the frequency band from 1 to 10 kHz a relative intensity noise level of $RIN = 2 \cdot 10^{-8} / \sqrt{\text{Hz}}$ is achieved. The structure at $f = 3\,\text{kHz}$ is caused by a resonance of the master laser driver. Unity gain of the intensity stabilisation loop is approx. $f_{\text{UG}} = 20\,\text{kHz}$. The free running intensity noise level is shown in black (upper graph), analyser noise is shown in green (lower graph). The out-of-loop reduction in intensity noise is smaller than the loop gain would suggest. This is caused by noise coupling into the non-common beam paths between the in-loop and the out-of-loop detector; this is described in more detail in the text.

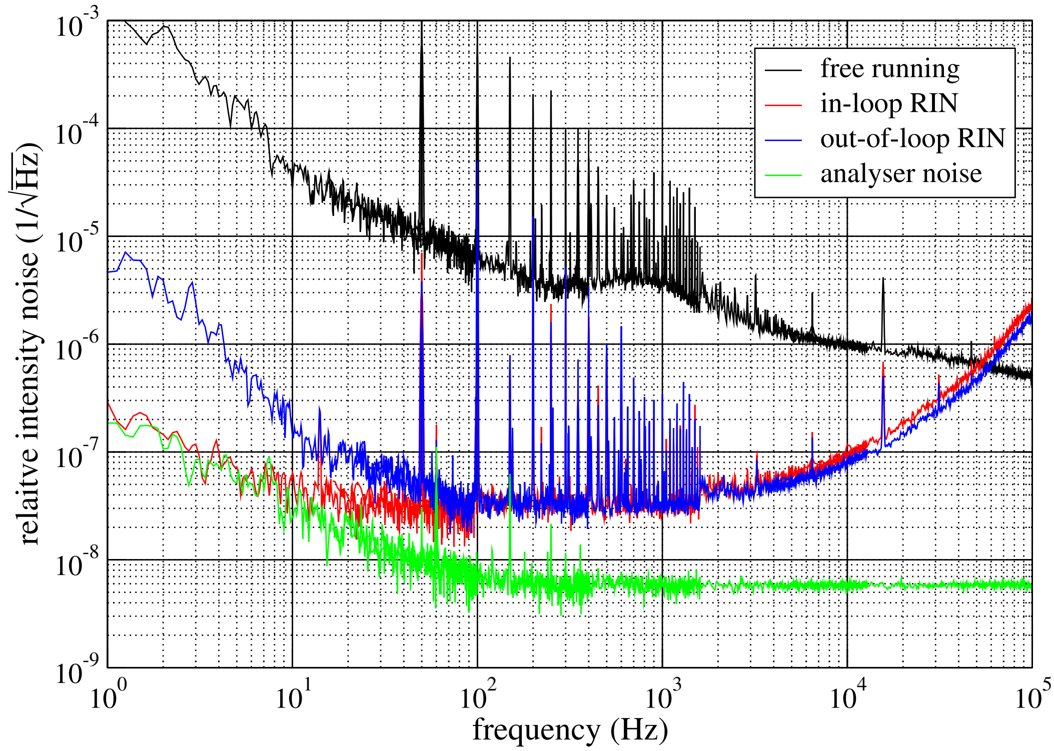

Figure 3.14: In-loop (red, lower middle graph) and out-of-loop (blue, upper middle graph) intensity noise of the injection locked laser system with active intensity stabilisation(first loop), detection scheme in vacuum. The free running intensity noise is shown in black, upper graph, the detection noise in green, lower graph.

3.5.3. Second stage: Stabilising the laser intensity after the second mode cleaner

The intensity stabilisation of the injection locked laser system is not completed with the first loop. The pre-stabilised laser light enters the first suspended mode cleaner and any beam geometry fluctuations of the light relative to the cavity eigen mode is transformed into intensity noise behind the mode cleaner. High intensity stability is needed at the beam splitter of the Michelson interferometer, though [3]. This calls for a second intensity stabilisation loop which detects the light behind the second mode cleaner and feeds back to the slave laser to stabilise the laser intensity directly before it enters the main interferometer.

The optical setup of the second loop is shown in figure 3.15. The light is detected at the output port of the second mode cleaner and the signal of the second intensity stabilisation servo is fed into the error point of the first loop. The designed control electronics is shown in appendix B.

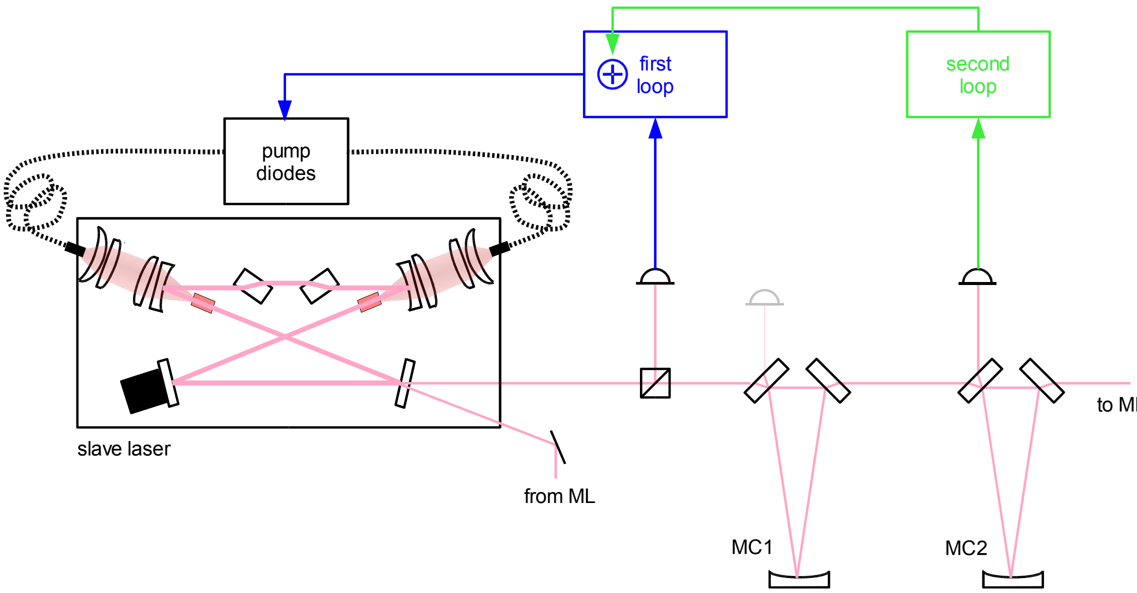

Figure 3.15: Schematic of complete intensity stabilisation scheme employed for the injection locked laser system at GEO 600. For the first intensity stabilisation loop the light is detected before it enters MC1, the signal is fed back to the pump current of laser diode A of the slave laser. The light for the second intensity stabilisation loop is detected at the output of the second mode cleaner, the control signal is fed into the error point of the first intensity stabilisation loop.

The resulting in-loop intensity noise is shown in figure 3.16. It corresponds to the designed open loop transfer function of the second loop. The out-of-loop intensity noise, measured with an independent photodetector, is given in figure 3.17. It is a more realistic measure of the relevant intensity noise at the beam splitter.

[3] Calculations show (Winkler 2002) that a relative intensity noise of $RIN = 10^{-8}/\sqrt{\text{Hz}}$ is tolerable if radiation pressure at the beam splitter is not to become an issue.

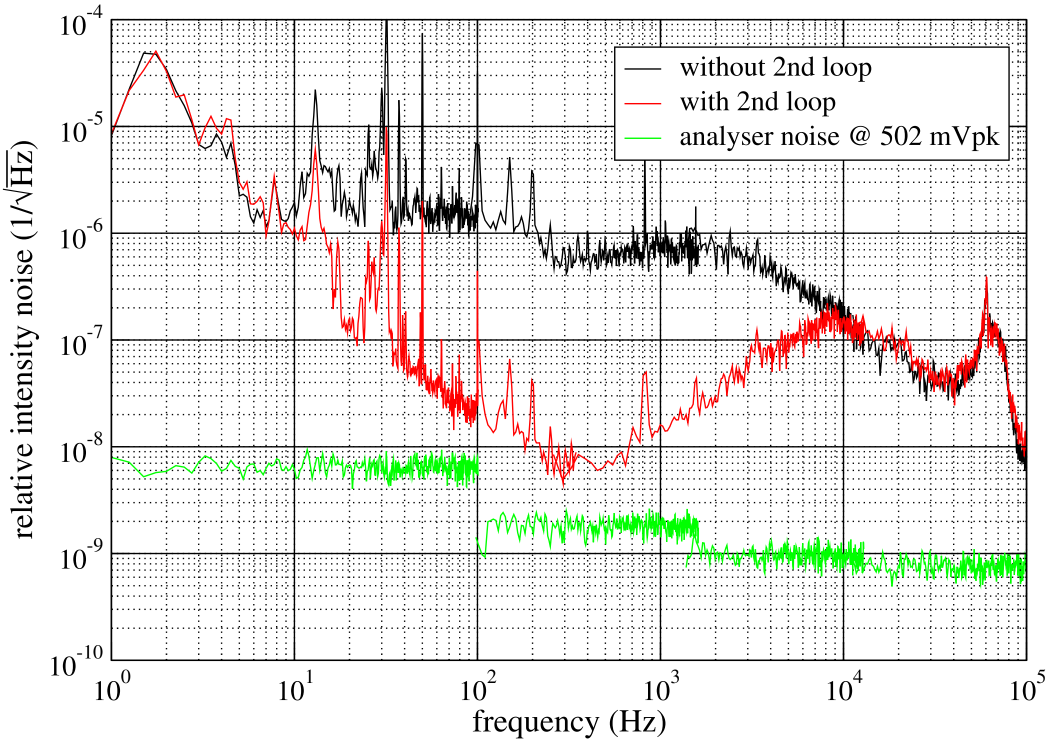

Figure 3.16: In-loop intensity noise of the injection locked laser system for GEO 600, measured behind MC2, with (in red, middle graph) and without (in black, upper graph) active second loop of the intensity stabilisation. The analyser noise is plotted in green (lower graph).

Feeding back the signal from the second loop into the error point of the first loop obviously has an effect on the intensity noise measured in front of the first mode cleaner. Figure 3.18 shows that the intensity noise before the first mode cleaner is significantly increased by the second intensity stabilisation loop. Nevertheless the first loop is used, as it enhances the dynamic range of the second loop.

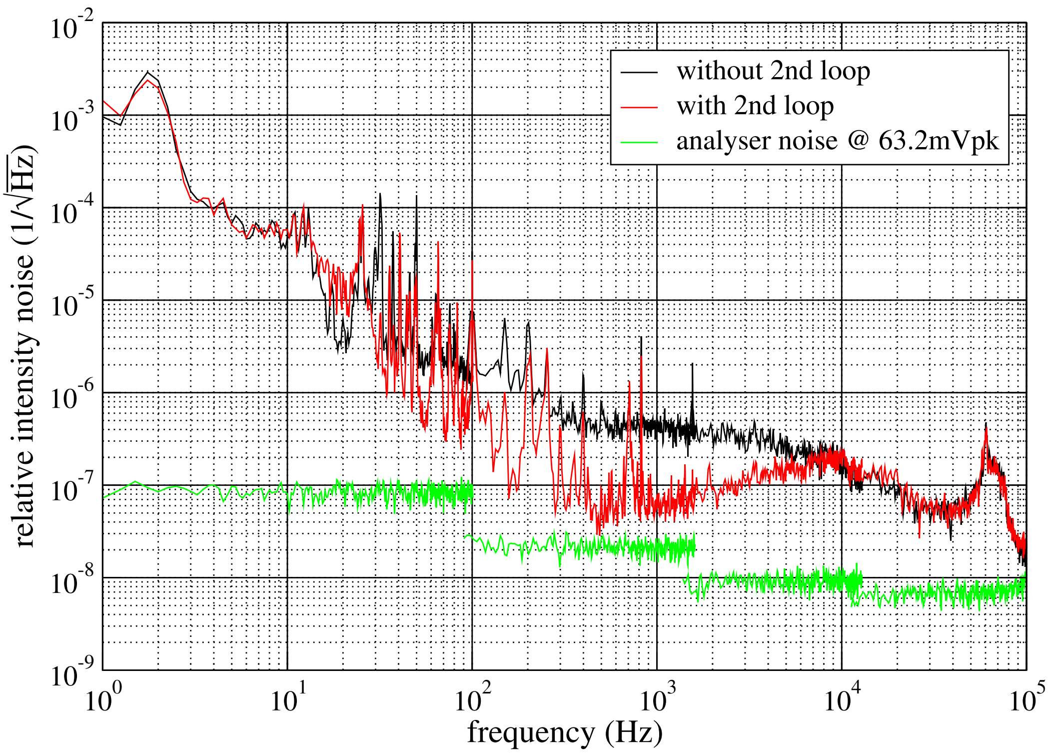

Figure 3.17: Out-of-loop intensity noise of the injection locked laser system for GEO 600, measured behind MC2, with (in red, middle graph) and without (in black, upper graph) active second loop of the intensity stabilisation.

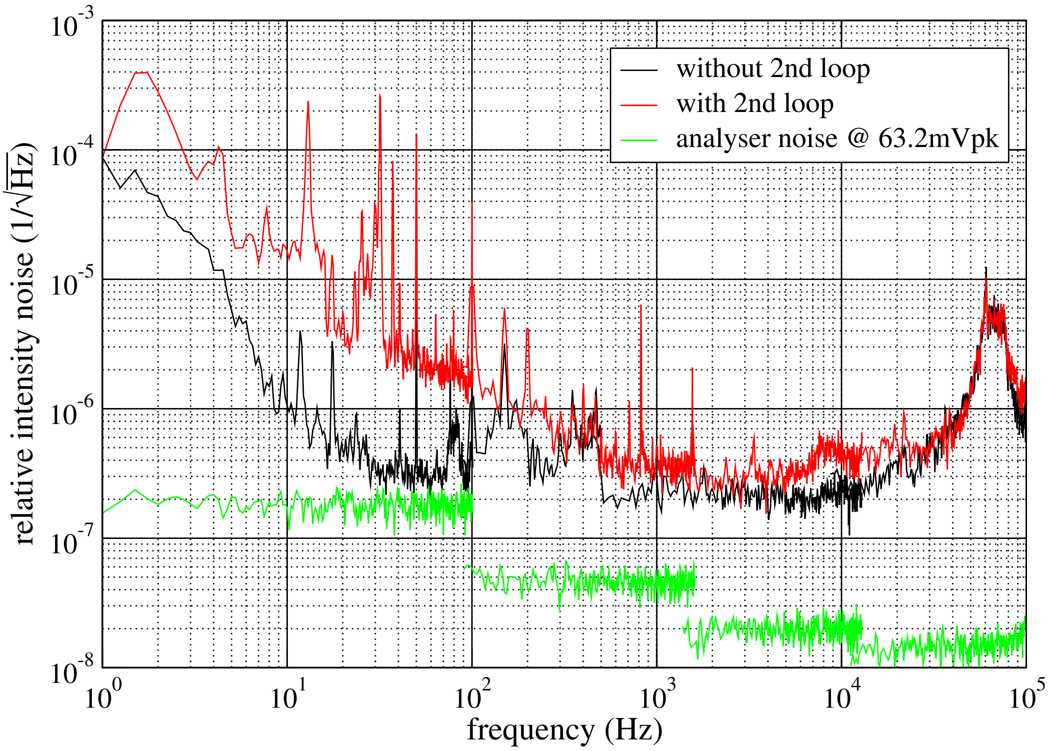

Figure 3.18: Intensity noise of the injection locked laser system in front of MC1 with (in red, upper graph) and without (in black, middle graph) active second intensity stabilisation loop (in both cases with active first intensity stabilisation loop). The second loop introduces excess intensity noise in the pre-stabilised laser system (i.e. in front of MC1), but reduces the intensity noise at the relevant point (i.e. at the input of the Michelson interferometer).

4. A new laser system for fundamental physics

As described in the predecessing chapter, laser diode pumped solid-state laser systems are exquisitely suited for precision measurements, e.g. as the light source for gravitational wave detectors such as GEO 600. The laser systems which are used here are monolithic or quasi-monolithic Nd:YAG lasers (Willke and the GEO 600 team 2004; Yang et al. 1996; Bondu et al. 2002; Abbott and the LIGO Science Collaboration 2004) and are characterised by inherently low noise in frequency, intensity and beam geometry (Freitag et al. 1995; Quetschke 2003). The ambitious requirements for use in a gravitational wave detector can only be achieved by active stabilisation of the observables, though.

When aiming at the suppression of noise in a laser system one inevitably encounters limits. Fundamental limits posed by the quantum nature of light, as i.e. shot noise, can only be overcome by sophisticated techniques such as squeezing (Slusher et al. 1985; Gea-Banacloche and Leuchs 1987). On the other hand, technical noise sources already make stabilisation of lasers down to fundamental limits difficult. The coupling of noise processes into one another further complicates the improvement of stabilisations and is therefore object of intensive investigations (Quetschke 2003).

In the course of the analysis of transfer functions between observables in our laser systems we found a very strong coupling between the pump current of the laser diode and the output frequency of the solid-state laser (Willke et al. 2000b). Due to the well-defined transfer function the pump current is well suited as an actuator for laser frequency. Frequency stabilisation via feedback to the pump current of the laser diode is called *current lock* (section 2.4.2).

Using the pump current as an actuator for the laser frequency must also result in a change of laser intensity. One would commonly expect a worsening of the intensity noise as a parasitic effect. But contrary to expectations, frequency stabilisation of a conventional NPRO via current lock even yields a small degree of intensity noise reduction in a limited frequency band! This result initiated a whole new era of experiments on a prototype laser system, which was aimed at a better understanding of the underlying causes for noise in solid-state lasers. These experiments and their results are described in this chapter.

To gain a better understanding of semiconductor lasers section 4.2 gives in introduction on the function principle of laser diodes. In section 4.3 the experiments are described which investigate the degree of coupling between pump and laser intensity noise in an NPRO pumped by one laser diode array. Based on these results the single-mode laser diode pumped NPRO was designed; its setup is described in section 4.4. Two experimental paths have to be pursued on the prototype laser system: On the one hand it is to be determined wether a suppression of the intensity noise of the single-mode pump source entails a stabilisation of the NPRO intensity noise [1]. These experiments on pump light stabilisation of the single-mode NPRO are discussed in section 4.5, also are the effects on the frequency noise

[1] It will be shown in section 4.3 that pump light stabilisation of a multi-mode laser diode array does not lead to a suppression of NPRO intensity noise; this result is in accordance with (Harb et al. 1997).

of the single-mode NPRO examined. On the other hand there are the promising results current lock on a conventional NPRO yielded (Willke et al. 2000b), which prompt investigation of current lock on the single-mode NPRO and its effect on laser intensity noise. These experiments are discussed in section 4.6. To achieve simultaneous reduction of intensity and frequency noise of the single-mode NPRO with control bandwidths above the resonant relaxation oscillations the experiments described in section 4.7 were conducted.

4.1. Conceptual formulation: The problem

When stabilising an observable of a laser system one makes use of one or more actuators. Ideally, this actuator only changes the one observable it is supposed to act upon. Unfortunately, all actuators exhibit parasitic coupling between observables. As an example we consider the piezo-electric actuator for the NPRO frequency. This transducer is contacted directly onto the NPRO crystal. When a voltage is applied to the piezo-electric actuator the optical path length in the active medium is changed via stress-induced birefringence, which causes a change of laser frequency. As an NPRO has the special characteristic of combining active medium and resonator in a monolithic structure, actuation with the piezo-electric element also causes mechanical stress on the laser crystal and thereby introduces excess beam pointing. The beam pointing then couples into intensity fluctuations, when the pointing beam is transmitted through an optical cavity or detected on a small-area photodetector. Also is the spatial beam shape changed, when the frequency of the laser is piezo-electrically actuated.

These parasitic coupling effects between observables in a laser system induced by actuators are a common problem in laser stabilisation, as in the stabilisation of the laser system for GEO 600. Experiments on the correlations between observables were therefore conducted in our group. In the course of these experiments it was found that the transfer function from pump current of the laser diode pump source of an NPRO to the NPRO frequency falls as the reciprocal of the Fourier frequency of the change over a wide frequency band (Quetschke 2003; Willke et al. 2000b). Due to this well-defined transfer function it is possible to use the pump current as an actuator for laser frequency (section 2.4.2).

Current lock evades many of the problems associated with frequency stabilisation using the more common piezo-electric actuator (limited bandwidth due to mechanical resonances and introduction of excess beam pointing). The frequency noise reduction achievable with the current lock method for a common NPRO is documented in the paper by Willke et al. (Willke et al. 2000b). It is to be expected that using the pump current as an actuator for the laser frequency also has an effect on the laser intensity noise; judging by the parasitic coupling between laser observables for other actuators (Quetschke 2003) an amelioration of intensity noise caused by current lock is not probable. But contrarily to expectations frequency stabilisation through current lock even results in a small intensity noise reduction (approx. 3 dB) in a narrow frequency band. This *current lock effect* must have its cause in the transfer functions from pump power to frequency as well as intensity of the NPRO: On the one hand, pump power fluctuations couple directly into fluctuations of the output power of the NPRO at Fourier frequencies well below the RRO (Harb et al. 1997). On the other hand frequency independent pump intensity fluctutations drive frequency fluctuations of the NPRO which decrease with Fourier frequency as $1/f$ (Day 1990): Pump power modulation leads to modulation of the deposited thermal energy in the active medium. This thermal modulation changes the index of refraction of the material as well as the length of the crystal; both phenomena result in a change of the optical path length in the Nd:YAG material. Hence any optical path length modulation causes a frequency modulation of the laser light. Since the laser crystal acts as a thermal low-pass filter, the effect of pump current modulation decreases with increasing modulation frequency. This explains the typical $1/f$ behaviour of the transfer function of frequency change per pump current modulation. Consequently intensity and frequency noise in an NPRO have the same cause, but the limits of simultaneous stabilisation had not yet been experimentally explored. To remedy this is the main objective of this work.

4.2. An introduction to laser diodes

All-solid-state laser systems have become increasingly important as light sources for optical communication, in laser based metrology (such as precision spectroscopy and LIDAR applications) and in other areas of scientific research. Laser diode pumped solid-state laser systems, such as Nd:YAG lasers, have numerous advantages over flashlamp pumped systems: The lifetime of laser diodes surpasses that of flashlamps by a factor of 500. Due to the much better spectral overlap of the laser diode emission spectrum with the absorption spectrum of the laser material higher system efficiency is achieved. Furthermore material degradation due to the high UV content in the flashlamp spectrum is evaded, which contributes to an improved lifetime of the laser. The compactness of these laser systems is another bonus. Only a few advantages are mentioned here; for a more extensive overview (Koechner 1996) is recommended.

Nearly all experiments in our group make use of diode lasers, either as a pump source for solid-state lasers (mostly Nd:YAG lasers) or directly as a spectroscopic light source. The next section will therefore deal with the basic function principles of diode lasers.

4.2.1. The function principle of semiconductor lasers

(Kneubühl and Sigrist 1991):

In a semiconductor the energy levels are not discrete, but are broadened into a quasi-continuum (*energy bands*). The outermost (partly) populated band is called *valence band*, the band which contains free carriers (carriers that are not "attached"to the ions) is the *conduction band*. Valence band and conduction band are separated by the *bandgap* E_g (see figure 4.1).

Due to the Pauli Principle the closely packed individual states in the bands can only be populated by two electrons with opposite spin. The population probability for a state with energy E follows the Fermi-Dirac statistic:

$$f(E) = \left[1 - e^{\frac{E-F}{kT}}\right]^{-1} \quad . \tag{4.1}$$

Here F denotes the energy of the Fermi level, k is the Boltzmann constant and T is the thermodynamic temperature. For $T = 0\,\mathrm{K}$ the Fermi level separates the fully populated

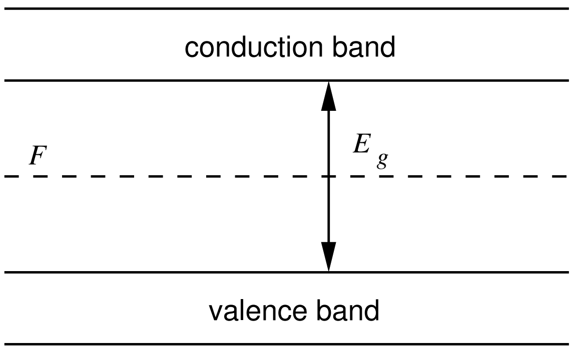

Figure 4.1: Band model of a semiconductor. E_g: bandgap, F: Fermi energy

from the empty states. For non-degenerate semiconductors the Fermi level lies completely in the bandgap, so that the valence band is completely filled and the conduction band is empty at zero temperature. The semiconductor is then a perfect isolator.

For laser action it is necessary to obtain a state of *inversion* (Siegman 1986; Svelto 1998). In the case of a semiconductor laser, where electrical pump power is directly converted into stimulated emission of coherent light, inversion is given when the population of the conduction band is larger than that of the valence band. This condition is achieved by a pumping process[2].

When electrons are lifted from the valence band into the conduction band through a pumping process, they quickly ($t \approx 10^{-13}$ s, (Kneubühl and Sigrist 1991)) fall into the lowest possible energy state in the conduction band. The equivalent happens to the defect electrons ('holes') produced in the valence band by the pump process: They are 'filled' by the electrons in the valence band, which occupy the lowest possible energy states, leaving defect electrons in the upper 'rim' of the band (fig.4.2).

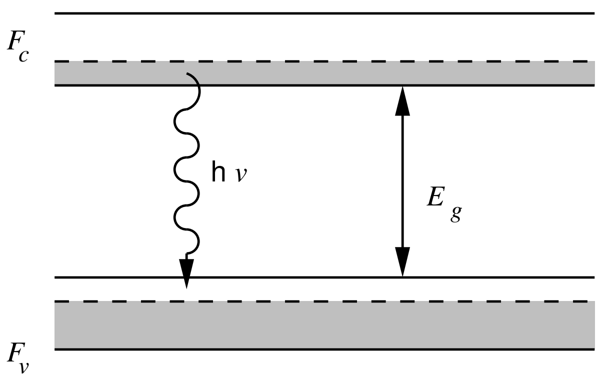

Figure 4.2: Inversion in a semiconductor laser. E_g: bandgap, hν: laser transition, F_c: quasi-Fermi level of the conduction band, F_v: quasi-Fermi level of the valence band

This situation is one of non-thermal equilibrium. The quasi-Fermi levels F_c and F_v of the

[2]In the case of a diode laser the pumping process is the injection of charge carriers into a p-n-junction.

conduction and the valence band correspond to the Fermi levels of an n-type respectively p-type semiconductor . Recombination of electrons in the conduction band with holes in the valence band occurs under emission of photons with energy hν, where h is Planck's constant and ν is the frequency of the emitted photon. Obviously, the condition

$$E_g < \mathrm{h}\nu < \mathrm{F_c} - \mathrm{F_v} \tag{4.2}$$

is fulfilled; the corresponding population probabilities depend on the quasi-Fermi levels:

$$f_c = \left[1 - e^{\frac{E-F_c}{kT}}\right]^{-1} \quad , \tag{4.3}$$

$$f_v = \left[1 - e^{\frac{E-F_v}{kT}}\right]^{-1} \quad . \tag{4.4}$$

As stated above laser action necessitates population inversion

$$\sigma = N_2 - N_1 > 0 \quad . \tag{4.5}$$

N_2 is the population of the upper laser level and is given by the population probability for electrons in the conduction band f_c times the probability for the absence of electrons in the valence band $(1 - f_v)$; equivalently N_1 is the population of the lower laser level, defined by $f_v \cdot (1 - f_c)$. σ denotes the population inversion.

The condition for laser action is therefore fulfilled, when

$$f_c(1 - f_v) - f_v(1 - f_c) > 0 \quad . \tag{4.6}$$

This condition is satisfied, when

$$F_c - F_v > E_2 - E_1 = \mathrm{h}\nu \quad , \tag{4.7}$$

with E_2 and E_1 being the energy of the upper and lower laser level, respectively.

As eq. 4.7 ist temperature independent, stimulated emission of recombination radiation will consequentially produce laser oscillation whenever population inversion is given and appropriate optical feedback is ensured.

4.2.2. Fundamental setup of semiconductor lasers

While the previous chapter dealt with undoped semiconductor materials, the most simple model of an actual laser diode consists of a p-doped region and an n-doped region brought into contact and thereby forming a p-n-diode. The doping concentration is larger than 10^{18} atoms/cm^3. Typical substrate materials are GaAlAs (for wavelengths around $\lambda = 800\,$nm) and InGaAsP (for wavelengths around $\lambda = 1.3\,\mu$m and $\lambda = 1.5\,\mu$m) (Kneubühl and Sigrist 1991). The band model of a p-n-junction is shown in figure 4.3.

Due to the doping the valence and conduction bands of the p- and the n-doped regions are shifted with regard to each other when the differently doped semiconductors are brought into contact. The Fermi level, though, is identical in both regions due to thermal

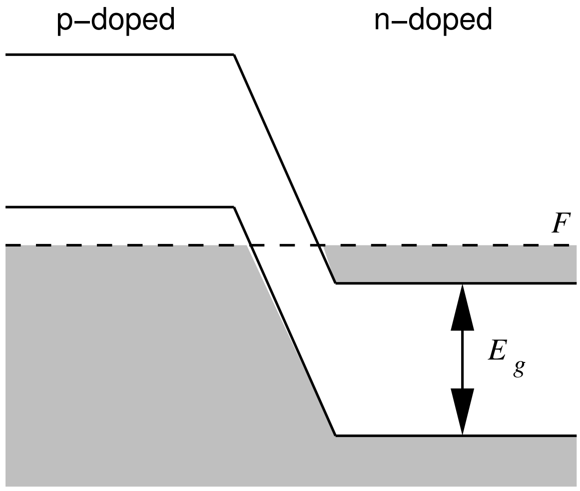

Figure 4.3: Band model of a p-n-junction without external voltages applied. E_g: bandgap, F: Fermi energy

equilibrium. As a result of the high doping it lies in the valence band of the p-doped region and in the conduction band of the n-doped region.

Applying a forward voltage V in the order of magnitude of the bandgap injects electrons from the n-region into the p-region; the Fermi level in the n-region is raised by the amount of eV relative to the Fermi level in the p-region, thermal equilibrium is no longer given. This fact is shown in figure 4.4.

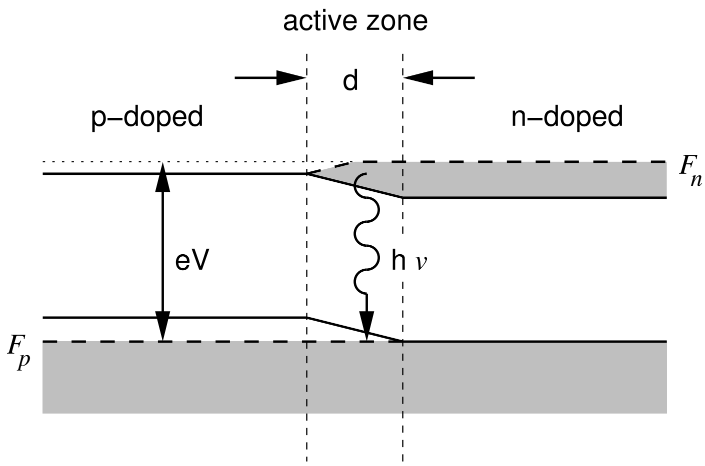

Figure 4.4: Band model of a p-n-junction with forward voltage applied. F_n: quasi-Fermi level of n-doped region, F_p: quasi-Fermi level of p-doped region, d: width of the active zone

There is now a narrow active zone d which contains electrons as well as holes. In accordance with eq. 4.5 the active zone shows inversion, so that electromagnetic radiation of frequency ν (as specified in eq. 4.2) is amplified. Laser emission is limited to this very narrow zone at the p-n-junction. The schematic setup of a p-n-diode laser is shown in figure 4.5.

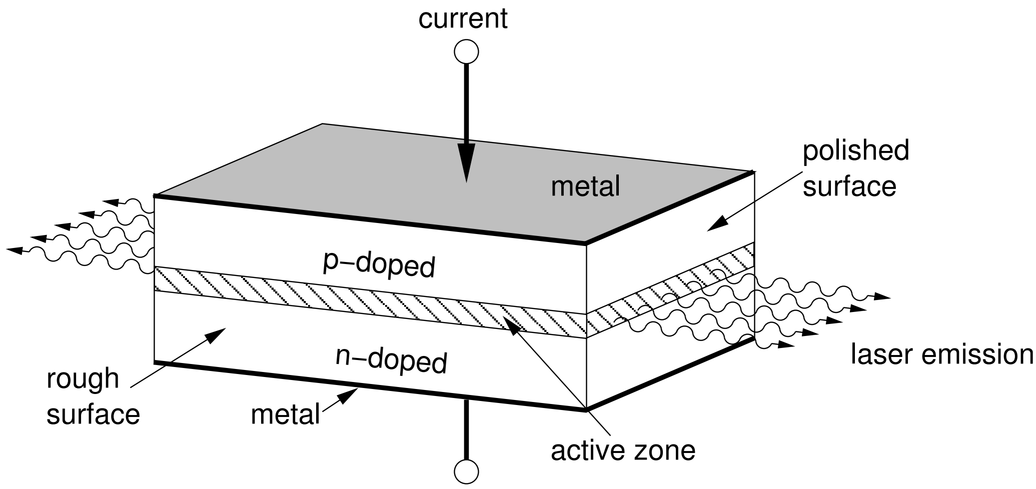

Figure 4.5: Schematic of a p-n-laser diode.

The inversion which is produced in the semiconductor is 'cleared' by stimulated emission (Svelto 1998; Siegman 1986). Optical feedback, which is necessary for any kind of laser, is obtained by multiple reflection of the accumulating laser light at the front faces of the semiconductor. The two polished front faces then form a Fabry-Perot resonator for the laser light. Splitting the semiconductor material at its crystalline boundaries results in relatively high reflection of the light at the semiconductor-air-interface ($\approx$ 32% for GaAs with a refraction index of $n = 3.6$, (Kneubühl and Sigrist 1991)), so that further coating of the facets is usually unnecessary. The side faces of the p-n-diode laser are kept rough to suppress laser oscillation in unwanted directions. As laser oscillation occurs only in the narrow active zone, which typically has a length of around 100 μm, the emitted laser beam shows a strong divergence of up to 50° (Siegman 1986; Kneubühl and Sigrist 1991).

The output power of a laser diode increases linearly with junction width (Koechner 1996). Unfortunately, the pump current in wide junctions tends to break up into filaments, so that the current does not flow evenly through the semiconductor . The current filamentation leads to localized damage of the faces and thereby reduces the device lifetime significantly. In order to avoid this effect the broad active stripe of the semiconductor laser is divided into multiple individual stripes, each permitting single transverse mode laser action. For this cause the upper metal contact of the semiconductor laser is periodically interupted by grooves of a high resistivity material. The lower metal contact remains unchanged. One can not, however, regard these multiple-stripe-geometry lasers as a compound of numerous individual single-emitter devices! With the described setup the stabilised total pump current through the semiconductor is split into a parallel connection over the number of narrow stripes. If momentarily a larger fraction of the current flows through one of these stripes, then obviously the current over the other stripes is reduced. There is therefore an anti-correlation between the emitters of a multi-stripe diode laser or *laser diode array* . This fact is mirrored in the experiments by Harb et al. (Harb et al. 1997). In agreement with these experiments this work shows that spatial truncation of the multi-mode diode laser beam by an aperture results in higher relative intensity noise (section 4.3.3).

Acutal diode laser configurations are more complex in order to obtain laser action at room temperature, lower threshold currents, longer lifetime and higher efficiency. The above is an introduction to the function principle of laser diodes. Detailed description of the different designs unfortunately goes beyond the scope of this work, but (Koechner 1996; Kneubühl and Sigrist 1991) are recommended for further reading.

4.3. Experiments with a laser diode array pumped NPRO

Commercially available NPROs use laser diode arrays as a pump source. An NPRO, type Mephisto 800 (InnoLight GmbH 2004), is pumped by two laser diode arrays, type SPL 2Y81 (from Osram Semiconductors), which emit $P = 1\,\mathrm{W}$ at a wavelength of $\lambda = 808\,\mathrm{nm}$. With this pump power the NPRO typically emits $P = 800\,\mathrm{mW}$ of laser light at a wavelength of $\lambda = 1064\,\mathrm{nm}$. The function principle and the design of the NPRO are described in appendix A.

The goal of the experiments described in this chapter is to gain a deeper understanding of the coupling mechanisms between pump intensity and laser frequency in solid-state laser systems. For this reason a simplified NPRO setup was designed, with only one fibre-coupled laser diode array as the pump source for the laser crystal. The experiments conducted with this laser diode array pumped NPRO are subject of this section, beginning with a description of the pump source (section 4.3.1) and going on to the experimental setup (section 4.3.2) and results of the implemented stabilisations (section 4.3.3).

4.3.1. The laser diode arrays SPL 2Y81 and 2F81

The laser diode arrays which are used as a pump source in commercially available NPROs (type Mephisto 800 (InnoLight GmbH 2004)) are Single Quantum Well Seperate Confinement Heterostructure (SQW-SCH) (Koechner 1996; Schmitt 2004) devices. They consist of different layers of variably aluminum-doped indium-gallium-arsenide in a strained layer quantum-well structure in a TO-220 package (Osram Opto Semiconductors 2003); a schematic of the layout is shown in figure 4.6. The active region of the laser diode array is $200\,\mu\mathrm{m}$ long, the junction width is $1\,\mu\mathrm{m}$. The 20 individual emitters of the laser diode array are electrically contacted in parallel to avoid filamentation of the current in the junction (section 4.2) and thereby increase the device lifetime.

Due to their design the emitted light is diffraction limited in the small dimension, but not in the large dimension. The intensity distribution of the light emitted by this kind of laser diode array can not be TEM_{00} (see appendix D), as the light stems from 20 'individual' emitters (see section 4.2). The laser beam is highly multimode and, in the free-beam case, resembles a striped rectangle, as shown in (Harb et al. 1997). The intensity of the individual stripes varies strongly over time.

The light from the laser diode array type SPL 2F81 can be fibre-coupled into a multimode fibre with numerical aperture $\mathrm{NA} = 0.22$ and core diameter $d = 200\,\mu\mathrm{m}$. For this cause the laser diode array is equipped with a graded-index (GRIN) lens contacted directly in front of the emitting chip. The resulting beam behind the fibre is shown in figure 4.7. The

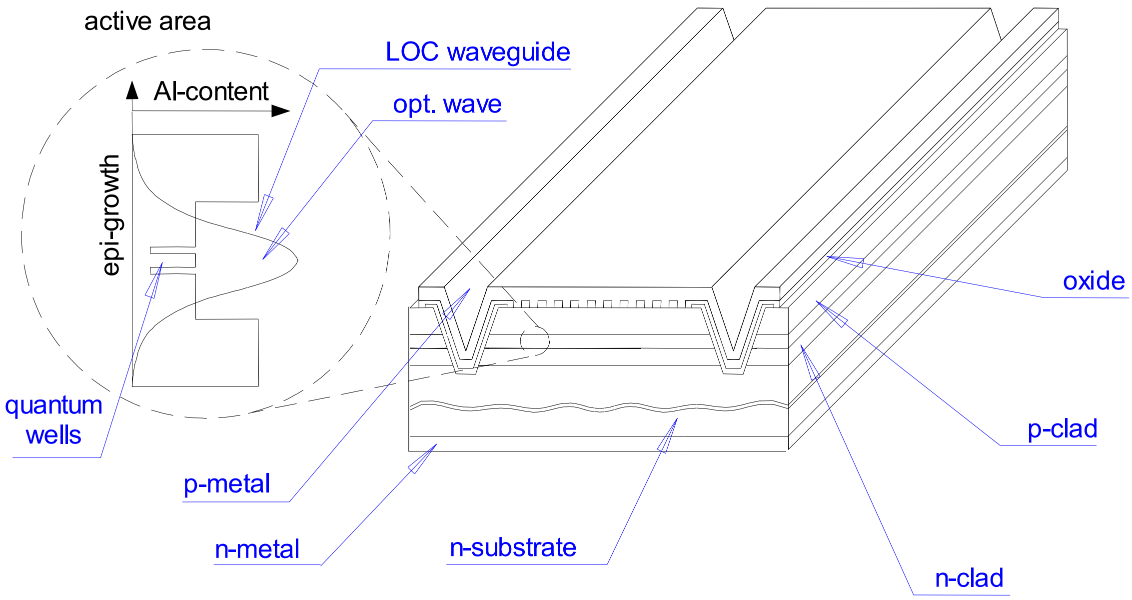

Figure 4.6: Schematic of a laser diode array, type SPL 2Y81. Picture courtesy of Dr. A. Schmitt, Osram Semiconductors,

beam is adequately round, but has a much larger divergence than a beam with TEM_{00} due to the fact that it is highly multi-mode; fibre-coupling with a multi-mode fibre naturally does not change this fact. The beam quality factor M^2 of this device is typically larger than 30. A static picture unfortunately does not reveal the most disturbing aspect of the intensity distribution of the fibre-coupled laser diode array: The intensity varies strongly and unpredictably over space and time. This is due to the anti-correlation of the emitters in the laser diode array.

4.3.2. Experimental setup

Experiments have shown (Willke et al. 2000b) that the intensity noise and the frequency noise in a conventional laser diode pumped NPRO are coupled, based on their dependence on pump intensity noise. A fibre-coupled laser diode array pumped NPRO was therefore constructed in order to investigate the effect of the pump geometry onto the intensity and frequency noise of an NPRO. The setup can be seen in figure 4.8.

As can be seen in figure 4.9 there is a good overlap of pump and laser mode in the NPRO crystal[3]; it is also striking to see how much larger the divergence of the pump light is (due to the multi-mode pump laser) with respect to the laser light.

[3] As described in appendix A the pump mode needs to be smaller than the NPRO laser mode for mode-selective pumping. Though figure 4.9 suggests that this is not the case here, transverse single-mode NPRO emission was given, as can be seen in figure 4.10. Due to the optical setup the beam profiles could not be measured with satisfying accuracy; the unavoidable errors are reflected by the fits. Yet the qualitative result and the strong difference in divergence are correct.

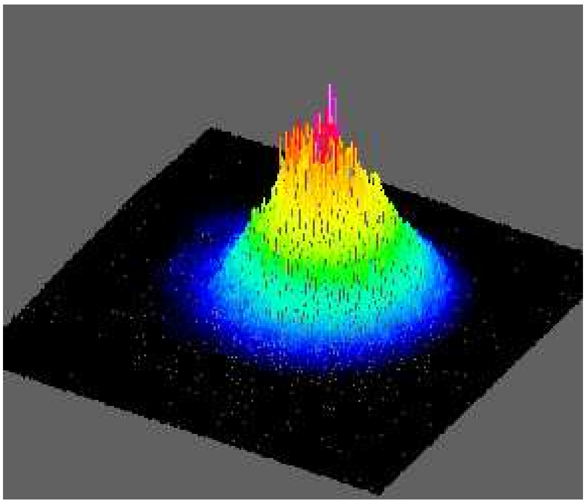

Figure 4.7: Farfield intensity distribution of a fibre-coupled laser diode array, type SPL 2F81, seen under an angle for better visibility of the beam profile which is not perfectly Gaussian and shows strong temporal variations!

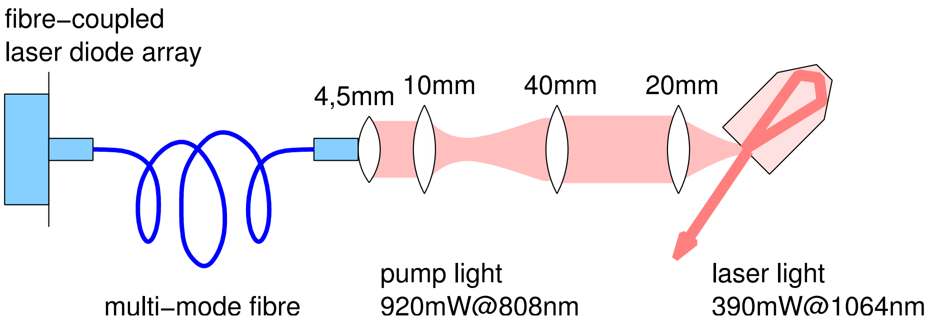

Figure 4.8: Experimental setup of the fibre-coupled laser diode array pumped NPRO.

The intensity distribution of the pump laser light varies strongly with time and is not a smooth Gaussian beam, as can be seen in figure 4.10, left hand side. The NPRO light resulting from this pump geometry is near-perfectly Gaussian, though (figure 4.10, right hand side), and does not fluctuate with time. As we will see, the temporally varying spatial inhomogeneities of the pump profile in combination with the imperfect mode overlap are the cause for the sub-optimal correlation between the observables NPRO intensity noise and NPRO frequency noise.

4.3.3. Experiments and discussion of the results

The fibre-coupled laser diode array pumped NPRO (see figure 4.8) was characterised in its observables. In order to determine the optimal operation parameters for the laser an electrical-to-optical slope of the fibre-coupled laser diode array was measured, shown in figure 4.11. The optical-optical slope of the fibre-coupled laser diode array pumped NPRO

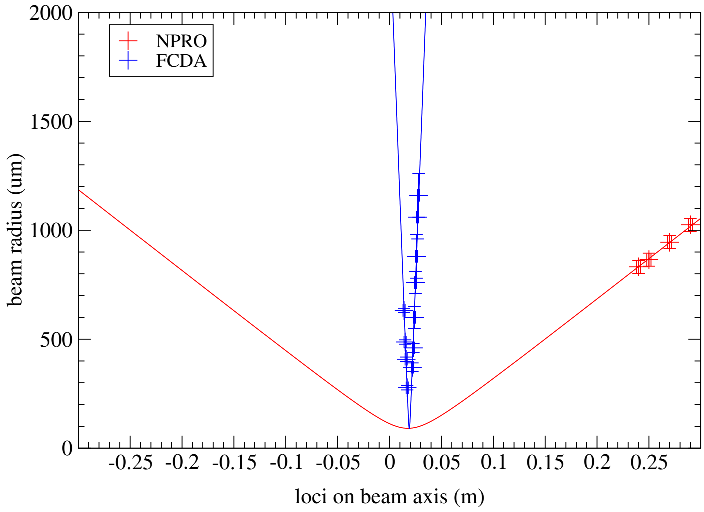

Figure 4.9: Beam profiles of the pump laser beam and the NPRO beam in the fibre-coupled laser diode array pumped NPRO.

is displayed in figure 4.12. Linear regression of the laser slope yields an efficiency of this NPRO of $\eta_{\text{opt}} = 37.5\,\%$.

A comparison between the free space propagation slope of the laser diode array and the slope measured behind the fibre shows a slight reduction of laser power due to the fibre coupling, which means that the laser beam emitted by the laser diode array is in some way cropped by the fibre-coupling. In accordance with (Harb et al. 1997) an increase of the relative intensity noise of the laser diode array is therefore to be expected and is confirmed by the following measurements.

Investigations of the effect an aperture has on the relative intensity noise of a laser diode array yielded the following results: The intensity noise of the laser diode array type SPL 2F81 was measured with and without fibre-coupling and is shown in figure 4.13. As a reference the relative intensity noise of a laser diode array type SPL 2Y81 was measured, with and without an aperture cropping the beam profile, the results can be seen infigure 4.14. From these measurements it is obvious that truncation of the laser beam emitted by a laser diode array leads to a significant increase in intensity noise.

The above measurements are in complete agreement with the results found in (Harb et al. 1997). The increase in relative intensity noise of a laser diode array is based on the anti-correlation of the emitters (see section 4.3.1). The intensity distribution over the beam profile varies strongly with time. This is caused by the fact that the 20 emitters of the laser diode array are contacted in parallel. The pump current is split up into 20 paths when it flows over the emitters. Depending on fluctuations of the semiconductor material or of environmental parameters the individual currents over the emitters vary. This variation of pump current in the different paths leads to a variation of the output intensity of the individual emitters, even though the net intensity integrated over the complete array is constant (corresponding to the stability of the pump current). An aperture introduced in the beam path of the laser diode array now truncates the beam. Light from some emitters

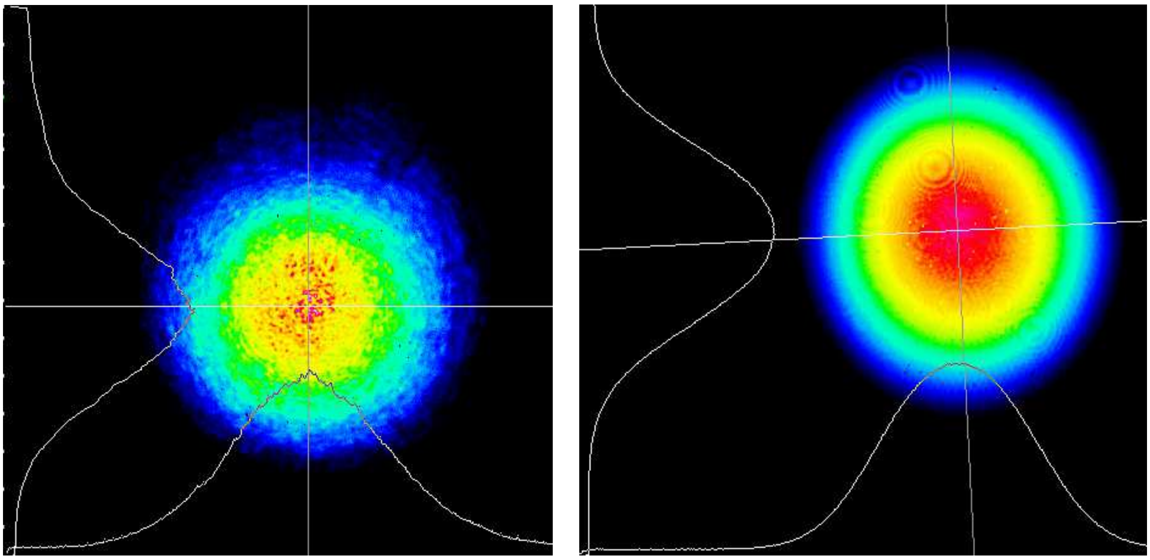

Figure 4.10: Intensity distribution of the fibre-coupled laser diode array SPL 2F81 (left hand side, strong fluctuations of the spatial profile with time) and of the fibre-coupled laser diode array pumped NPRO (right hand side, stable profile).

is therefore not taken into account in the detection of intensity. If at some given time the blocked emitters show an intensity maximum, then the detected intensity reaches an intensity minimum and vice versa. Any aperture in the beam path therefore introduces intensity fluctuations in the detection, even though the overall intensity remains constant.

Pump light stabilisation of the fibre-coupled laser diode array pumped NPRO

Below the resonant relaxation oscillations pump intensity fluctuations couple directly into NPRO intensity noise (Harb et al. 1997). If there is a firm coupling between the pump light intensity fluctuations and the resulting laser light fluctuations, then it should be possible to attain intensity noise reduction of the NPRO light by detecting a fraction of the pump light and feeding back an appropriate control signal to the pump current. This *pump light stabilisation* experiment was conducted on the fibre-coupled laser diode array pumped NPRO; a schematic of the experiment is shown in figure 4.15.

The photodetector used for stabilisation is called *in-loop* photodetector, as it is part of the control loop. Closing the pump light stabilisation control loop and reading out the resulting intensity noise on the in-loop detector leads to the measurement shown in figure 4.16. A reduction of the in-loop pump light intensity noise of more than 40 dB is achieved by this method.

Measuring the pump light with an independent, *out-of-loop* photodetector, however, yields a more truthful expression of the 'real' pump light intensity noise with active pump light stabilisation and is displayed in figure 4.17. As is clearly visible there the realised out-of-loop pump intensity noise suppression with pump light stabilisation is much weaker than in-loop. This fact is an example for the well-known *in-loop / out-of-loop problem* (see section 2.5) and stems from the fact that disturbances couple into the experiment in the

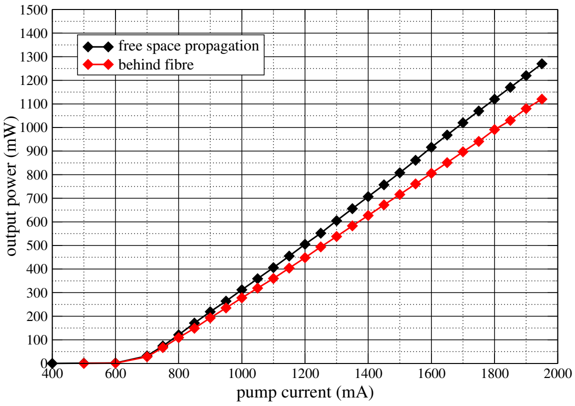

Figure 4.11: Slope of the fibre-coupled laser diode array, type SPL 2F81, no. 085104 (fibre from Ocean Optics).

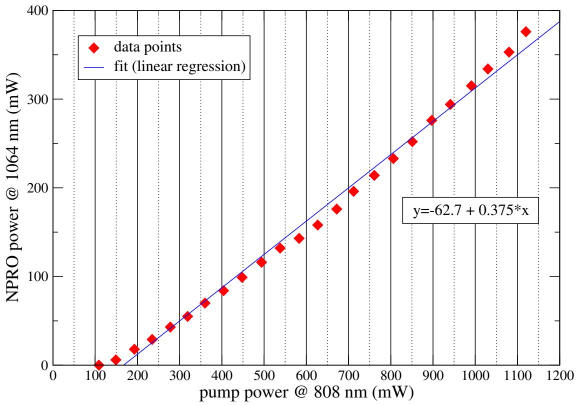

Figure 4.12: Optical-optical slope of the fibre-coupled laser diode array pumped NPRO.

non-common beam path after the point of stabilisation (here between the in-loop and the out-of-loop detector).

Looking at the resulting intensity noise of the NPRO with and without active pump light stabilisation (figure 4.18) reveals hardly any reduction of intensity noise at all, even though the pump light stabilisation electronics obviously works (as can be seen in the in-loop measurement in figure 4.16).

Figure 4.18 shows that it is not possible to stabilise the NPRO intensity noise by suppressing the intensity noise of its multi-mode pump. The anti-correlation between the emitters of the multi-mode laser diode array in combination with unavoidable apertures in the path of the pump beam destroys the coupling between pump and NPRO intensity noise .

Since pump light stabilisation does not lead to a reduction of NPRO intensity noise it is not worth measuring the frequency noise of the NPRO with and without pump light stabilisation as the coupling does not hold in the first step. A different pumping scheme needs to be designed in order to investigate the coupling effects further.

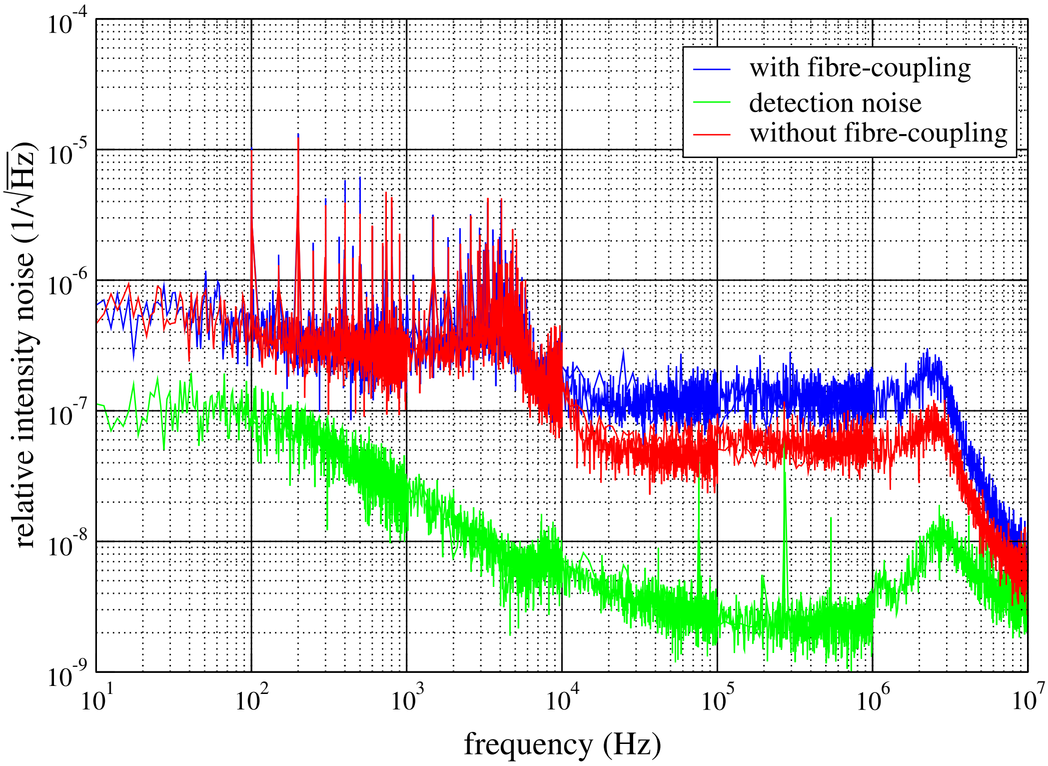

Figure 4.13: Relative intensity noise of a laser diode array type SPL 2F81, with (blue, upper graph) and without (red, middle graph) fibre-coupling. The fibre-coupling acts as an aperture and thereby increases the relative intensity noise. Detection noise is shown in green (lower graph).

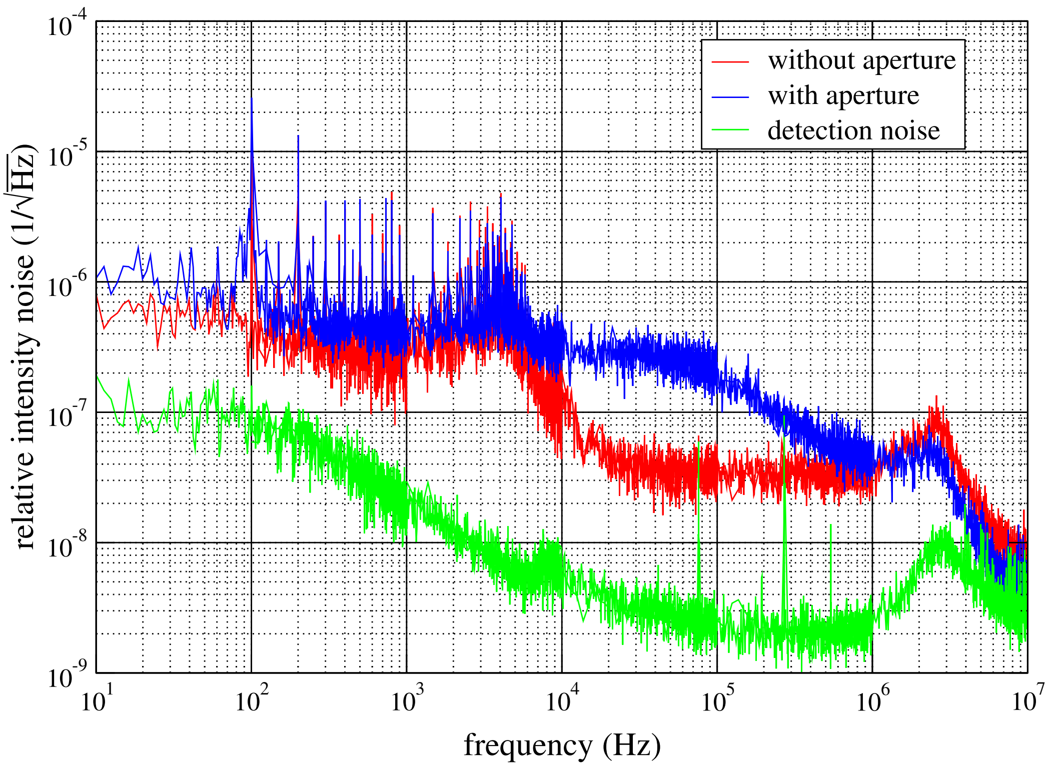

Figure 4.14: Relative intensity noise of a laser diode array type SPL 2Y81, with (blue, upper graph) and without (red, middle graph) a pinhole as a beam aperture. The increase of relative intensity noise due to the introduced aperture is clearly visible. Detection noise is shown in green (lower graph).

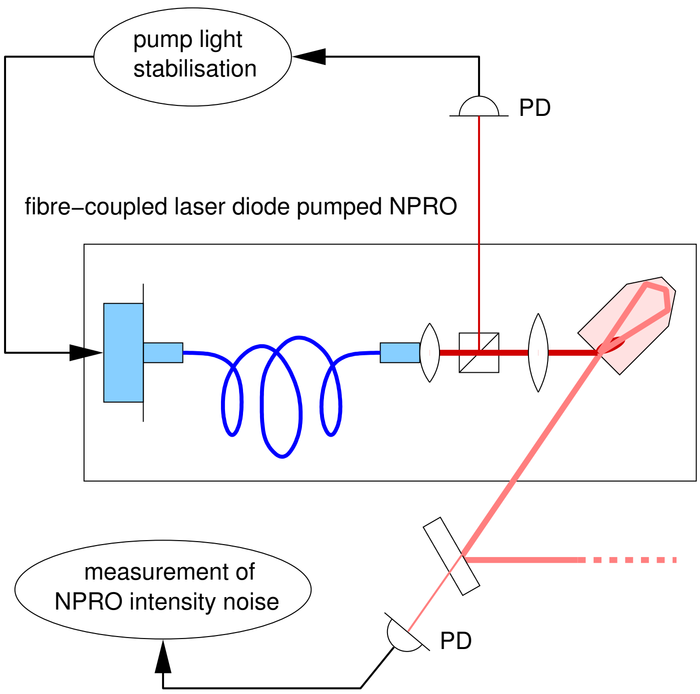

Figure 4.15: Schematic of the pump light stabilisation experiment on the fibre-coupled laser diode array pumped NPRO. The pump light is detected by a photodetector (PD) and the control signal is fed back to the pump current of the laser diode array. The resulting NPRO intensity noise is detected by second photodetector. For a measurement of the out-of-loop intensity noise of the laser diode array an independent photodetector was placed at the position of the NPRO crystal.

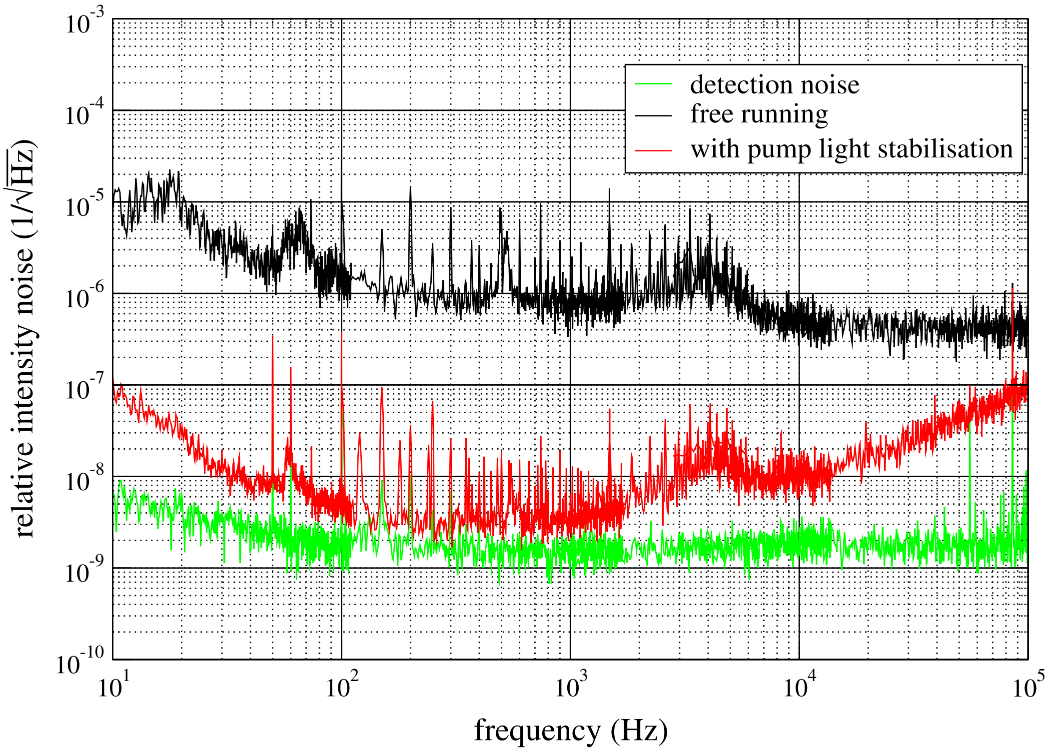

Figure 4.16: In-loop intensity noise of the fibre-coupled laser diode array, type SPL 2F81, with and without active pump light stabilisation. The free running intensity noise of the laser diode array (black, upper graph) is reduced by the servo gain to the level shown in red (middle graph). The lower graph (green) shows the detection noise.

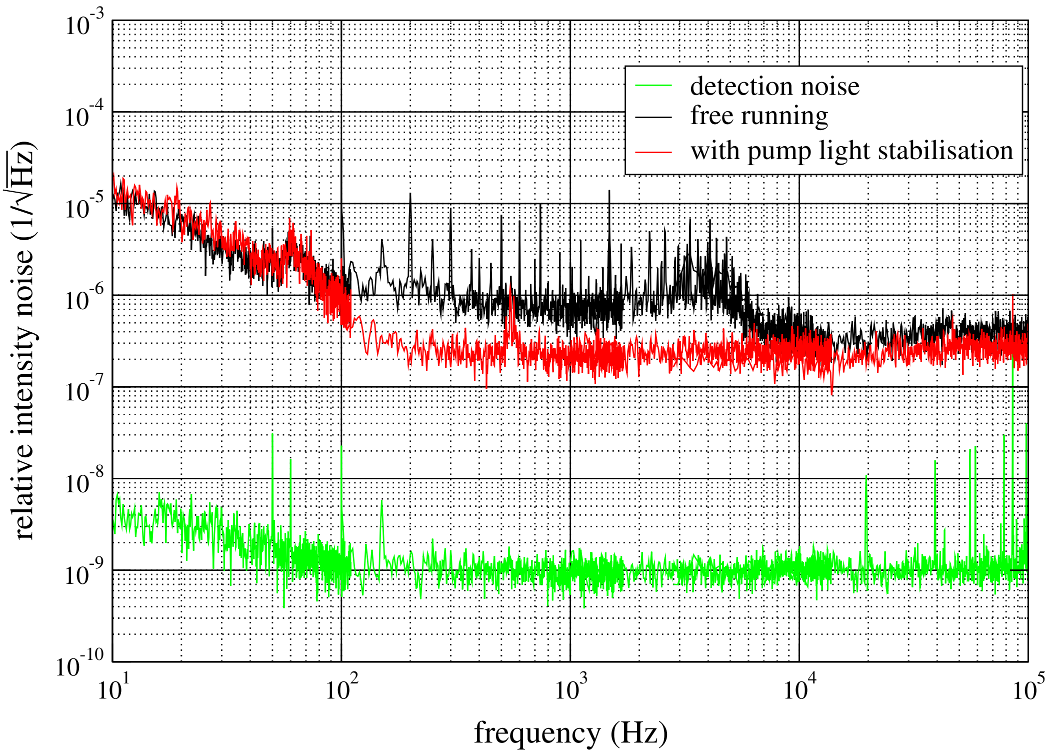

Figure 4.17: Out-of-loop intensity noise of the fibre-coupled laser diode array, type SPL 2F81, with (shown in red, middle graph) and without (shown in black, upper graph) active pump light stabilisation. Even though the stabilisation is not gain limited (see figure 4.16) the intensity noise reduction of the laser diode array measured with an independent (out-of-loop) photodetector is small. The detection noise is shown in green (lower graph).

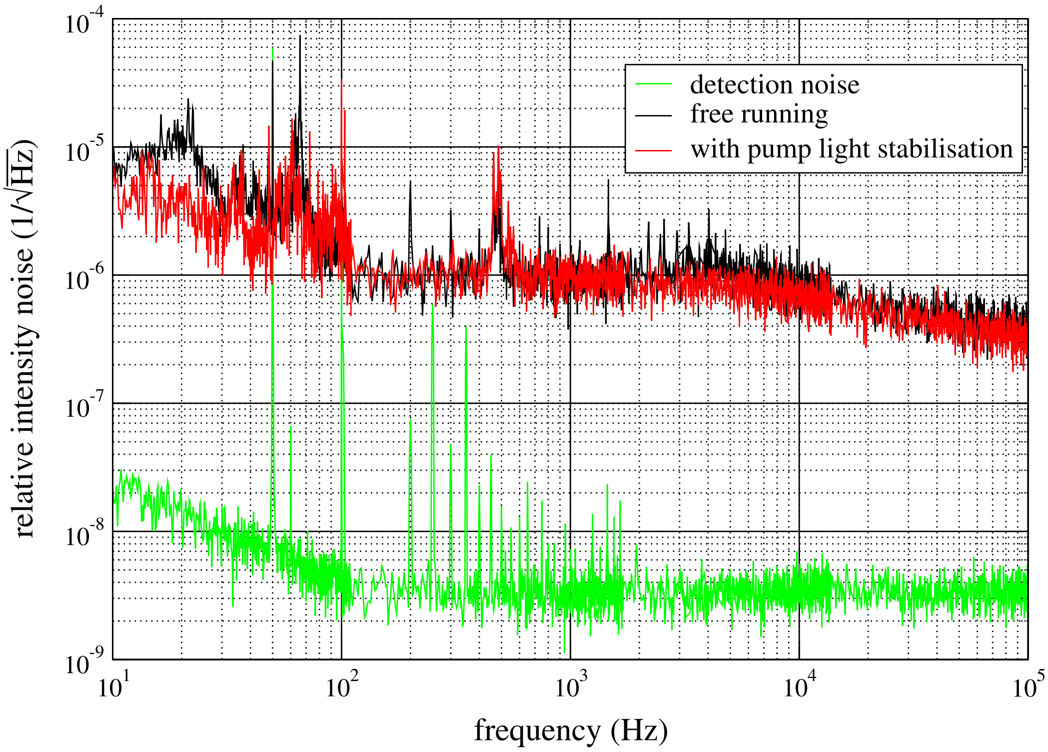

Figure 4.18: Intensity noise of the fibre-coupled laser diode array pumped NPRO, with (in red) and without (in black) active pump light stabilisation. No significant reduction of intensity noise is achieved in the laser diode array pumped NPRO by pump light stabilisation. The detection noise is shown in green (lower graph).

4.4. The prototype laser system

In an NPRO with a multi-mode pump source the frequency noise suppression from current lock is very high, but the corresponding intensity noise suppression is nearly negligible (Willke et al. 2000b). Also is a reduction of NPRO intensity noise by stabilisation of the pump intensity not possible, as shown in section 4.3.3. Both of these observations are based on the fact that a multi-mode pump source does not drive NPRO intensity and frequency fluctuations equally; the coupling between the two does not hold for this pump geometry. This is caused by the following effect: The pump intensity fluctuations in the overlap area of pump and laser mode lead to intensity noise of the NPRO (Harb et al. 1997). All but $1/e^2$ of the initial pump intensity is absorbed in the first few millimeters of the laser active material (see calculation in appendix A), but a fraction of the pump power remains in non-overlap sections where the pump beam is larger in diameter than the laser mode. The remaining pump power introduces heat in the laser material which has an effect on the laser frequency, but not on the laser intensity. As the pump profile is spatially inhomogeneous and varies with time the heat input varies accordingly, causing laser frequency noise. This is the reason why the degree of simultaneous intensity noise reduction for current lock in a multi-mode pumped NPRO is so small. Figure 4.19 illustrates the geometry.

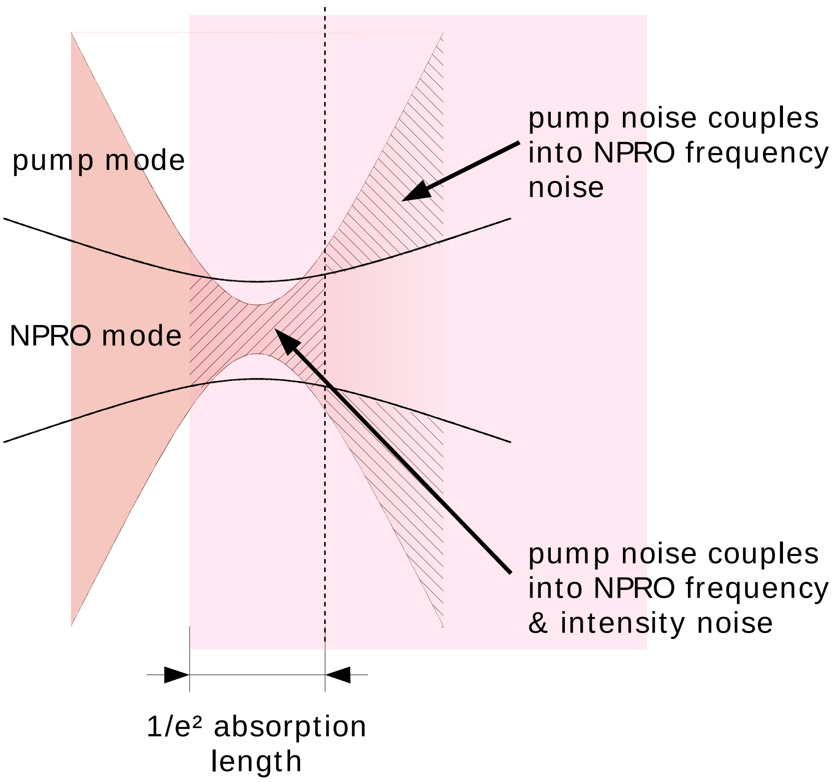

Figure 4.19: Illustration of the overlap between multi-mode pump and single-mode laser beam in an NPRO.

The previous section 4.3 showed that coupling of pump intensity noise into the two observables intensity noise and frequency noise of the NPRO depends strongly on the characteristics of the pump source. The anti-correlations in the intensity of the laser diode array emitters in combination with unavoidable apertures in the beam path largely reduce this coupling. To circumvent this problem a new laser system was designed, the so-called *single-mode NPRO*. The prerequisite for this laser system is a pump source, where the intensity distribution of the beam profile does not vary with time; ideally this is a single-mode laser diode. The new laser system with optimised pump geometry was designed to investigate wether an increase in the degree of simultaneous intensity and frequency noise suppression in current lock can be achieved. A schematic of the prototype laser system can be seen in figure 4.20 and a photograph is shown in figure 4.21.

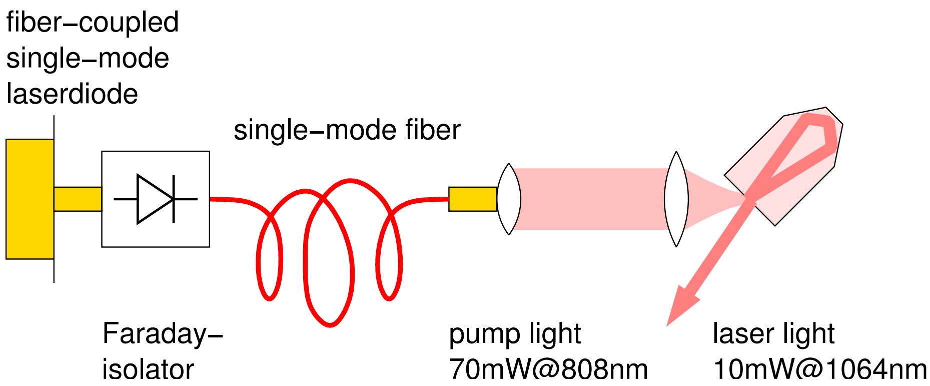

Figure 4.20: Schematic of the fibre-coupled single-mode laser diode pumped NPRO.

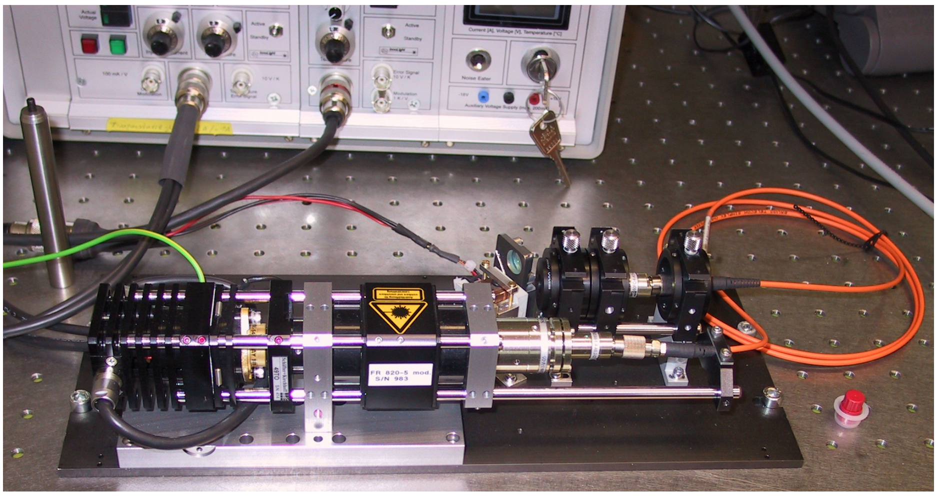

Figure 4.21: Photograph of the fibre-coupled single-mode laser diode pumped NPRO.

4.4.1. Experimental configuration of the single-mode laser diode pumped NPRO

The single-mode NPRO consists of a fibre-coupled single-mode laser diode, the light of which is mode matched into an NPRO crystal with extended tuning range (ETR-NPRO). The laser crystal needs a reduced threshold, as the pump module only emits around $P = 70\,\mathrm{mW}$ of pump light at $\lambda = 808\,\mathrm{nm}$. The laser then emits approximately $P = 10\,\mathrm{mW}$ of light at $\lambda = 1064\,\mathrm{nm}$. Conventional ETR-NPRO crystals have a threshold of $P_{\mathrm{thr}} \approx 80\,\mathrm{mW}$, which is realised by a coating of the front facet with a transmissivity of $T_{\mathrm{s}} = 2.5\,\%$ for the s-polarisation respectively $T_{\mathrm{p}} = 5.9\,\%$ for the p-polarisation. To reduce the laser threshold for the prototype laser system the front facet of the NPRO crystal has $T_{\mathrm{s}} = 1.3\,\%$ and $T_{\mathrm{p}} = 3.0\,\%$ (Bode 2004). The prototype NPRO was assembled at InnoLight GmbH.

Pump source: The single-mode laser diode

The implemented pump module is constructed on Microbank-system by Schäfter & Kirchhoff GmbH. The pump module consists of a single-mode laser diode from SDL / JDS Uniphase, type 5422-H1-810, which nominally emits light at $\lambda = 810 \pm 4\,\mathrm{nm}$. The implemented laser diode emits light at $\lambda = 813\,\mathrm{nm}$ at room temperature. It is possible to tune the emission wavelength of a laser diode to the absorption maximum of Nd:YAG (which lies at $\lambda = 808.6\,\mathrm{nm}$, compare figure 4.25, which shows the absorption spectrum of Nd:YAG around $\lambda = 800\,\mathrm{nm}$) by changing the operation temperature; the tuning coefficient is $0.3\,\mathrm{nm/K}$. In this setup cooling of the laser diode fibre assembly reduced the fibre coupling efficiency drastically. The NPRO was therefore pumped not at the dominant absorption maximum at $\lambda = 808.6\,\mathrm{nm}$, but instead the smaller absorption maximum at $\lambda = 813\,\mathrm{nm}$ was used for pumping. The absorption length at $\lambda = 813\,\mathrm{nm}$ is approximately a factor of three longer as opposed to that at $\lambda = 809\,\mathrm{nm}$, but single transverse mode operation of the model NPRO was nevertheless given.

Single-mode emission of the pump laser diode is only guaranteed if the pump current does not exceed a certain limit; the power of the emitted light is $P = 150\,\mathrm{mW}$ at a pump current of $I = 167\,\mathrm{mA}$, the slope efficiency of the laser diode without fibre coupling is $1.00\,\mathrm{W/A}$ (SDL / JDS Uniphase 2002). Fibre-coupling reduces the emitted light power due to unavoidable apertures in the optical path: The light emitted by the single-mode laser diode is collimated, passes a Faraday isolator (to avoid fatal back-reflections into the laser diode), is formed by anamorphotic optics (which reduces the 3:1 ellipticity of the beam, caused by the emitter dimensions) and is again collimated to be matched into the fibre. The polarisation-maintaining 'Panda'-fibre has a core diameter of $5.3\,\mu\mathrm{m}$ and a numerical aperture of $NA = 0.13$.

The pump light of the single-mode laser diode exhibits a significantly different intensity noise spectrum than a laser diode array (for comparison: figure 4.13 shows the relative intensity noise of the laser diode array with and without fibre-coupling). The intensity noise of the single-mode laser diode is shown in figure 4.23. A plateau in the spectrum is visible in the frequency region from 10 Hz to 3 kHz, which is followed by a $f^{3/2}$ decrease in intensity noise from 3 kHz to 50 kHz. White pump light intensity noise drives 1/f frequency noise of an NPRO, this is stated in (Day 1990). It will be interesting to find what the frequency noise spectrum of the single-mode NPRO looks like with the characteristic of the single-mode pump source.

The pump light power of $P_{\mathrm{pump}} = 70\,\mathrm{mW}$ emitted by the pump module behind the fibre

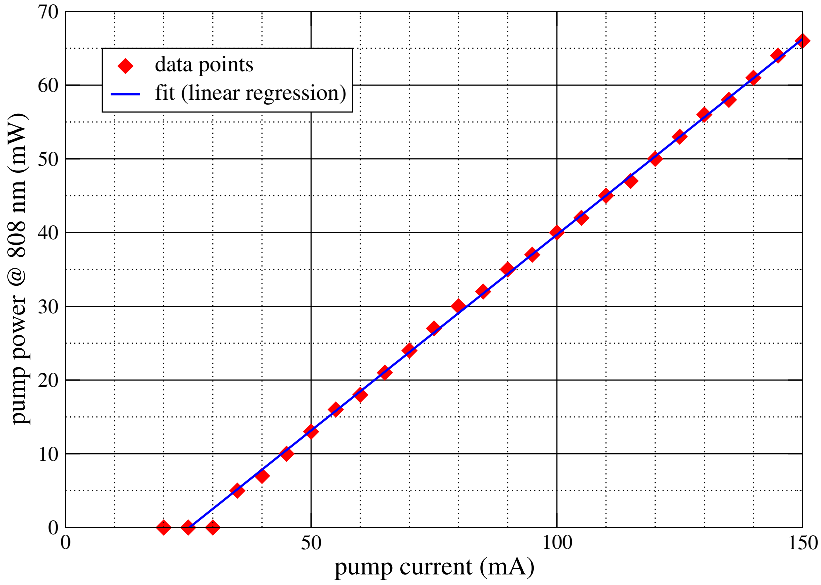

Figure 4.22: Electrical-optical slope of the single-mode laser diode no. BA 080, type 5422-H1-810.

coupling is passed through a telescope (see schematic in figure 4.20) which matches the beam to the ETR-NPRO crystal Eigenmode. When the ETR-NPRO is pumped by the single-mode pump source with a pump power of $P_{\text{pump}} = 70\,\text{mW}$ at $\lambda_{\text{pump}} = 813\,\text{nm}$, the laser emits $P = 10\,\text{mW}$ of laser light at $\lambda = 1064\,\text{nm}$. The laser slope yields an optical-optical efficiency of $\eta_{\text{opt}} \approx 50\,\%$ and is shown in figure 4.24.

As is visible in figure 4.24, the laser slope is not perfectly smooth and also not completely reproducable. This probably owes to the fact that tuning the pump current of the single-mode laser diode results in *mode hops* of the emitted light. A short estimate supports this theory:

Assuming that the length of the semiconductor emitter is 200μm, the resulting free spectral range FSR of the diode laser cavity (formed by the polished front faces, which are 200μm apart) is

$$\text{FSR} = \frac{c}{2L} \Rightarrow \text{FSR} = 7.5 \cdot 10^{11}\,\text{Hz} = 750\,\text{GHz} \quad . \tag{4.8}$$

With wavelenght $\lambda = 808\,\text{nm}$ the frequency ν is

$$\nu = \frac{c}{\lambda} \Leftrightarrow \nu = 370\,\text{THz} \quad . \tag{4.9}$$

The relation

$$\frac{\Delta\nu}{\nu} = \frac{\Delta\lambda}{\lambda} \tag{4.10}$$

holds with $\Delta\nu = \text{FSR}$ and ν, λ as above and yields

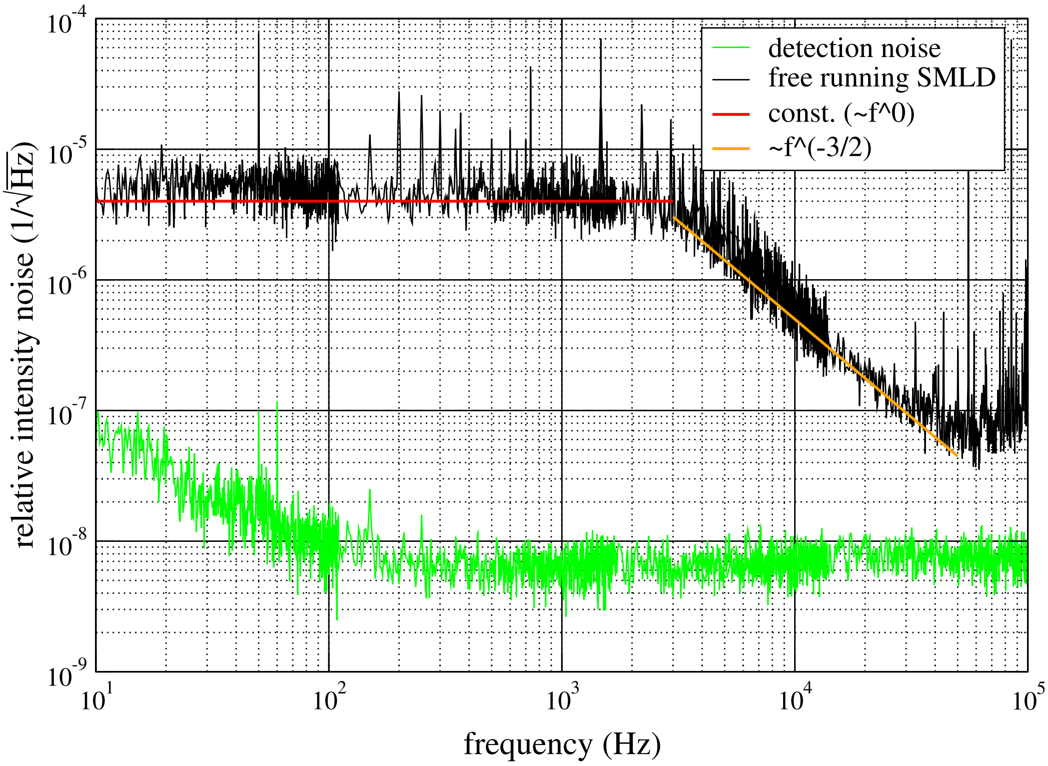

Figure 4.23: Intensity noise of the single-mode laser diode no. BA079, type 5422-H1-810 (black, upper graph) with fits. Detection noise (lower graph) is shown in green.

$$\Delta\lambda = \lambda \cdot \frac{\mathrm{FSR}}{\nu} \quad , \tag{4.11}$$

$$\Delta\lambda = 1.6\,\mathrm{nm} \quad . \tag{4.12}$$

Equation 4.12 states that modehops of the single-mode laser diode are seperated by a wavelength spacing of $\Delta\lambda = 1.6\,\mathrm{nm}$. As the absorption profile of Nd:YAG, shown in figure 4.25 (Mao et al. 2002), varies strongly over wavelength, it is plausible that mode hops of the single-mode laser diode can produce the effect seen in the slope in figure 4.24. On the other hand another effect comes into play: Due to the varying absorption coefficient of the Nd:YAG material over pump wavelength, there is also a variation in the residual pump light behind the NPRO crystal, clearly visible with an infrared viewer. During the measurement of the NPRO slopes no pump light filter was used, so the detected light is always the superposition of (dominating) NPRO light and (residual) pump light.

The resulting free running intensity noise of the fibre-coupled single-mode laser diode pumped NPRO is shown in figure 4.26. It can be seen that the resonant relaxation oscillation lies at a lower frequency (around $f = 130\,\mathrm{kHz}$) than in a conventional NPRO (around $f = 500\,\mathrm{kHz}$). This is explained by the fact that the frequency of the resonant relaxation oscillation is approximately proportional to the square root of the pump power (Svelto

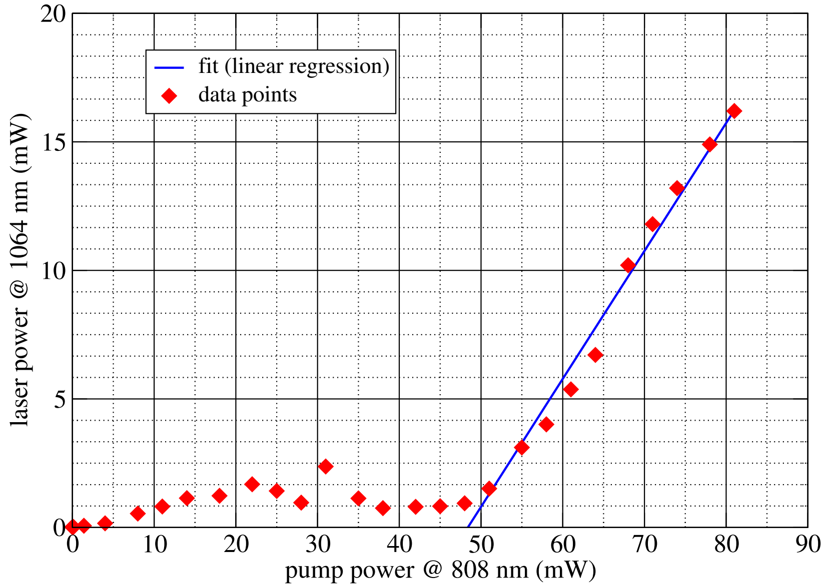

Figure 4.24: Optical-optical slope of the fibre-coupled single-mode laser diode pumped NPRO; diode laser no. BA 080. A modehop of the laser diode can be seen around $P_{\text{pump}} = 35\,\text{mW}$, which causes the laser to cease emitting again above the actual laser threshold of $P_{\text{pump}} = 30\,\text{mW}$. Stable laser emission is achieved for pump powers above $P_{\text{pump}} = 50\,\text{mW}$; the linear regression of the optical-to-optical efficiency (in blue, solid graph) uses only the data points above this pump power. For measurements the laser is operated in the linear regime.

1998; Siegman 1986), and the available pump power for the single-mode NPRO is much lower than that of a laser diode array pumped NPRO.

The single-mode NPRO is not equipped with a piezo-electric actuator contacted to the crystal. The crystal temperature, however, can be controlled by use of a Peltier element beneath the crystal and a temperature controller from InnoLight GmbH, with an accuracy on the order of millikelvin. In order to be able to use the pump current as an actuator for the laser system it is necessary to provide a modulation input for current modulation. As single-mode laser diodes are especially prone to fatal accidents caused by electrical transients, special care has to be taken when modulating the pump current. It has to be made sure that the current driver is well de-coupled from any parasitic ground and that switching transients are avoided. The design of the control electronics necessary to fulfil these requirements is described in appendix B. The *modulation box* constructed directly next to the single-mode laser diode was built at Schäfter & Kirchhoff GmbH by a design from the author in cooperation with InnoLight GmbH; the pin connections are given in table 4.1.

Experiments conducted on the prototype laser system are described in the following section.

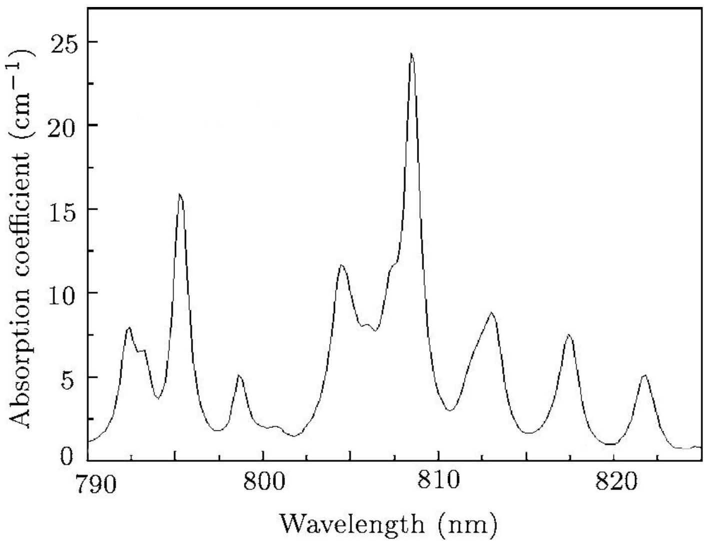

Figure 4.25: Absorption spectrum of Nd:YAG with a concentration of 3.0 at.% , taken from (Mao et al. 2002).

4.4.2. Optical setup

Experiments investigating the effects of a single-mode pump on the NPRO need a variety of analysis tools: different photodetectors for the detection of intensity noise and heterodyne control signals as well as different optical cavities for frequency analysis. This section will deliver a description of the optical setup for the various experiments conducted on the single-mode NPRO .

For the above described tasks one needs at least the following tools:

- a photodetector for detection of a fraction of the pump light,
- a photodetector for detection of a fraction of the single-mode NPRO light,
- a rigid optical resonator as a reference to frequency stabilise the single-mode NPRO by means of the current lock technique,
- a photodetector in reflection of this cavity for the control loop,
- a second optical resonator for independent frequency noise analysis,
- a photodetector in reflection of the second cavity for the control loop.

The optical resonators are explained in the following; for an overview of the implemented photodetectors see appendix C.

The optical resonators used in these experiments were designed in our group and built by REO; they are extensively used in the laser lab as well as at the site of the gravitational wave detector GEO 600 and at the LaserZentrumHannover e.V. for laser beam analysis and stabilisation purposes. The two most commonly used resonators are described here.

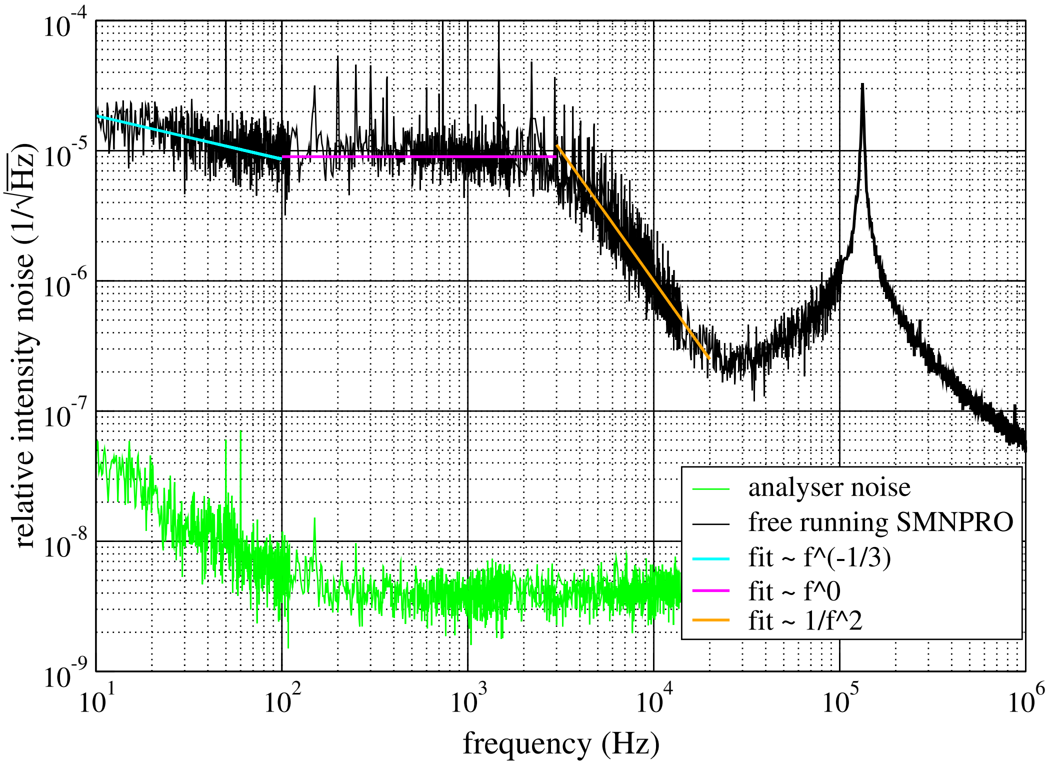

Figure 4.26: Free running intensity noise of the fibre-coupled single-mode laser diode pumped NPRO (shown in black, upper graph) with fits. Detection noise (lower graph) is shown in green.

Reference cavity

The so-called *reference cavity* is a rigid three-mirror optical ring resonator with ultra-high finesse ($F \approx 58000$). Ring resonators display the obvious advantage that light leaving the cavity (either reflected or transmitted) uses a different beam path than the incoming beam. From a controls point of view this is a convenient optical simplification. Another advantage is the fact that back reflections into the laser are avoided.

There is no actuator for the length of the reference cavity. Instead, the resonator is quasi-monolithically constructed of ULE (an ultra-low-expansion glass by Corning) to ensure the highest possible temperature stability. Also, the resonator is placed in ultra-high vacuum ($p \approx 10^{-9}$ mbar) to inhibit strongly disturbing effects of air currents and accoustics.

Mode cleaner

The *mode cleaner* has a setup similar to that of the reference cavity, as it also is a three-mirror optical ring resonator. An alias for the mode cleaner is *pre-mode cleaner* (in order to be able to differentiate between the suspended mode cleaners at the site of GEO 600 and the table top device described here). There are three different configurations of this resonator: One with an aluminum spacer, one with a spacer made of Invar, the last made of ULE; the latter two designs are optimised for better thermal stability. The three mirrors are glued to the spacer. The finesse of the mode cleaner is $F_s \approx 4000$ for the s-polarisation and $F_p \approx 200$ for

purpose	connector type	pin connections
current modulation	SMA (gold)	core: to LD anode tab: to LD cathode
pump light monitor	Binder 712	1: monitor photodiode anode 2: n.c. 3: monitor photodiode cathode
drive current	Binder 680	1: LD anode 2: peltier anode 3: NTC 4: NTC 5: peltier cathode 6: laser diode cathode 7: n.c.

Table 4.1: Pin assignment of the modulation box for the single-mode laser diode.

the p-polarisation. The mode cleaner is commonly used for beam quality analysis of the various laser systems, but can also be used as a frequency reference or frequency analyser. This can only be achieved, though, if the mode cleaner is placed in vacuum. In air the stability of the mode cleaner is not sufficient for frequency stabilisation of an NPRO, as the inherent frequency stability of the NPRO then exceeds that of the resonator.

A more complete overview of the optical resonators (technical details, schematics, photographs) can be found in (Quetschke 2003; Brozek 1999).

4.5. Pump light stabilisation on the single-mode laser diode pumped NPRO

As mentioned at the beginning of this chapter, there are two experimental paths to be pursued on the single-mode NPRO: current lock of the single-mode NPRO to the reference cavity and pump light stabilisation of the single-mode NPRO. The latter is described in this section. The results of section 4.3.3 showed that pump light stabilisation of a multi-mode pumped NPRO does not entail a suppression of the NPRO intensity noise. As described before, the reason for this unfortunate fact are the spatial inhomogeneities of the pump beam which vary with time. This is remedied by the design of the single-mode NPRO, which employs a single-mode laser diode as its pump source (the setup is shown in figure 4.20). Pump light stabilisation of the single-mode NPRO should now lead to a suppression of pump intensity noise as well as NPRO intensity noise. The effect on NPRO frequency noise is to be determined.

4.5.1. Experimental setup

For the pump light stabilisation the following optical setup (figure 4.27) was realised: The light of the single-mode NPRO is modematched into the mode cleaner. A small fraction of the NPRO light is detected by a photodetector behind a pick-off plate (an uncoated substrate made of BK7 with a wegde, angle 2°). The internal monitor photodiode of the single-mode laser diode is used for detection of the pump intensity noise. The photo current produced in the monitor photodiode is fed to the input stage of the pump light stabilisation electronics (for a detailed description of the electronics see appendix B), where the current is converted into a voltage by a transimpedance amplifier stage. The resulting control signal at the end of the electronics is passed to the end stage, a transistor current bypass, which is directly connected to the modulation input of the single-mode laser diode. The resulting in-loop intensity noise of the pump laser diode is detected on the monitor photodiode. Due to the compact setup it was not possible to detect the out-of-loop intensity noise of the pump laser diode on an independent photodetector, but detection of the single-mode NPRO intensity noise is the best possible measure of out-of-loop suppression. For measurement of the frequency noise of the single-mode NPRO with and without pump light stabilisation the mode cleaner is locked to the single-mode NPRO via its piezo-electric transducer. The error and the feedback signal of this control loop are a measure for the frequency noise of the single-mode NPRO and deliver a frequency noise spectrum when adequately calibrated.

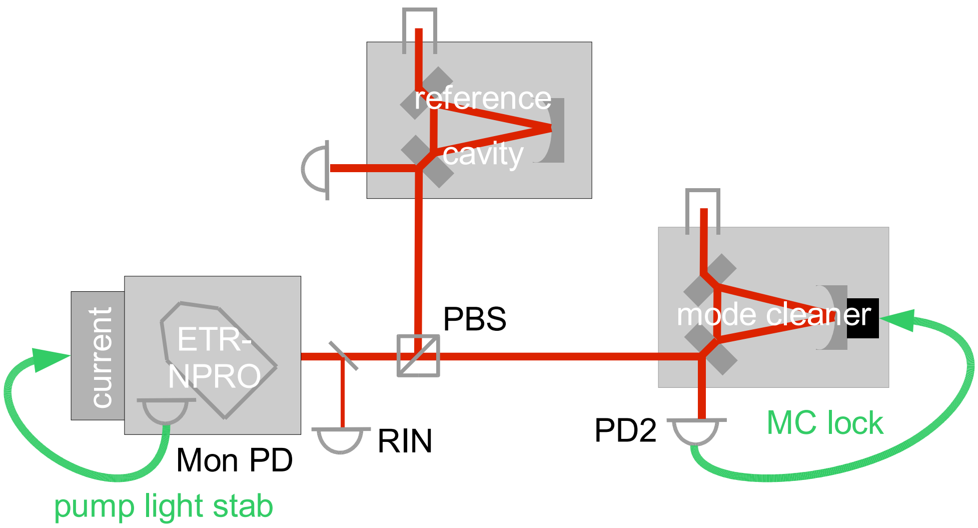

Figure 4.27: Schematic of the optical setup around the single-mode NPRO for pump light stabilisation. RIN: photodetector for measurement of relative intensity noise, PD2: photodetector in reflection of mode cleaner (for Pound-Drever-Hall method), MonPD: internal monitor photodiode in single-mode laser diode.

4.5.2. Results and discussion

Figure 4.28 shows the free running and in-loop intensity noise of the single-mode laser diode. Obviously the pump light stabilisation electronics works as designed, a suppression of the intensity noise by a factor of 40 dB is achieved. Unity gain of the loop is here $f \approx$ 50 kHz. The structure in the in-loop intensity noise of the single-mode laser diode visible at 3 kHz might be caused by saturation of an electronic stage; a structure at this frequency is well-known as a feature of the current driver electronics for the laser diode. In an in-loop measurement noise coupling into the loop at any point should be reduced by the loop gain of the pump light stabilisation electronics.

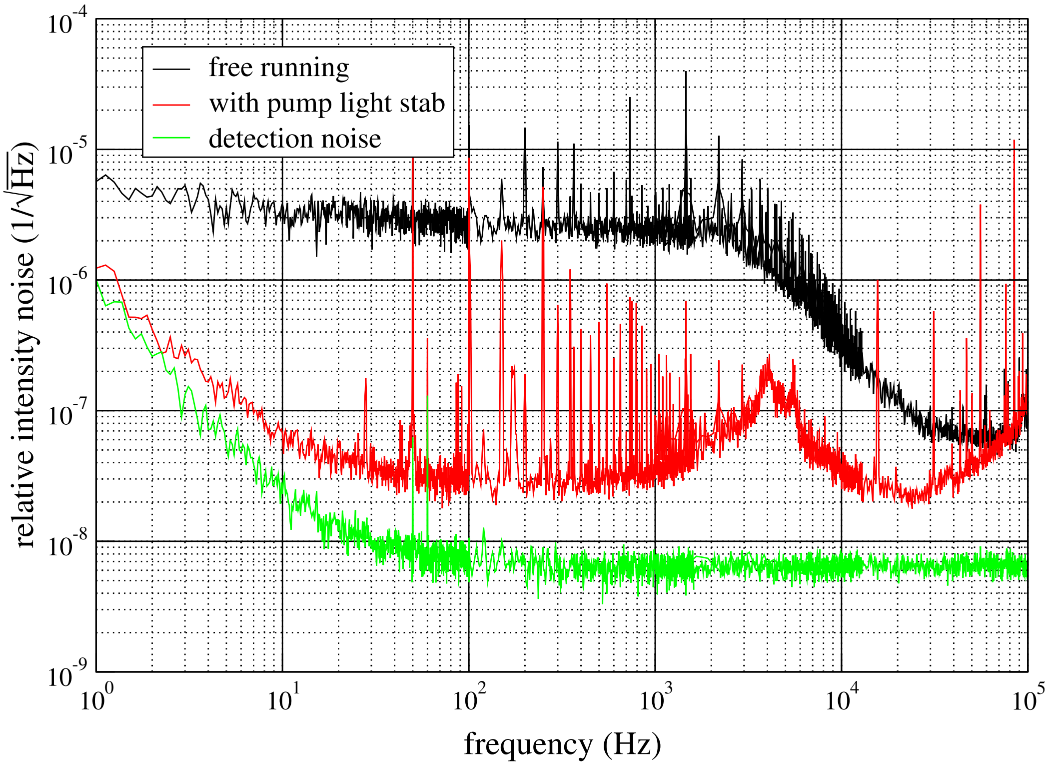

Figure 4.28: In-loop intensity noise of the single-mode laser diode with and without active pump light stabilisation. The free running intensity noise of the single-mode laser diode is shown in black (upper graph), the in-loop intensity noise in red (middle graph). The structure at 3 kHz visible in the in-loop measurement is likely to be caused by saturation of an electronic stage, probably the current driver electronics for the laser diode, though in-loop any noise should be reduced by the loop gain of the pump light stabilisation electronics. Detection noise is plotted in green (lower graph).

The resulting intensity noise of the single-mode NPRO with and without pump light stabilisation is displayed in figure 4.29. It is visible that the intensity noise suppression of the pump light results in an intensity noise suppression of the NPRO (by $\geq$ 20 dB) in this system, This is an unprecedented result [4]. As opposed to figure 4.28 unity gain is at a lower frequency ($f \approx 15\,\mathrm{kHz}$), as the proportional gain was chosen differently. The increase in intensity noise for frequencies above $f = 10\,\mathrm{kHz}$ is caused by the resonance structure of the resonant relaxation oscillations at $f \approx 100\,\mathrm{kHz}$. Acoustic noise coupling into the loop at frequencies between $f = 100\,\mathrm{Hz}$ and $f = 1\,\mathrm{kHz}$ cause additional structures in the spectrum. The overall intensity noise suppression in the single-mode NPRO is lower than the in-loop

[4]As seen in section4.3 pump light stabilisation of a multi-mode laser diode array does not entail an intensity noise reduction of the NPRO.

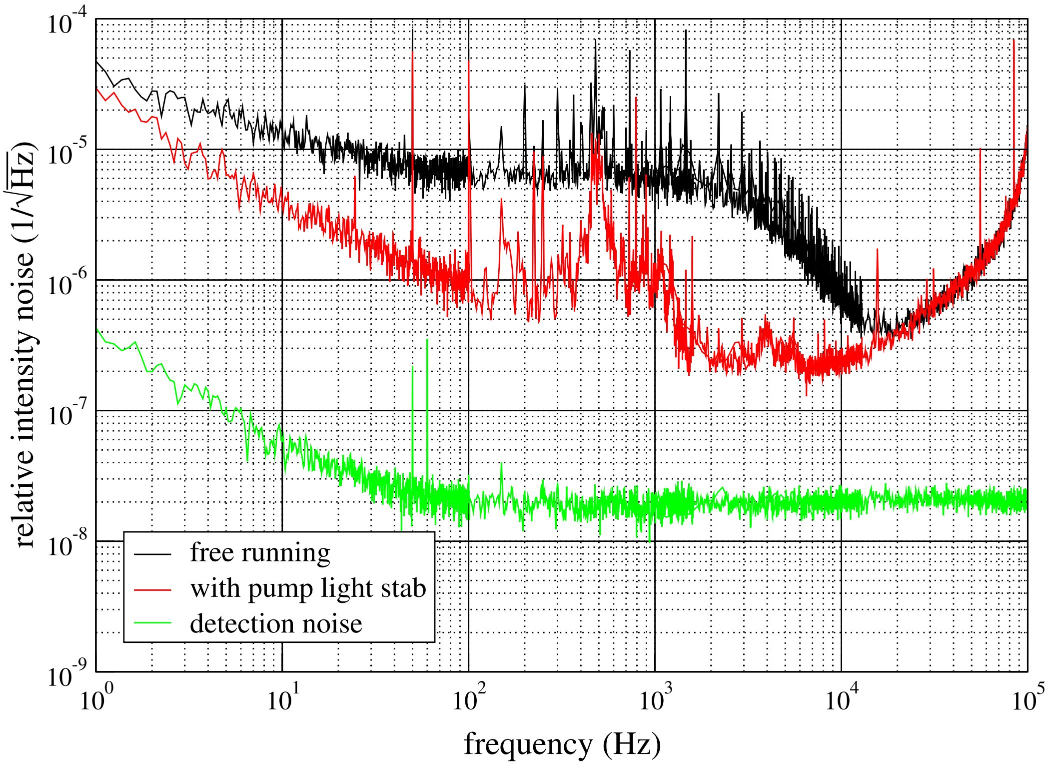

Figure 4.29: Relative intensity noise of the single-mode NPRO with and without active pump light stabilisation. The free running intensity noise of the single-mode NPRO is shown in black (upper graph), the in-loop intensity noise in red (middle graph). The increase in intensity noise above unity gain is caused by the resonant relaxation oscillations of the NPRO, the noise in the in-loop graph between 100 Hz and 1 kHz is caused by acoustics. Detection noise is plotted in green (lower graph).

intensity noise reduction of the single-mode laser diode, especially in the frequency range below $f = 100\,\text{Hz}$. This is most likely a manifestation of 1/f noise, as no other structures pointing to resonances of any kind are discernible.

The frequency noise of the single-mode NPRO can be measured with the mode cleaner, as described in the above section. This measurement yields the frequency noise spectrum shown in figure 4.30, where it is clearly visible that the NPRO intensity noise suppression of 20 dB reached via pump light stabilisation is passed on to the frequency noise! A reduction of the frequency noise of the single-mode NPRO with active pump light stabilisation in the same order of magnitude as in the NPRO intensity noise is achieved by this stabilisation. This is proof of the coupling of intensity noise and frequency noise in the single-mode NPRO based on pump light intensity fluctuations. Unity gain again lies at $f \approx 15\,\text{kHz}$. The acoustics coupling into the loop between $f = 100\,\text{Hz}$ and $f = 1\,\text{kHz}$ also appear in the frequency noise spectrum. For frequencies above $f = 10\,\text{kHz}$ the measured frequency noise spectra are limited by the electronic noise of the demodulation electronics.

The results of the pump light stabilisation experiments with the single-mode NPRO are

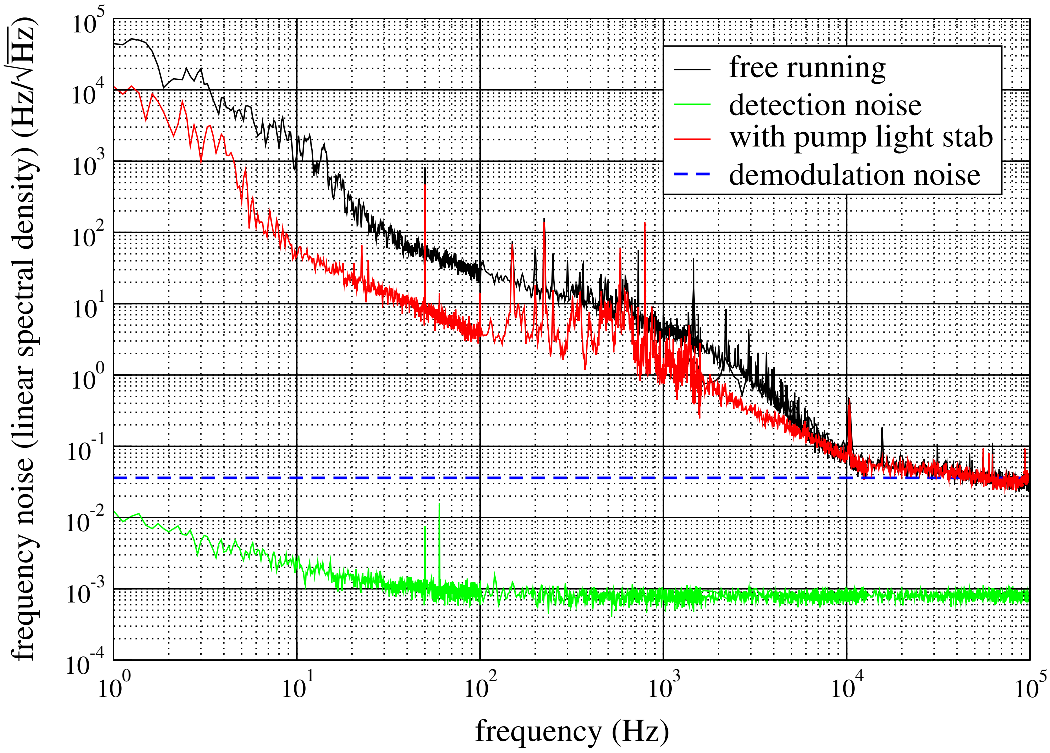

Figure 4.30: Frequency noise of the single-mode NPRO with and without active pump light stabilisation. The free running frequency noise of the single-mode NPRO is shown in black (upper graph), the in-loop frequency noise in red (middle graph). The excess frequency noise between 100 Hz and 1 kHz is caused by acoustics; the frequency noise is limited above 10 kHz by the noise of the demodulation electronics (blue, dashed). Detection noise is plotted in green (lower graph).

to be submitted to Applied Physics B (Heurs et al.).

4.6. Current lock on the single-mode laser diode pumped NPRO

Section 4.5 showed that intensity stabilisation of the single-mode NPRO pump source results in a reduction of NPRO intensity noise as well as frequency noise. Current lock of the single-mode NPRO pursues the alternative experimental path: The frequency fluctuations of the laser are detected with a Pound-Drever-Hall-scheme and suppressed by feedback to the drive current of the single-mode pump source. Due to the current lock effect a reduction of NPRO intensity noise is to be expected, the degree of which is yet to be determined. This section deals with the current lock experiments conducted on the single-mode NPRO and gives a discussion of the results achieved.

4.6.1. Experimental setup

To frequency stabilise the single-mode NPRO via current lock the following optical/electrical configuration was realised: The light of the free running single-mode NPRO is passed through a resonant electro-optic modulator (New Focus, model 4003 M), where phase modulation sidebands at $\Omega = 29.02\,\text{MHz}$ are imprinted on the light. The beam is then divided into two nearly equal fractions by a (polarisation independent) power beam splitter. The transmitted light is mode matched into the reference cavity. The light in reflection of the reference cavity is detected on a photodetector, the signal is appropriately phase shifted and then demodulated by a mixer. The resulting error signal is fed to the current lock control electronics (see appendix B), and the control signal reaches the end stage of the electronics. The end stage is connected to the modulation box next to the laser diode. The control signal causes the correct amount of drive current to be bypassed from the laser diode; the end stage is a current sink, as this design provides higher saftey against accidental application of reversed voltages or transients to the sensitive laser diode. For a schematic of the control loop see figure 4.31.

4.6.2. Results and discussion

Current lock of the single-mode NPRO to the reference cavity results in a reduction of the in-loop frequency noise. This is not a surprising result, as the suppression of noise in the control loop is easily achievable (for a treatment of the in-loop / out-of-loop problem see section 2.5) and only limited by the loop gain. In figure 4.32 it can be seen that the free running frequency noise of the single-mode NPRO goes roughly as 1/f. A more detailed anaylsis shows that the frequency noise spectrum has to be divided into sections, where the characteristics vary. In the frequency band from 1 Hz to 30 Hz the linear spectral density of frequency noise is proportional to $1/f^2$, from 30 Hz to 3 kHz it goes as 1/f, from 3 kHz to 10 kHz it again falls as $1/f^2$ (from 10 kHz on the measurement is limited by electronic noise of the demodulation scheme). This behaviour of the frequency noise is atypical for an NPRO. It might be explained in the following way: (Day 1990) shows, that white pump light intensity noise is the cause for 1/f frequency noise in an NPRO; a causality based in the thermal lowpass of the active material. The pump light intensity noise of the single-mode NPRO, though, is not frequency independent, but exhibits the intensity noise spectrum shown in figure 4.26. It is therefore not surprising to find that f^n pump light intensity noise

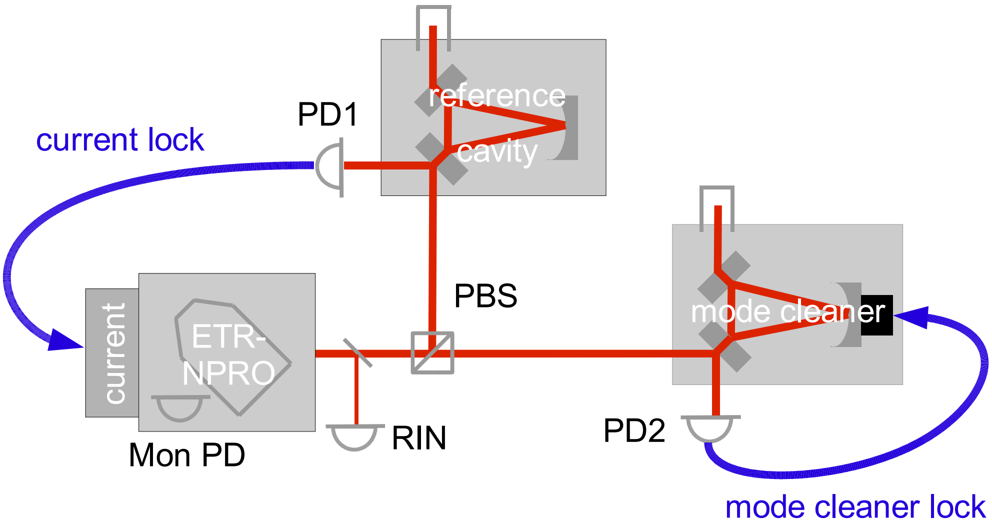

Figure 4.31: Schematic of the optical setup around the single-mode NPRO for current lock. RIN: photodetector for measurement of relative intensity noise, PD1: photodetector in reflection of reference cavity (for Pound-Drever-Hall method), MonPD: internal monitor photodiode in single-mode laser diode.

drives f^{n-1} frequency noise of the single-mode laser diode pumped NPRO. This hypothesis deserves further investigation in the future.

The in-loop frequency noise reduction of the single-mode NPRO shown in figure 4.32 corresponds to the open loop gain of the current lock electronics: The free running frequency noise is suppressed by a factor of $\geq$ 60 dB at 10 Hz. Unity gain of the loop is approximately $f = 4$ kHz. The measurement of frequency noise above $f \approx 10$ kHz is limited by the electronic noise of the demodulation path [5].

Stabilising the mode cleaner via its piezo-electric actuator to the single-mode NPRO (which itself is stabilised to the reference cavity via current lock) gives a measure of the out-of-loop frequency noise of the current lock stabilised single-mode NPRO and is shown in figure 4.33. The out-of-loop frequency noise suppression is around 30 dB in the bandwidth of the control loop. At low Fourier frequencies the out-of-loop frequency noise is limited by detection noise; for Fourier frequencies as of approximately $f = 100$ Hz the suppression is gain limited. As of $f = 10$ kHz the measurement is limited by the electronic noise of the demodulation path. Acoustic noise at frequencies between $f = 100$ Hz and $f = 1$ kHz couples into the loop via the non-common beam path, clearly visible as structures in the out-of-loop frequency noise spectrum.

The resulting intensity noise of the frequency stabilised single-mode NPRO can be seen in figure 4.34. The coupling between frequency noise and intensity noise in the single-mode NPRO holds and yields an intensity noise suppression in current lock of the same degree

[5]Above unity gain the error point (the output of the mixer) is a measure for the free running frequency noise, but below unity gain the frequency noise is proportional to the feedback signal and is therefore not limited by demodulation noise.

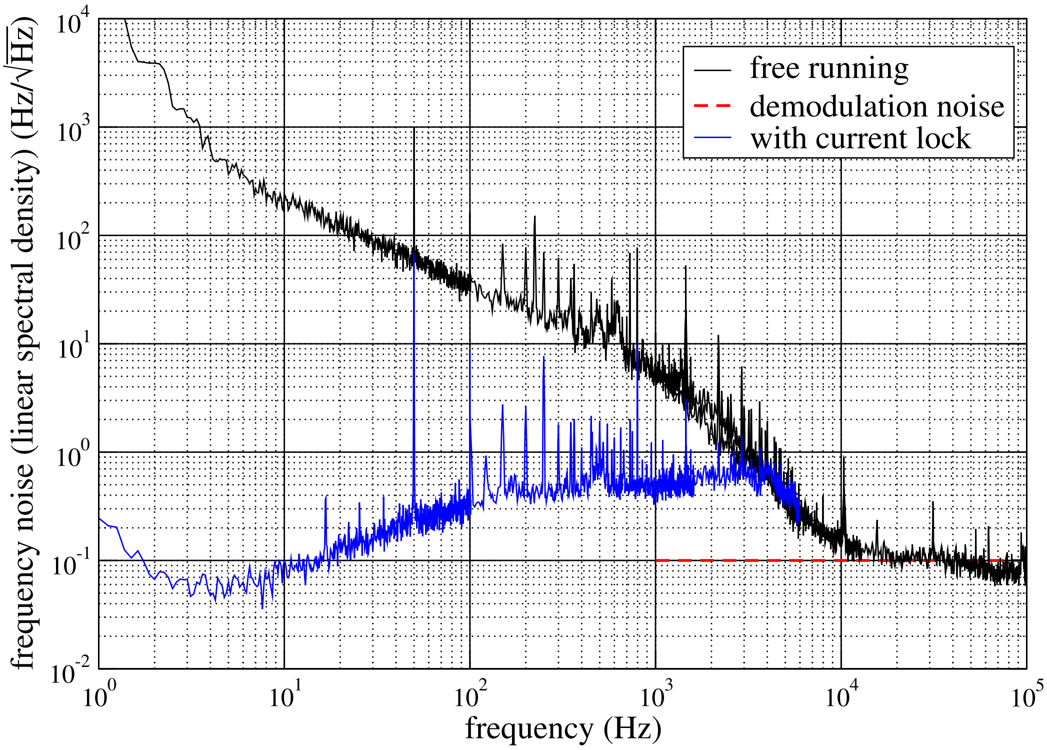

Figure 4.32: In-loop frequency noise of the single-mode NPRO with and without active current lock. The free running frequency noise of the single-mode NPRO is shown in black (upper graph), the in-loop frequency noise in blue (lower graph). Unity gain lies at $f \approx 4\,\mathrm{kHz}$. Above 10 kHz the frequency noise measurement is limited by the noise of the demodulation electronics (red, dashed).

as the out-of-loop frequency noise suppression, namely up to 30 dB. A result of this kind is completely unprecedented in the field.

The results of this section show that control of the spatially well defined and temporally controlled laser diode pump source leads to a significant simultaneous reduction of both frequency and intensity fluctuations when merely the frequency noise is detected and reduced by feedback to the laser diode pump current. The cause for this is the coupling between laser intensity and frequency noise. Pump light intensity fluctuations drive NPRO intensity noise in the frequency regime below the resonant relaxation oscillation. On the other hand the heat deposited in the laser active material by the pump source with temporally varying intensity causes fluctuations of the optical path length for the laser light, which in turn leads to laser frequency noise. In the single-mode NPRO both effects are coupled. The results of the current lock experiments conducted with the single-mode NPRO have been published in Optics Letters (Heurs et al. 2004).

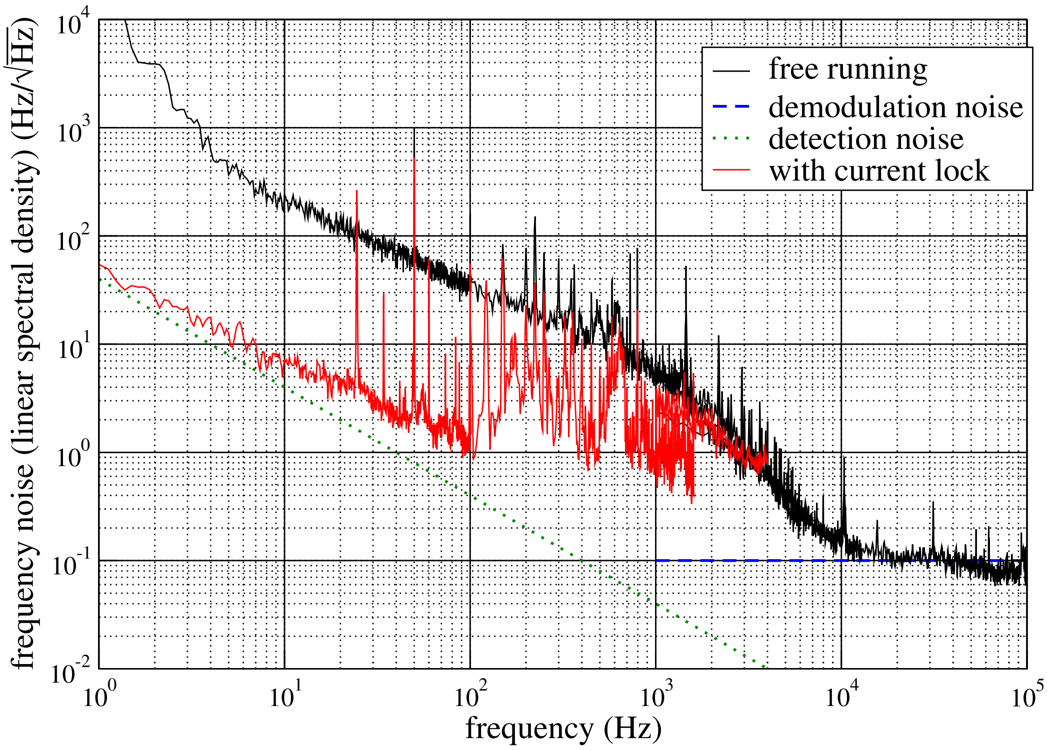

Figure 4.33: Out-of-loop frequency noise of the single-mode NPRO with and without active current lock. The free running frequency noise of the single-mode NPRO is shown in black (upper graph), the out-of-loop frequency noise in red (lower graph). Above 10 kHz the frequency noise is limited by the noise of the demodulation electronics (blue, dashed). For frequencies below 100 Hz the out-of-loop measurement is limited by detection noise (dark green, dotted). The excess frequency noise in the out-of-loop measurement between 100 Hz and 1 kHz is caused by acoustics coupling into the non-common beam path (between in-loop and out-of-loop detector.)

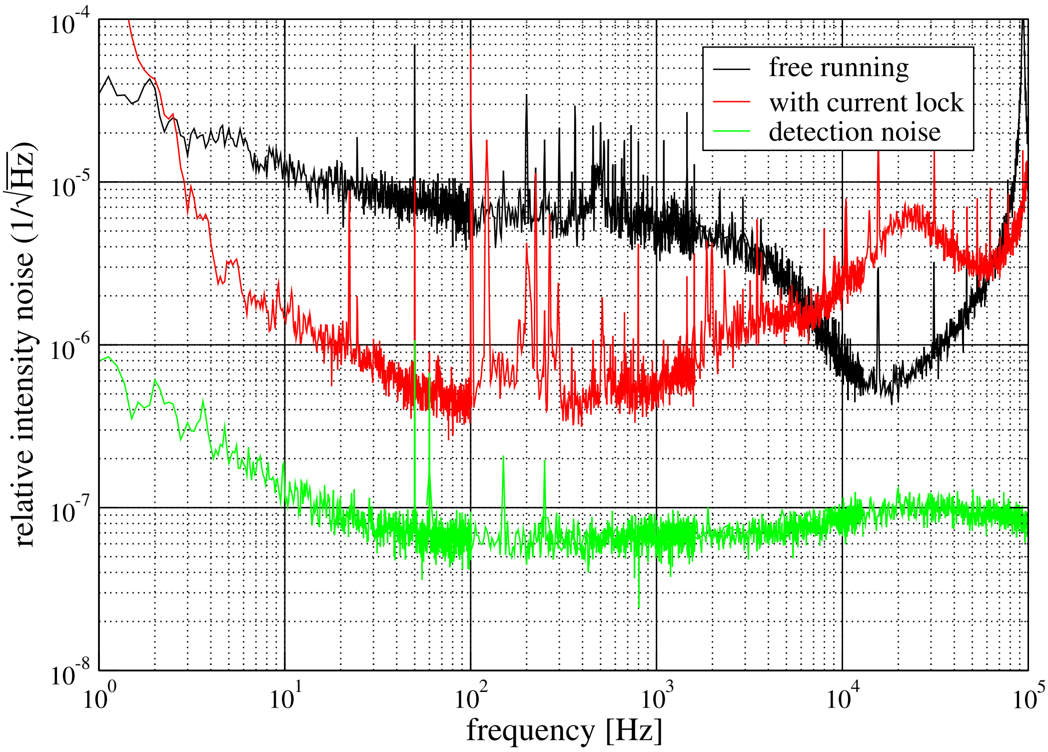

Figure 4.34: Relative intensity noise of the single-mode NPRO with and without active current lock. The free running intensity noise of the single-mode NPRO is shown in black (upper graph), the intensity noise with active current lock in red (middle graph). The structure around 22 kHz is caused by the servo bump of the current lock stabilisation. Detection noise is plotted in green (lower graph).

4.7. Increasing the control bandwidth - simultaneous reduction of intensity and frequency noise in the single-mode NPRO up to the resonant relaxation oscillations

The measurements conducted with the single-mode NPRO in section 4.5 (pump light stabilisation) and section 4.6 (current lock) show unprecedented results in the simultaneous reduction of frequency and intensity noise. Due to the design of the control electronics the achievable bandwidths are limited to frequencies below the resonant relaxation oscillations, though. It is desirable to increase the bandwidth of electronics to determine wether a stabilisation beyond the resonant relaxation oscillations is possible. In principle this should be the case since the transfer functions from pump current to pump intensity, NPRO intensity and NPRO frequency respectively are defined and can be measured.

In addition to this it is interesting to know wether a stabilisation of the single-mode NPRO intensity noise (not the pump source) leads to a significant reduction of its frequency noise. In a commercial, multi-mode pumped NPRO the noise eater electronics (see appendix A) reduces the resonant relaxation oscillations and also leads to a reduction of low frequency intensity noise to a degree of typically 20 dB. Additionally it causes a slight reduction in frequency noise (of less than a factor of two) , as shown in (Brozek 1999).

4.7.1. Experimental setup

A noise eater electronics was adapted for use with the single-mode NPRO; the optical setup with the noise eater control loop and the mode cleaner loop for the measurement of frequency noise is shown in figure 4.35.

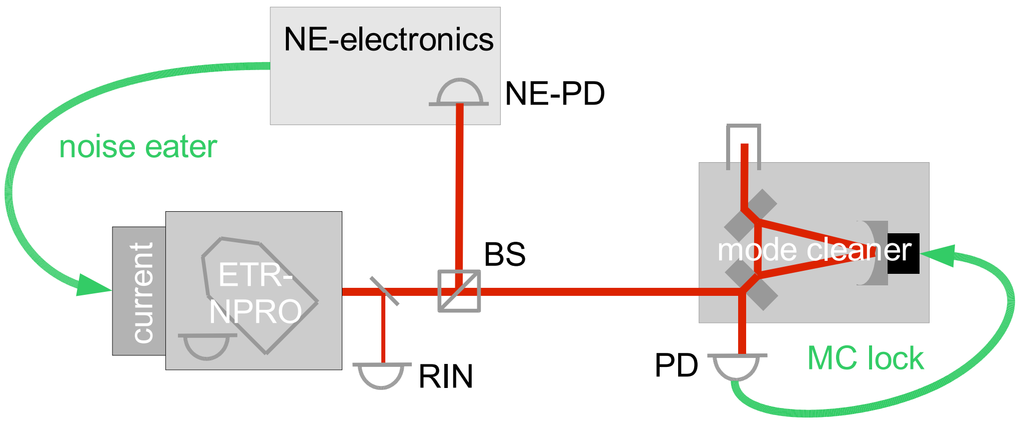

Figure 4.35: Schematic of the noise eater intensity stabilisation experiment on the single-mode NPRO. RIN: photodetector used for out-of-loop measurement of the NPRO intensity noise, BS: power beam splitter, NE-PD: photodetector implemented on the noise eater electronics, PD: photodetector in reflection of the mode cleaner for measurement of frequency noise.

A fraction of the single-mode NPRO light ($P \approx 1\,\mathrm{mW}$) is detected by the photodiode (an InGaAs device from PerkinElmer, type C30641 (PerkinElmer Optoelectronics 2001)) implemented on the noise eater electronics. The noise eater has a current driver end stage and its output is contacted in parallel to the single-mode laser diode. The dynamic range of the end stage has to be modified for this system.

A wedged glass plate in the single-mode NPRO light path provides a pick-off beam for the measurement of intensity noise. The photodetector with high bandwidth (see appendix C) employs an InGaAs photodiode type C30641 (PerkinElmer Optoelectronics 2001) and delivers an out-of-loop measurement of the single-mode NPRO intensity noise.

The remaining light from the single-mode NPRO is modematched into the mode cleaner which is used as an analyser cavity for the frequency noise of the laser. By means of a Pound-Drever-Hall detection scheme the mode cleaner is locked to the single-mode NPRO. Adequately calibrated the feedback and the error point signal of the mode cleaner locking loop then yield the frequency noise of the single-mode NPRO with and without active noise eater.

4.7.2. Results and discussion

The resulting out-of-loop intensity noise of the single-mode NPRO with active noise eater is shown in figure 4.36. The noise eater completely damps out the resonant relaxation oscillations at $f = 120\,\mathrm{kHz}$ and also reduces the intensity noise by more than 20 dB at $f = 1\,\mathrm{kHz}$. The increase in intensity noise at $f = 800\,\mathrm{kHz}$ is the servo bump. The structure at $f \approx 4\,\mathrm{kHz}$ in the free running intensity noise is caused by the drive electronics of the single-mode laser diode.

The frequency noise of the single-mode NPRO with and without active noise eater is measured by locking the mode cleaner to the laser by feeding back to the piezo-electric transducer of the mode cleaner. The resulting frequency noise can be seen in figure 4.37. In average the reduction in frequency noise is considerably weaker than the intensity noise suppression, though the resonant relaxation oscillations in the frequency noise spectrum at $f = 120\,\mathrm{kHz}$ are completely suppressed. An average suppression of a factor of three is attained in the frequency band from 30 Hz to 150 Hz and from 2 kHz to 4 kHz when the noise eater is active. The lesser frequency noise reduction in comparison to the intensity noise suppression is partly caused by excess noise coupling into the detection in the non-common beam path behind the beam splitter between noise eater and mode cleaner (compare figure 4.35). The path length to the mode cleaner is not minimised due to technical reasons. Vibrations of optical components and fluctuations in the index of refraction of the air cause disturbances which compromise the measurement. Additionally the measurement is most likely to be limited by the detection noise of the mode cleaner, as investigations in our group point to the fact that the intrinsic frequency noise of the mode cleaner in vacuum lies at the same level as the reduced frequency noise in figure 4.37 for frequencies below $f = 10\,\mathrm{kHz}$.

The above measurements demonstrate the possibility of stabilising frequency and intensity of the single-mode NPRO simultaneously and with control bandwidths beyond the resonant relaxation oscillations. The transfer of the achieved intensity noise suppression to the frequency noise is worsened by incoupling noise, though. The next logical step is therefore to stabilise the frequency of the single-mode NPRO with a control bandwidth larger

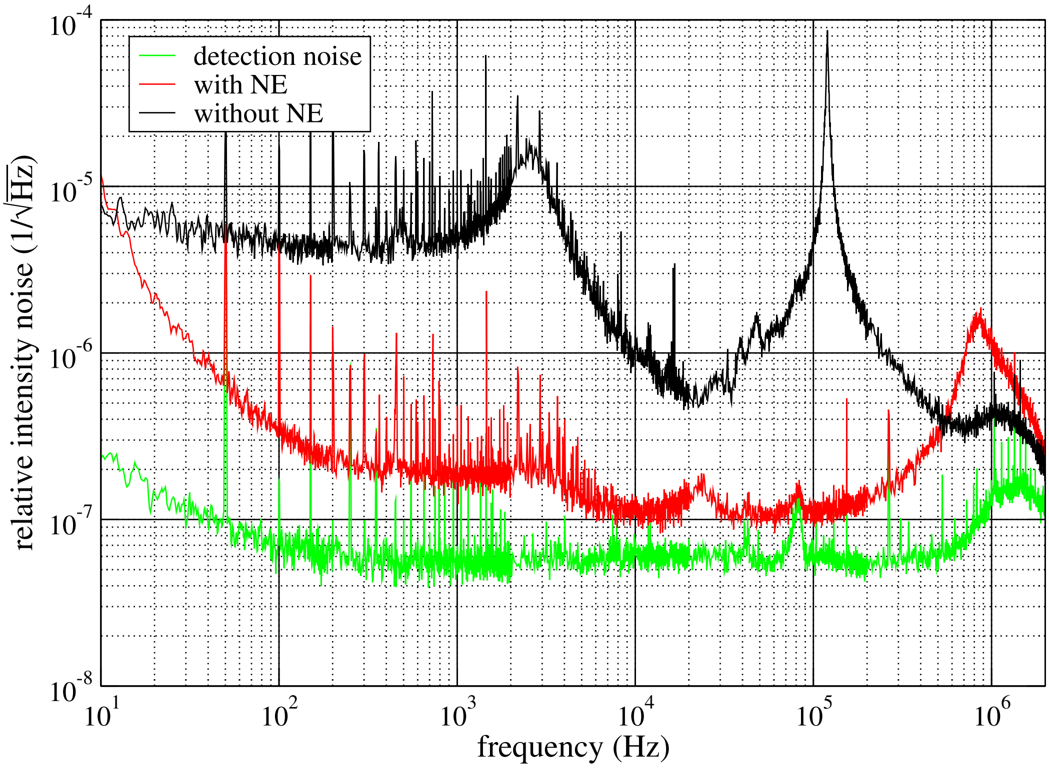

Figure 4.36: Relative intensity noise of the single-mode NPRO with and without noise eater. The free running intensity noise of the single-mode NPRO is shown in black (upper graph), the out-of-loop intensity noise with active noise eater in red (middle graph). The structure around 800 kHz is caused by the servo bump of the noise eater electronics. Detection noise is plotted in green (lower graph).

than the resonant relaxation oscillation frequency and to determine the degree of simultaneously achievable intensity noise reduction. This will be subject of ongoing work.

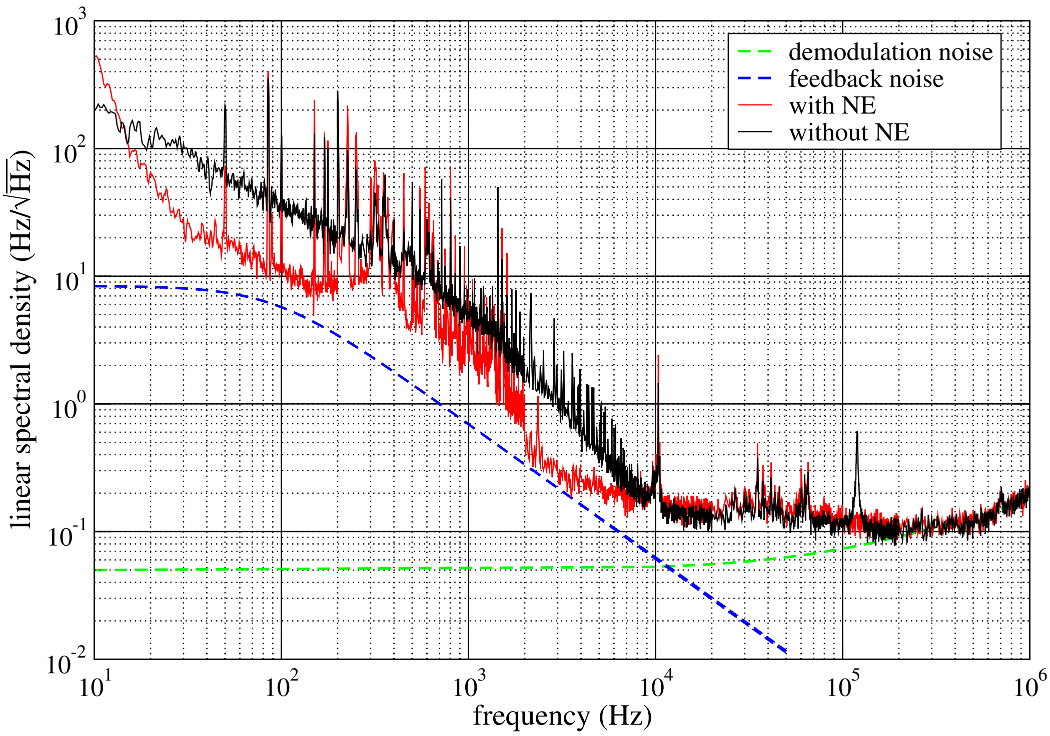

Figure 4.37: Frequency noise of the single-mode NPRO with and without noise eater. The free running frequency noise of the single-mode NPRO is shown in black (upper graph), the frequency noise with active noise eater in red (lower graph). Demodulation noise (lower fit, green dashed) contains noise of the mixer and the photodetector, HVmon noise is shown in blue, dashed (upper fit). The resonant relaxation oscillations visible in the free running frequency noise at 120 kHz are completely suppressed by the noise eater. An average suppression of a factor of three is attained in the frequency band from 30 Hz to 150 Hz and from 2 kHz to 4 kHz when the noise eater is active. The measurement is bound to be limited by detection noise of the mode cleaner. Excess noise is introduced in the beam path between the noise eater and the mode cleaner , clearly visible in the spectrum between 200 Hz and 2 kHz.

5. Prospects

This thesis demonstrates that laser diode pumped Nd:YAG lasers are superb light sources for precision interferometry. The experiments and their results described in chapter 3 show how the injection locked high power laser system for the interferometric gravitational wave detector GEO 600 is stabilised in its observables laser intensity and frequency to fully comply with the ambitious requirements. The intensity stabilisation is focus of this chapter, describing the realisation of the first and second intensity stabilisation control loop to reach the necessary specifications. With the first loop an out-of-loop intensity stability of $RIN = 2 \cdot 10^{-8} / \sqrt{\text{Hz}}$ at $f = 2\,\text{kHz}$ is reached. In the identical lab laser system intensity stabilisation with the first loop and a detection scheme in vacuum yields an out-of-loop intensity stability of $RIN = 3 \cdot 10^{-8} / \sqrt{\text{Hz}}$ from $f = 100\,\text{Hz}$ to from $f = 1\,\text{kHz}$. The second loop realised at the site of GEO 600 achieves an out-of-loop intensity stability of $RIN = 5 \cdot 10^{-8} / \sqrt{\text{Hz}}$ at $f = 500\,\text{Hz}$.

and a detection scheme in vacuum

Besides being well suited for implementation in precision experiments, monolithic laser diode pumped NPROs are an interesting and worthy experimentation subject of fundamental physics. The experiments conducted in chapter 4 yield outstanding new results in the field of simultaneous laser stabilisation. The novelty of these results lies in the large degree of simultaneous stabilisation of two seemingly unconnected observables, the laser intensity and the laser frequency, by detection of and feedback to only one of the two. Simultaneous noise reductions in the range of 30 dB in frequency and intensity have been realised with the techniques of pump light stabilisation and current lock.

Future generation gravitational wave detectors call for even higher stability of their light sources. It is therefore crucial to understand the limits of the existing stabilisations; only then will we ever be able to reach the fundamental limits of laser stability. The prototype laser system introduced in chapter 4, the single-mode NPRO, opens the door for new stabilisation concepts, posing the possibility of stabilising both laser intensity and frequency by means of merely one stabilisation loop. The single-mode NPRO itself does not supply enough output power to act as e.g. the master laser for an injection locked high power laser system, though. Developments enhancing the output power of the single-mode NPRO must be pursued and might be realised by using a tapered amplifier as a near single-mode pump source with increased pump power of $P_{\text{pump}} \approx 500\,\text{mW}$.

The single-mode NPRO in principle has the potential of allowing for a non-demolition measurement. By detecting solely the frequency of the system and feeding back to the pump current as the actuator, simultaneous intensity noise suppression is achieved with the expected frequency noise reduction. This is accomplished without the need to detect the laser intensity. Under normal conditions intensity stabilisations are shot noise limited, this poses a fundamental limit to the obtainable intensity noise suppression. Shot noise limited frequency stabilisation can in principle be honed to a better stability level: By increasing the steepness of the frequency discriminator (by using an optical cavity with a higher finesse) very high suppressions of frequency noise are feasible. Through the coupling of intensity and frequency noise in the single-mode NPRO the intensity noise can simultaneously be suppressed to or possibly even below the shot noise limit. A step towards this goal will soon be undertook by stabilisation of the single-mode NPRO frequency beyond the resonant relaxation oscillation frequency with enhanced gain and the investigation of its effect on the intensity noise.

Additional attention should be directed toward self-injection locking experiments of the slave laser. Self-injection locking is accomplished by placing a mirror in one of the slave laser output ports. Using an optical resonator instead of the self-injection locking mirror ought to lead to frequency stabilisation of the slave laser. If successful, this scheme would eliminate the need for a master laser, thereby significantly simplifying the laser system.

A. Appendix: The non-planar ring oscillator (NPRO)

The **N**on-**P**lanar **R**ing **O**scillator (NPRO) is a laser diode pumped, monolithic ring laser of high intrinsic frequency and amplitude stability[1]. Due to their performance characteristics (stability, efficiency, reliability) NPROs are destined for high stability applications, for instance as the master laser for the gravitational wave detector GEO 600, as described in chapter 3. Due to its potential in laser stabilisation the NPRO is also subject of ongoing investigations concerning laser dynamics as well as fundamental stabilisation limits, which are described in chapter 4.

The NPRO design is based on the original works by Kane and Byer (Kane and Byer 1985) conducted in the 1980's. Meanwhile various modified NPRO designs exist, differing in laser material, crystal geometry and pump sources. The commercially available NPROs used in this work are of the Mephisto 800-type (InnoLight GmbH 2004) from InnoLight GmbH (www.innolight.de). To supplement the overview given in chapter 3.2.1 the design of the NPRO is treated in more detail in this appendix. The design of the modified NPRO used for the experiments in chapter 4, however, is described there; the differences mainly concern the pump geometry, not the fundamental crystal / resonator design (and thereby the function principle).

The *active medium* of the NPRO is a crystal consisting of a laser-active material (in our case neodymium doped yttrium aluminum garnet (Nd^{3+}:$Y_3Al_5O_{12}$), short Nd:YAG, with a doping concentration of typically 1 %). The crystal dimensions are $3 \times 8 \times 12\,\mathrm{mm}^3$. The geometry of the NPRO crystal can be seen in figure A.1: The pump light with a wavelength of $\lambda_{\mathrm{pump}} = 808\,\mathrm{nm}$ enters the crystal at point A of the front facet, which is anti-reflex coated for the pump wavelength to typically 90 %. The absorption spectrum of Nd:YAG varies strongly with wavelength and also depends on the doping concentration (for an absorption spectrum of Nd:YAG with a doping concentration of 3 % see figure 4.25). The peak neodymium absorption line lies at $\lambda = 808.6\,\mathrm{nm}$, the corresponding absorption coefficient at this pump wavelength is $\alpha = 7.3\,\mathrm{cm}^{-1}$ for a doping concentration of 1 % (Mao et al. 2002). Inserting this value in the Lambert-Beer-law of absorption (Thorne et al. 1999)

$$I(z) = I_0 \cdot e^{-\alpha \cdot z} \quad , \tag{A.1}$$

one sees that all but $1/e^2$ of the initial pump intensity I_0 is absorbed in the Nd:YAG crystal over the first 2.7 mm.

The high *intrinsic frequency stability* of the NPRO is mainly due to its monolithic design: The *laser resonator* is formed by the specially facetted end faces of the laser crystal. There are no external mirrors which introduce mechanical vibrations, thereby causing frequency noise, nor is there the need for frequent re-alignment – a fact which contributes to the high *reliability* of the system. Total internal reflection at the points B, C and D at the rear facets

[1] The older, ambiguous alias for the NPRO, MISER, stands for **M**onolithic **I**solated **S**ingle-**E**nd-**P**umped **R**ing laser. This name emphasises yet other important characteristics of the NPRO, namely the end-pumping scheme as well as the unidirectionality of laser emission by use of the Faraday effect.

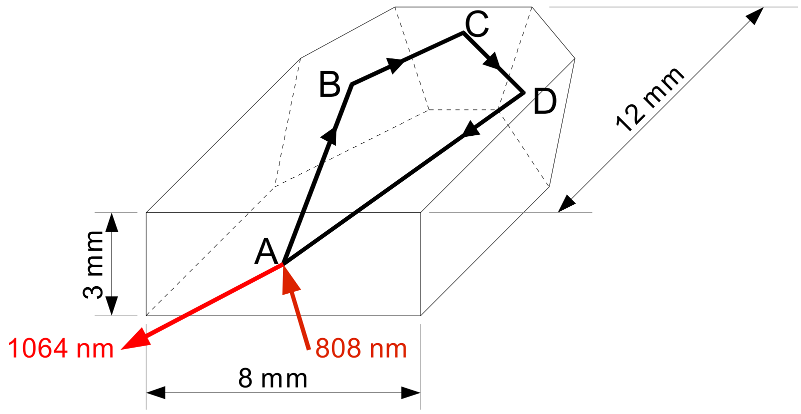

Figure A.1: Schematic of the common NPRO geometry and of the beam path in the crystal. A: point at the front facet where the pump light enters and the laser beam leaves the crystal; B, C and D: points at the rear crystal facets respectively the top surface (C) where the beam path is defined by total internal reflection at the crystal boundaries.

of the crystal leads to the illustrated beam path of the laser emission at $\lambda = 1064\,\text{nm}$. The output face of the crystal has a dielectric coating with a reflectivity of $R_S = 97.5\,\%$ for s-polarised and $R_P = 93.0\,\%$ for p-polarised light for the laser wavelength of $\lambda = 1064\,\text{nm}$. In the typical NPRO design thermal lensing in the crystal (caused by the pumping process) is compensated by the concave front face (radius of curvature $R = -2000\,\text{mm}$, (Quetschke 2003)) of the NPRO, in effect fulfilling the stability criterion for the laser resonator /producing a stable laser resonator[2]. The overall round trip length in the NPRO crystal is 51.8 mm

Figure A.2 shows the typical pumping scheme for an NPRO. Two best form lenses with a focal length of $f_1 = 20\,\text{mm}$ modematch the pump light of each of the two pump laser diode arrays (which have perpendicular polarisation) onto a polarising beam splitter. The superpositioned spots of the laser diode arrays are then imaged onto the front face of the NPRO crystal by a third best form lens with focal length $f_2 = 20\,\text{mm}$. This *end-pumping scheme* allows for *mode selective pumping*: Over the absorption length the pump spot in the NPRO crystal has a smaller waist size (optimally $w_{\text{pump}} = 85\,\mu\text{m}$) than the resulting laser beam $w_{\text{NPRO}} \approx 180\,\mu\text{m}$, which leads to transverse single-mode emission of the NPRO and a corresponding *high beam quality* factor of $M^2 \leq 1.1$.

Without further measures the ring laser design of the NPRO leads to bidirectional laser emission, and for each propagation orientation there are two possible orthogonal polarisations. There are consequently four possible emission eigen modes, but only the laser mode with the smallest losses will oscillate in the NPRO. An *optical diode* introduces different losses for the individual modes in the following way, leading to unidirectional operation: Due to the non-planar beam path in the NPRO the laser beam experiences a reciprocal rotation of its polarisation (i.e. a polarisation rotation which depends upon the direction of

[2]NPRO crystals designed for lower threshold (such as the single-mode NPRO of chapter 4) have a plane input facet to account for the lower pumping power and the corresponding weaker thermal lens.

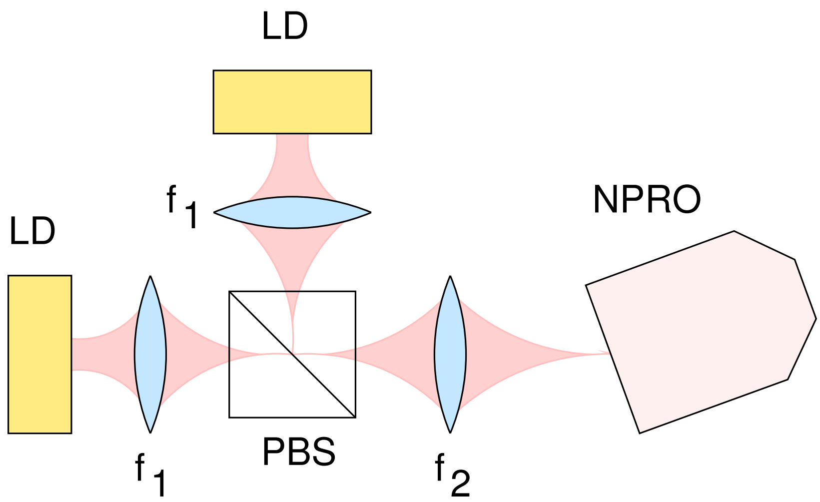

Figure A.2: Schematic of the pump geometry of a commercial NPRO, type Mephisto 800 (InnoLight GmbH 2004). LD: pump laser diode, PBS: polarising beam splitter, NPRO: laser crystal, focal lengths $f_1 = 20\,\mathrm{mm}$, $f_2 = 20\,\mathrm{mm}$.

beam propagation) at the reflection points B, C and D. A magnetic field applied along the optical axis of the material causes optical activity due to the *Faraday effect*. Nd:YAG has a non-vanishing Verdet constant of $103\,^\circ\mathrm{T}^{-1}\mathrm{m}^{-1}$, therefore placing a permanent magnet under the NPRO crystal leads to a non-reciprocal polarisation rotation (independent of the orientation of beam propagation). The effects of both the reciprocal and the non-reciprocal polarisation rotation are summed in the resonator, partly compensating each other for one propagation orientation, but cumulating for the other. The output face of the NPRO has a dielectric coating (stated above) differing for s- and p-polarisation, which acts as the polariser of the optical diode. This dielectric coating introduces excess loss for the unwanted s-polarisation. Of the two remaining eigen modes with p-polarisation one propagation direction has a higher p-polarisation content than the other, consequently this is the preferred mode with the lowest losses, leading to unidirectional emission.

With a pump power of $P_{808\mathrm{nm}} = 1\,\mathrm{W}$ an NPRO typically emits $P_{1064\mathrm{nm}} = 300\,\mathrm{mW}$ of output power; with $P_{808\mathrm{nm}} = 2\,\mathrm{W}$ the output power easily reaches the specified $P_{1064\mathrm{nm}} = 800\,\mathrm{mW}$ and can often be tweaked to $P_{1064\mathrm{nm}} = 1\,\mathrm{W}$, resulting in an optical-optical slope efficiency of $\eta_{\mathrm{NPRO}} = 50\,\%$. Slope efficiencies of $\eta_{\mathrm{NPRO}} = 60\,\%$ have been reached (Freitag 1994). The laser threshold for a common NPRO (Mephisto 800) is $P_{\mathrm{thr}} = 660\,\mathrm{mW}$, though designs for reduced threshold (for instance the single-mode NPRO) exist, where it can be as low as $P_{\mathrm{thr}} = 30\,\mathrm{mW}$.

The *resonant relaxation oscillations* exhibited by an NPRO are an artefact of the transient behaviour when lasing begins. By pumping the laser inversion is built up and the laser reaches threshold, resulting in the onset of laser emission. By stimulated emission the inversion is cleared, consequentially pushing the medium below threshold again, causing laser emission to cease[3]. Continued pumping rebuilds inversion and the process starts anew,

[3]This is a description of the dynamic processes during the onset of lasing. Please keep in mind that in steady-state the value of inversion is clamped.

but with smaller amplitude as the system approaches steady-state, resulting in damped sinusoidal oscillations around the steady-state value of inversion. The resonant relaxation oscillations are quasi the steady-state echo of this process. (Koechner 1996) gives a comprehensive analysis of this behaviour.

As an approximation the frequency of the resonant relaxation oscillations is proportional to the square root of the pump power (Svelto 1998), for a Mephisto 800 they are around $f_{\mathrm{RRO}} \approx 500\,\mathrm{kHz}$. In the intensity noise spectrum the resonant relaxation oscillation peak can lie 40 to 60 dB above the spectrum. To suppress the resonant relaxation oscillations commercially available NPROs can have a *noise eater* implemented. This control electronics detects a fraction of the NPRO light and feeds back to the pump current of the pump laser diodes. The noise eater suppresses the resonant relaxation oscillations by typically 40 to 60 dB, but it also reduces the intensity noise below the resonant relaxation oscillations by typically 20 dB.

B. Appendix: Designed control electronics

In the course of this thesis different control electronics for the various stabilisation tasks were designed. For documentation purposes the schematics of the electronics are given here. Eagle (version 3.5 and 4.09r2 from CadSoft) was used for the design of the schematics and the board layout.

B.1. Injection locking electronics

The injection locking electronics for the high power laser system for GEO 600 was revised several times in the years it has been employed. It was last changed in 2001 when an autolocking circuit was implemented. The autolocking electronics relocks the system within milliseconds after a lock loss; typical relock times are $t < 100\,\mathrm{ms}$. The design also includes optional notch filters to compensate for resonances of the slave laser piezo-electric transducer and a lock control, which verifies if the laser is in injection lock by means of the error signal level.

The essential sheets of the schematic are given here; supplies etc. are omitted for clarity. Since 2002 the current status of the electronics is unchanged.

B.2. Universal servo for frequency stabilisation of an NPRO

Frequency stabilisation of an NPRO to a cavity (or vice versa) is a common task in our group. The basic control problem is always similar, which is why I designed a universal servo for this purpose. The actual servo can easily be modified (proportional gain, cut-off frequencies, optional integration stages, filters) by exchange of part values, whereas the design of the end stage(s) accounts for most of the possible actuators (piezo-electric transducer of either the NPRO or the tunable cavity, drive current of the pump laser diode(s) and NPRO crystal temperature).

The universal servo is used as a frequency stabilisation servo for the injection locked lab laser system 3.4.1 and can be used for frequency stabilisation of the front end for the high power laser for the Advanced LIGO pre-stabilised laser system. Due to its versatility other groups can make use of this electronics, too. The schematic of the universal servo is shown in figure B.4 (servo and crossover network) and B.5 (temperature control).

B.3. Intensity stabilisation of the GEO 600 laser system

An active intensity stabilisation for the injection locked high power laser system is needed to fulfil the specifications for GEO 600. The requirements and the conditions are described in section 3.5, as well as the results achieved with the two intensity stabilisation loops. The designed control electronics is shown here for documentation purposes. Power supplies etc. have been omitted for clarity.

Figure B.6 shows the servo of the first loop as well as the hard-wired comparator circuit which determines wether the signals are in range. Figure B.7 is the Sallen-Key low-pass filtered voltage reference for the intensity stabilisation, as the first loop pursues a DC-coupled stabilisation scheme. Figure B.8 gives the schematic of the second loop. The signal to the second loop is high-pass filtered at $f = 0.2\,\mathrm{Hz}$. The electronics of the first loop exists as an Eagle layout, whereas the second loop was hard-wired on a piggyback circuit board.

The compound control signal (of first and second loop) is fed to the current bypass endstage (shown in figure B.9) which is connected in parallel to laser diode A of the slave laser pump diodes. Schottky diodes protect the laser diode against accidental reverse biasing. A current modulation input facilitates transfer function measurements of the slave laser.

B.4. Pump light stabilisation electronics for intensity stabilisation of the single-mode NPRO

Conventional NPROs are often equipped with an intensity stabilisation - the so-called noise eater - which detects a fraction of the NPRO light and feeds back to the pump current of the pump laser diodes, mainly to suppress the resonant relaxation oscillations of the NPRO. The pump light stabilisation used in section 4.5 instead uses a fraction of the pump light, detected by the internal monitor photodiode of the single-mode laser diode, to feed back to the pump current and thereby stabilise the *pump power* of the single-mode NPRO. As can be seen in section 4.3.3 an attempt at stabilising the output power of a laser diode array pumped NPRO by stabilisation of the pump power is not successful.

In the case of the single-mode NPRO stabilisation of the pump intensity not only results in a reduction of NPRO intensity noise, but also entails a suppression of NPRO frequency noise. A detailed description of the experimental setup and the results of the pump light stabilisation are given in section 4.5. The electronics designed for pump light stabilisation of the single-mode NPRO is shown in figure B.10.

The pump light stabilisation electronics was especially designed for intensity stabilisation of the single-mode NPRO, which is why much care was taken to ensure that the very sensitive single-mode laser diode is not destroyed by transients. The end stage is a current bypass transistor stage with an additional Schottky diode against accidental reverse biasing of the laser diode. The transistor is an n-channel enhanced mode MOSFET which is controlled by a voltage at its gate. When the voltage at the gate goes from rail to rail (max. $\pm 15\,\mathrm{V}$) between 0 and 20 mA of pump current are bypassed through the transistor instead of passing through the single-mode laser diode. This causes a variation of output intensity.

B.5. Current lock electronics for frequency stabilisation of the single-mode NPRO to the reference cavity

As shown in section 2.4.2 the drive current of the pump laser diodes is a superb actuator for NPRO frequency (see also (Willke et al. 2000b)). The current lock technique (frequency stabilisation by use of the actuator pump current) is explained in section 2.4.2, and the complete chapter 4 deals with the optimisation of the coupling between pump intensity and laser frequency. In the single-mode NPRO current lock results not only in frequency noise reduction, but also in a high degree of simultaneous intensity noise suppression.

The control electronics for current lock of the single-mode NPRO is shown in figure B.11. The end stage is very similar to that of the pump light stabilisation, since both electronics were designed for current modulation of the same sensitive single-mode laser diode.

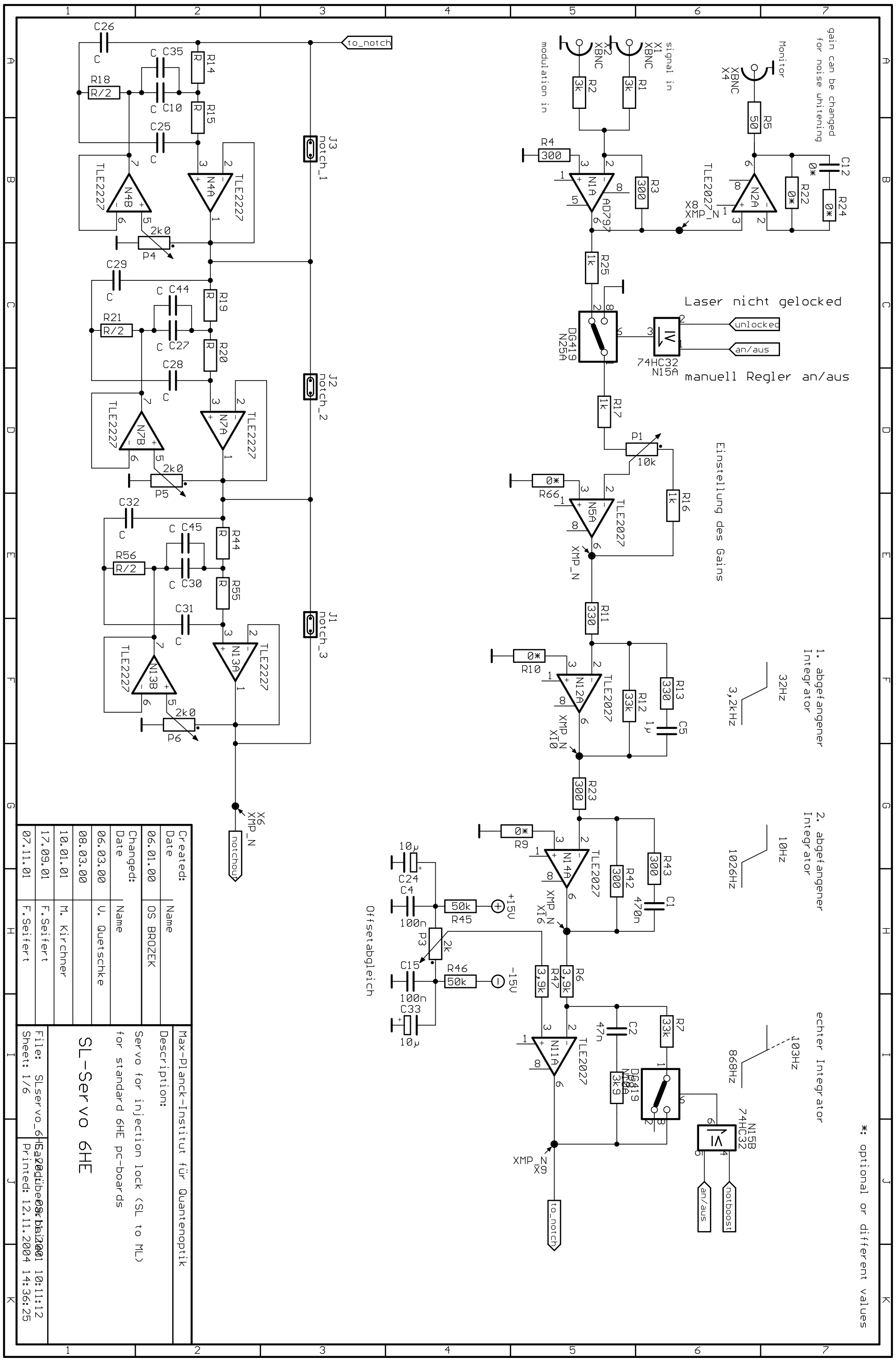

Figure B.1: Schematic of the injection lock servo, which is used for injection locking of the high power laser system for GEO 600. Sheet 1 shows the actual servo as well as the optional notch filters which can be used to compensate for resonances of the piezo-electric transducer of the slave laser.

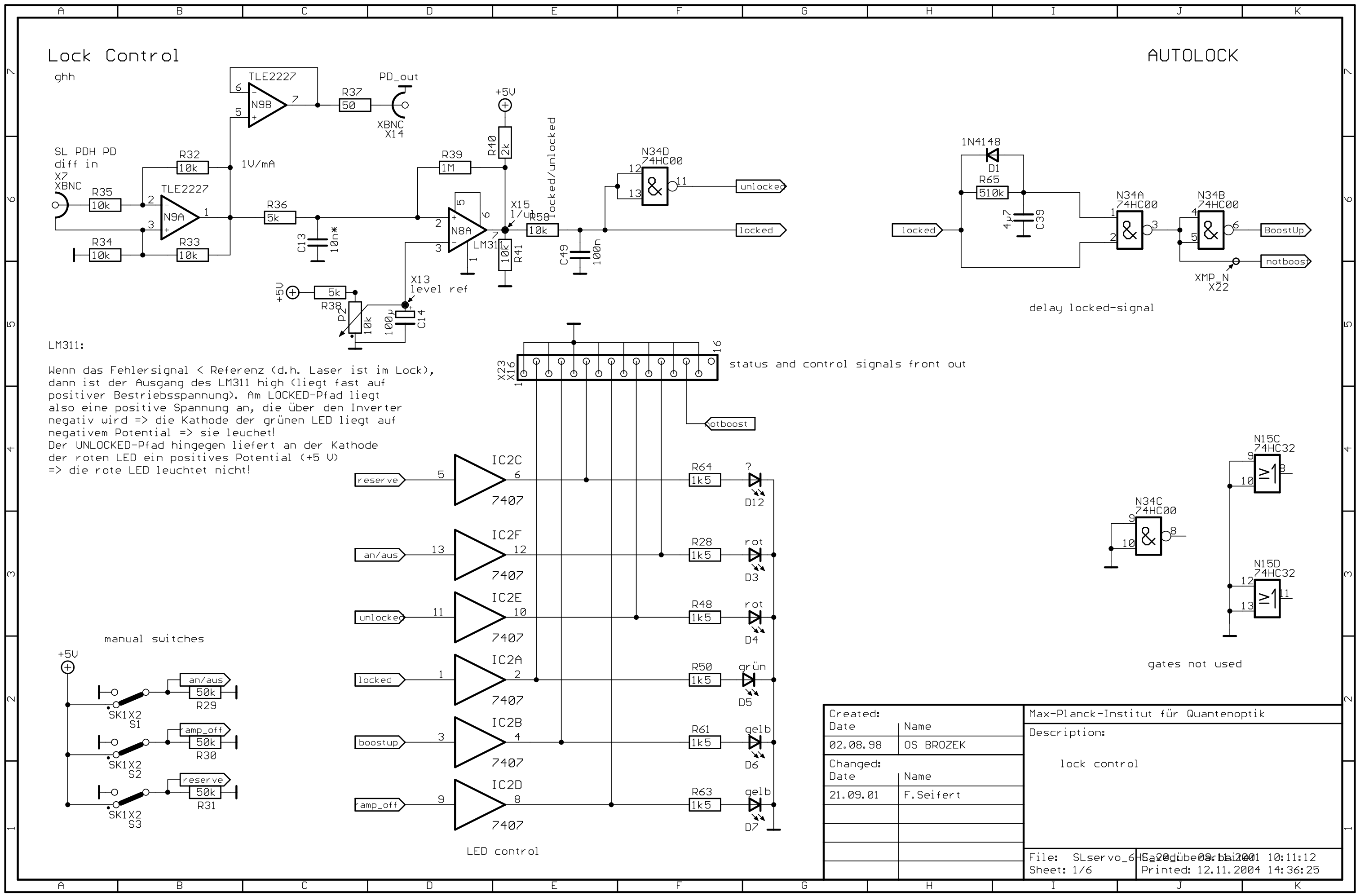

Figure B.2: Schematic of the injection lock servo, which is used for injection locking of the high power laser system for GEO 600. Sheet 5 shows the lock control which verifies wether the laser is still in injection lock. If the laser has fallen out of lock the comparator LM311 delivers a signal which powers an indicator LED.

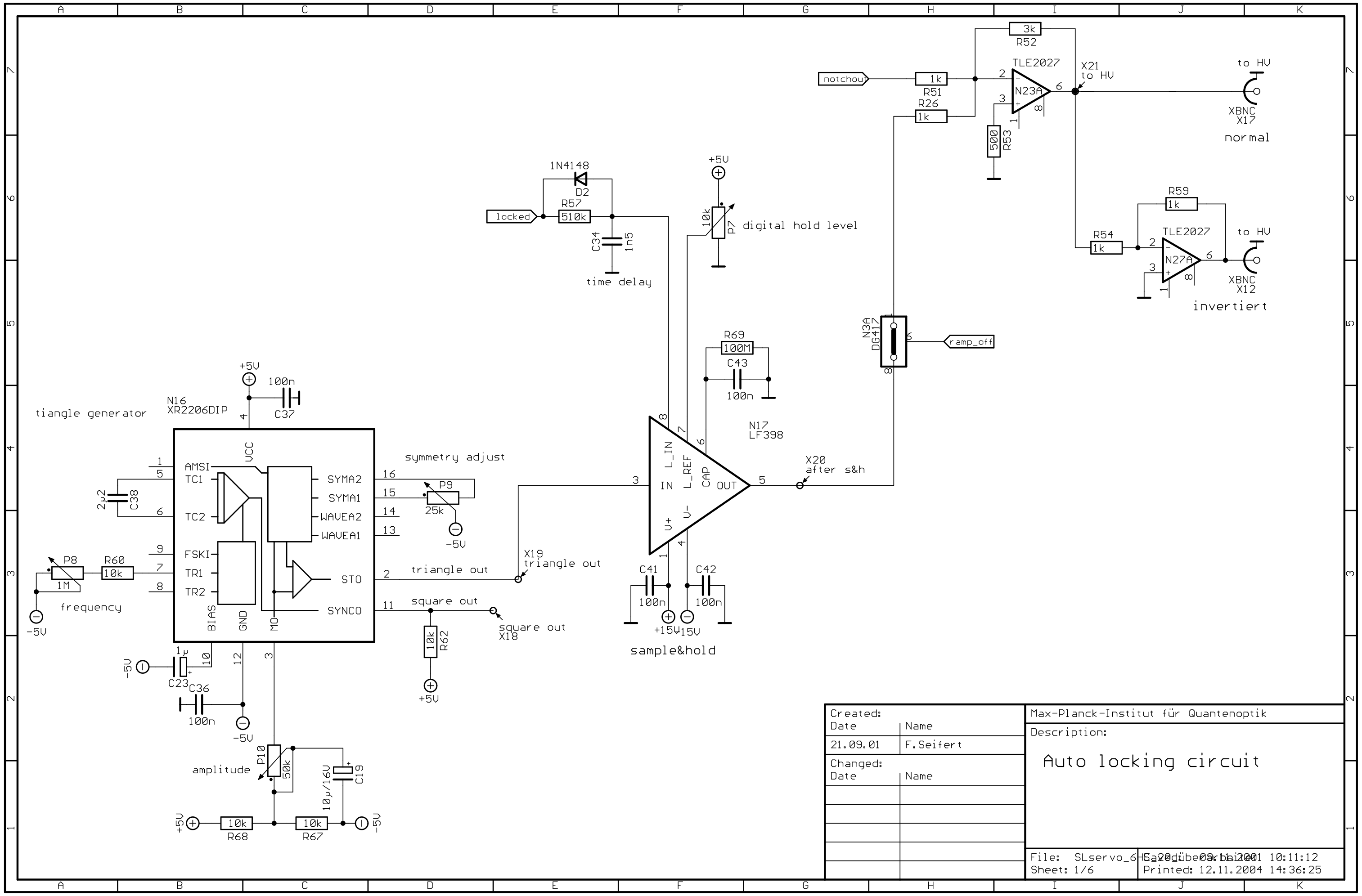

Figure B.3: Schematic of the injection lock servo, which is used for injection locking of the high power laser system for GEO 600. Sheet 6 shows the autolocking circuit. If the laser has fallen out of injection lock the ramp generator delivers a voltage ramp which drives the slave laser piezo-electric element and yields a Pound-Drever-Hall error signal. The system then acquires lock when the error signal is near zero.

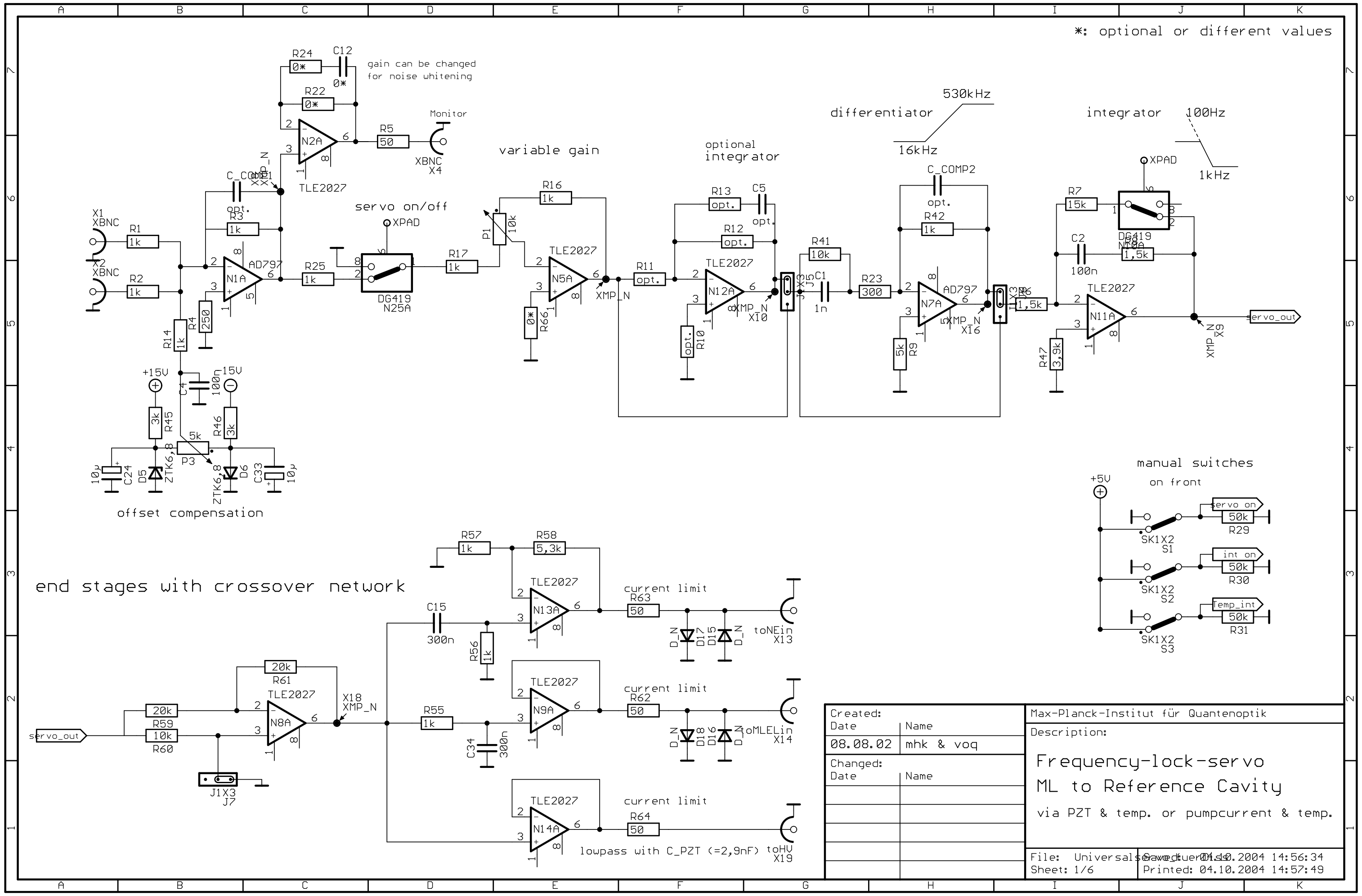

Figure B.4: Schematic of the universal servo, which can be used for frequency stabilisation of an NPRO to an optical cavity or vice versa. The end stages allow for the use of a combination of different actuators, the servo itself can easily be modified for different stabilisation tasks.

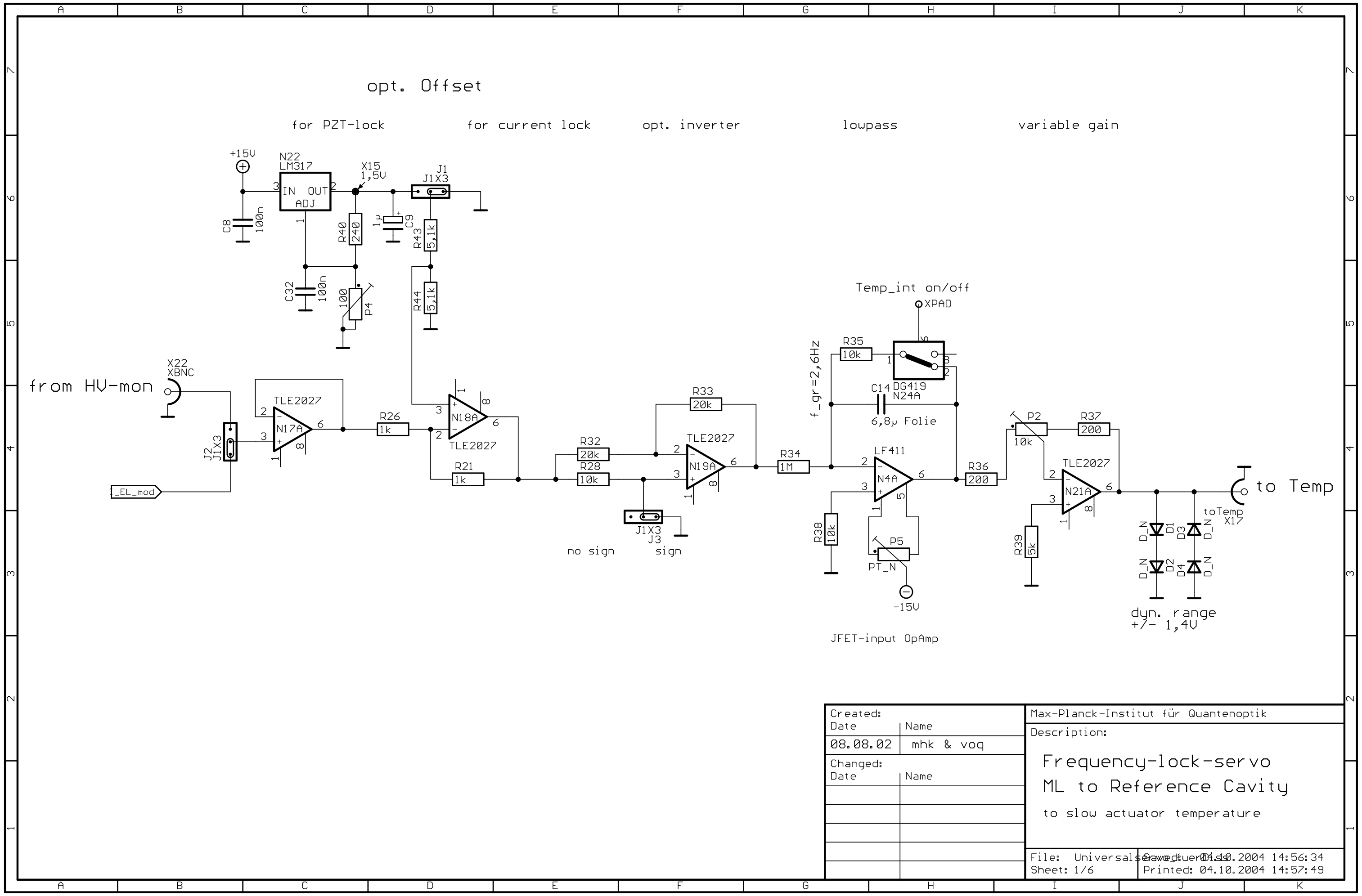

Figure B.5: Schematic of the universal servo, which can be used for frequency stabilisation of an NPRO to an optical cavity or vice versa. The temperature control stage shown here increases the dynamic range of the servo.

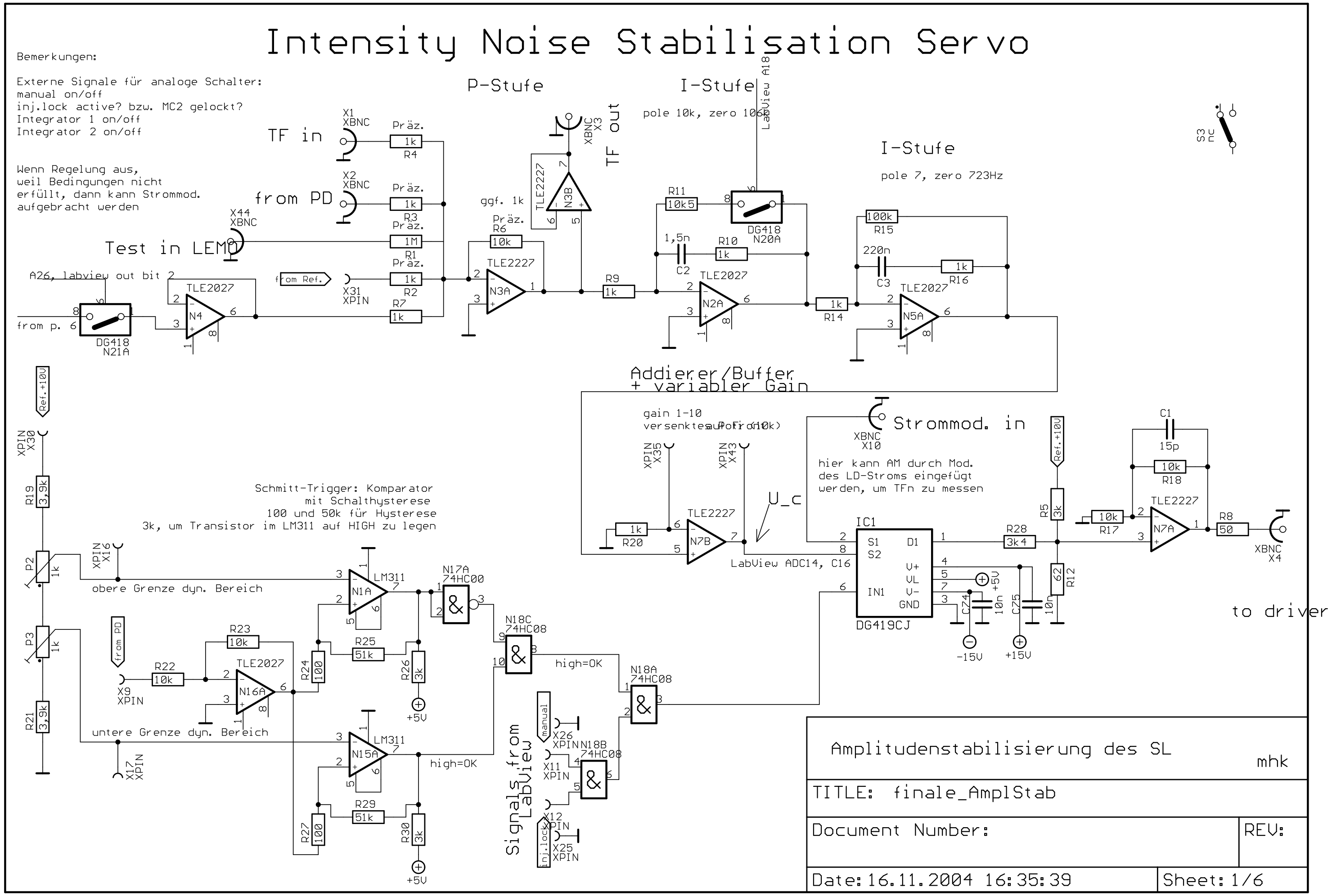

Figure B.6: Schematic of the first loop of the intensity stabilisation servo. Shown here is the servo as well as the comparator circuit for the input range of the signals. The signal from the servo is fed to a current bypass driver end stage, which is shown in figure B.9.

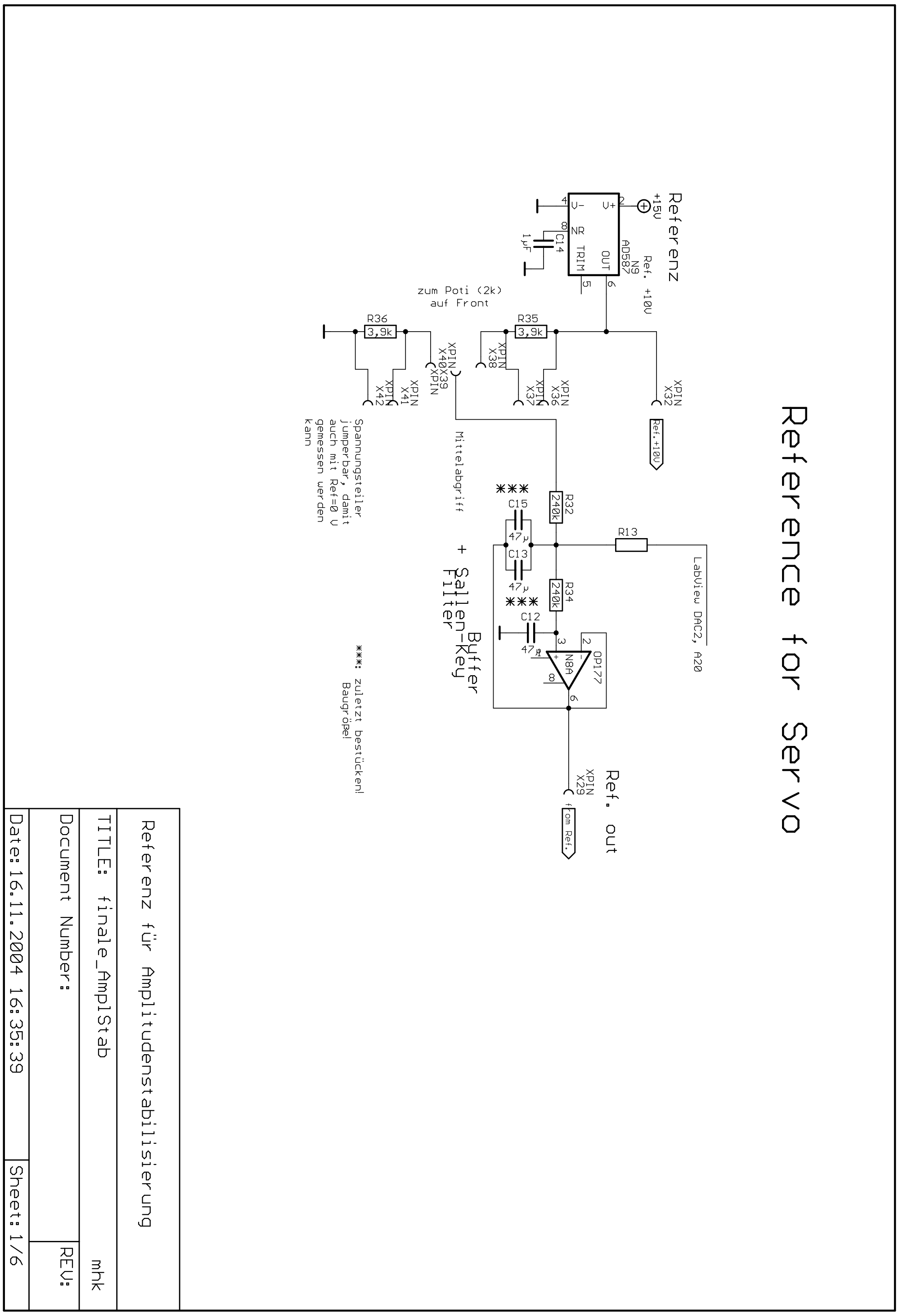

Figure B.7: Schematic of the voltage reference of the first loop of the intensity stabilisation servo. A Sallen-Key low-pass filtered AD587 is used as a low-noise voltage reference.

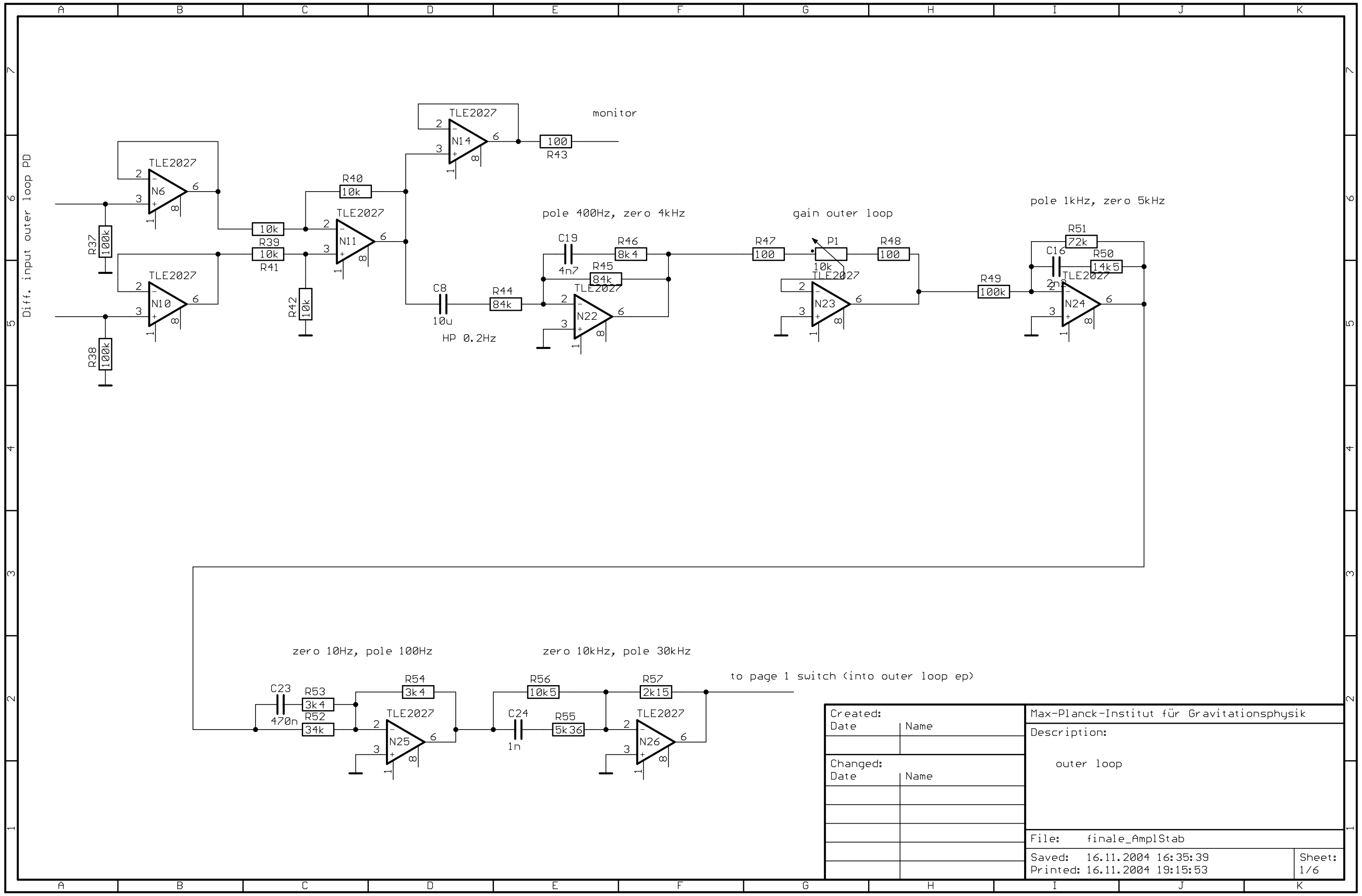

Figure B.8: Schematic of the second loop of the intensity stabilisation servo. This loop is not part of the layout of the first loop, but is added onto the first loop by a piggyback circuit.

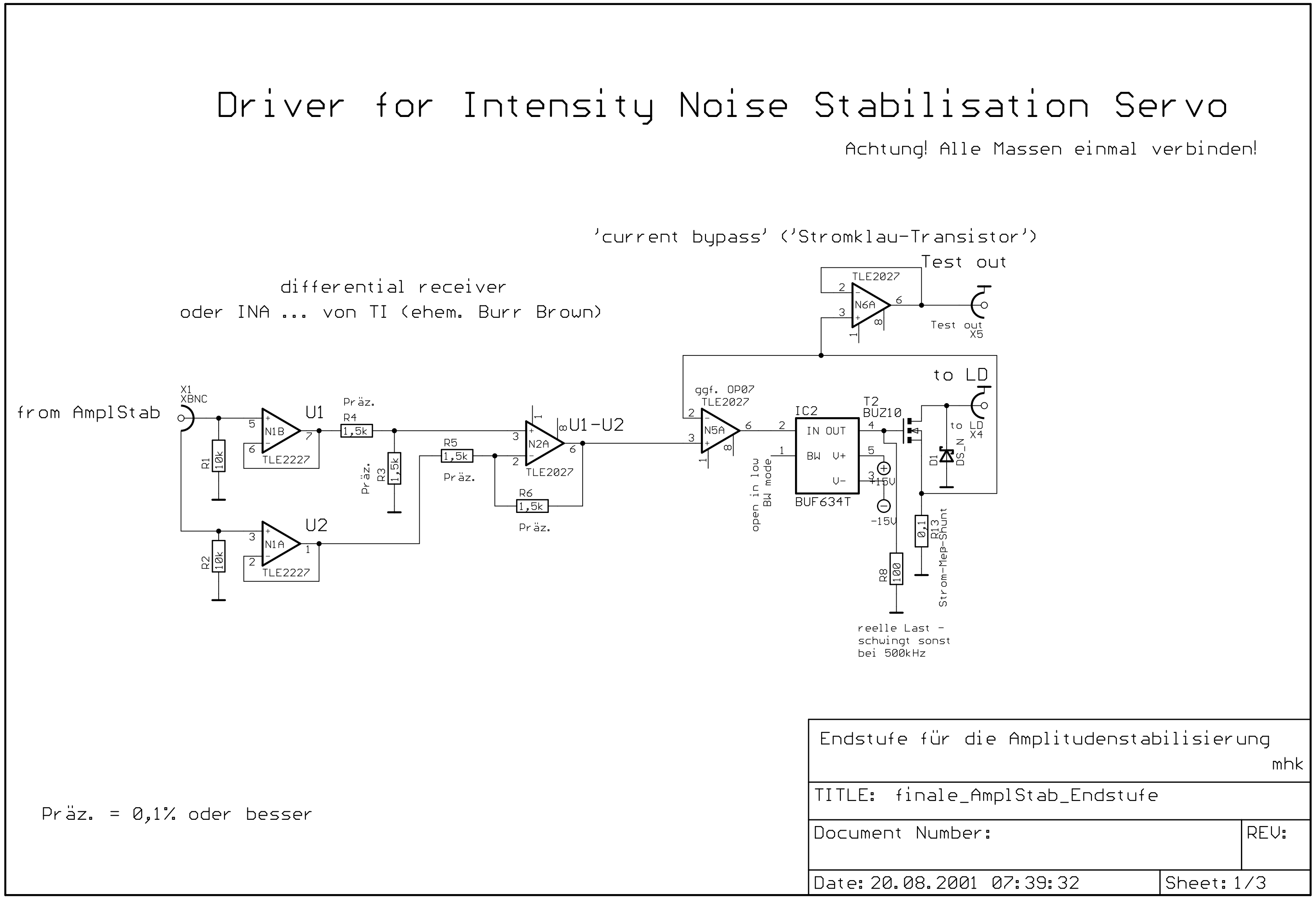

Figure B.9: Schematic of the endstage for intensity stabilisation of the GEO 600 laser system. The endstage is a current bypass, contacted in parallel to laser diode A of the slave laser pump diodes.

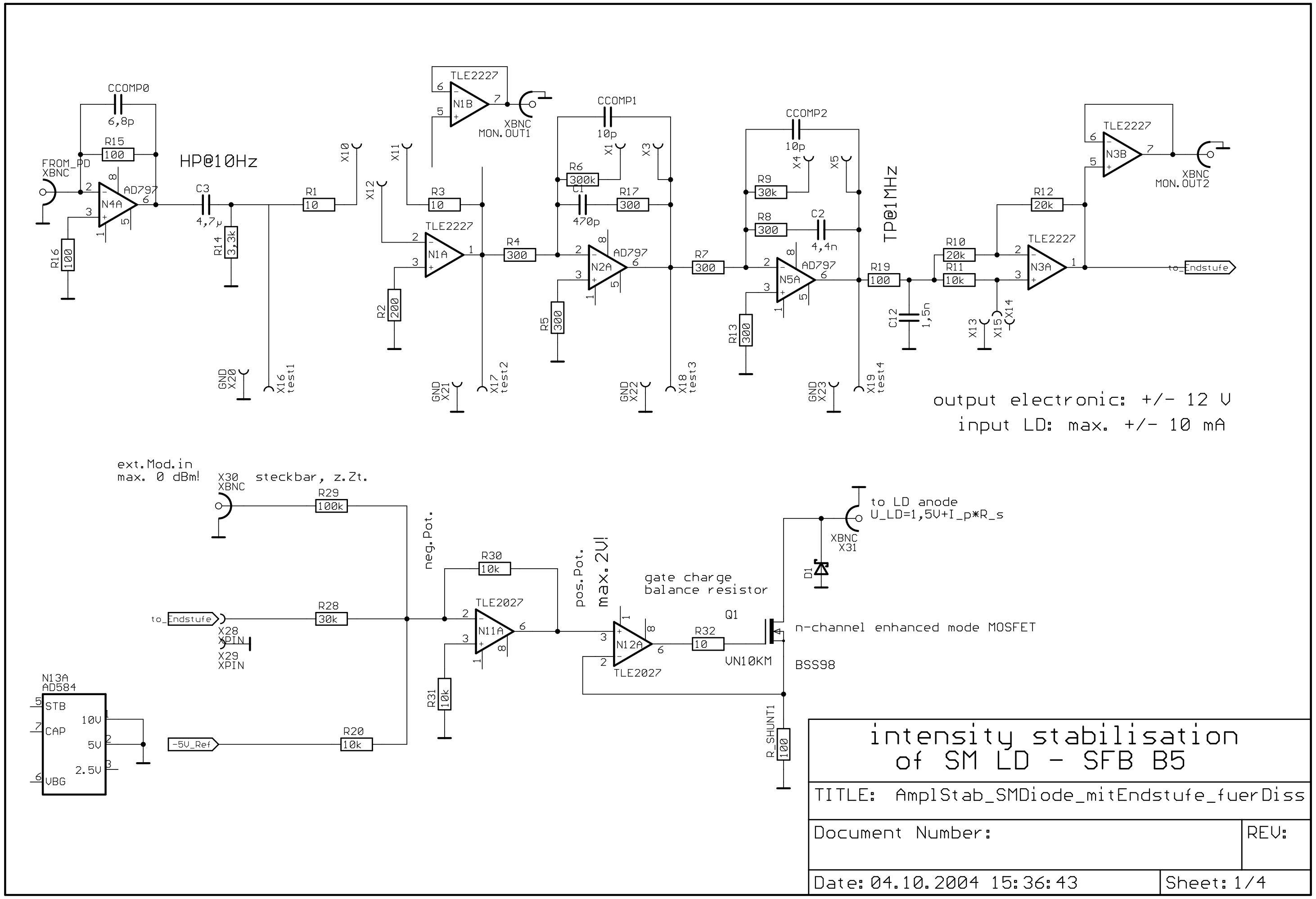

Figure B.10: Schematic of the pump light stabilisation electronics. A fraction of the pump light of the single-mode NPRO is detected by the internal monitor photodiode of the single-mode pump laser diode; this signal is used for intensity stabilisation of the pump power, which in the case of the single-mode NPRO results in intensity noise reduction of the NPRO light and simultaneous frequency stabilisation. The results are shown in figure 4.29 (intensity noise) and 4.30 (frequency noise).

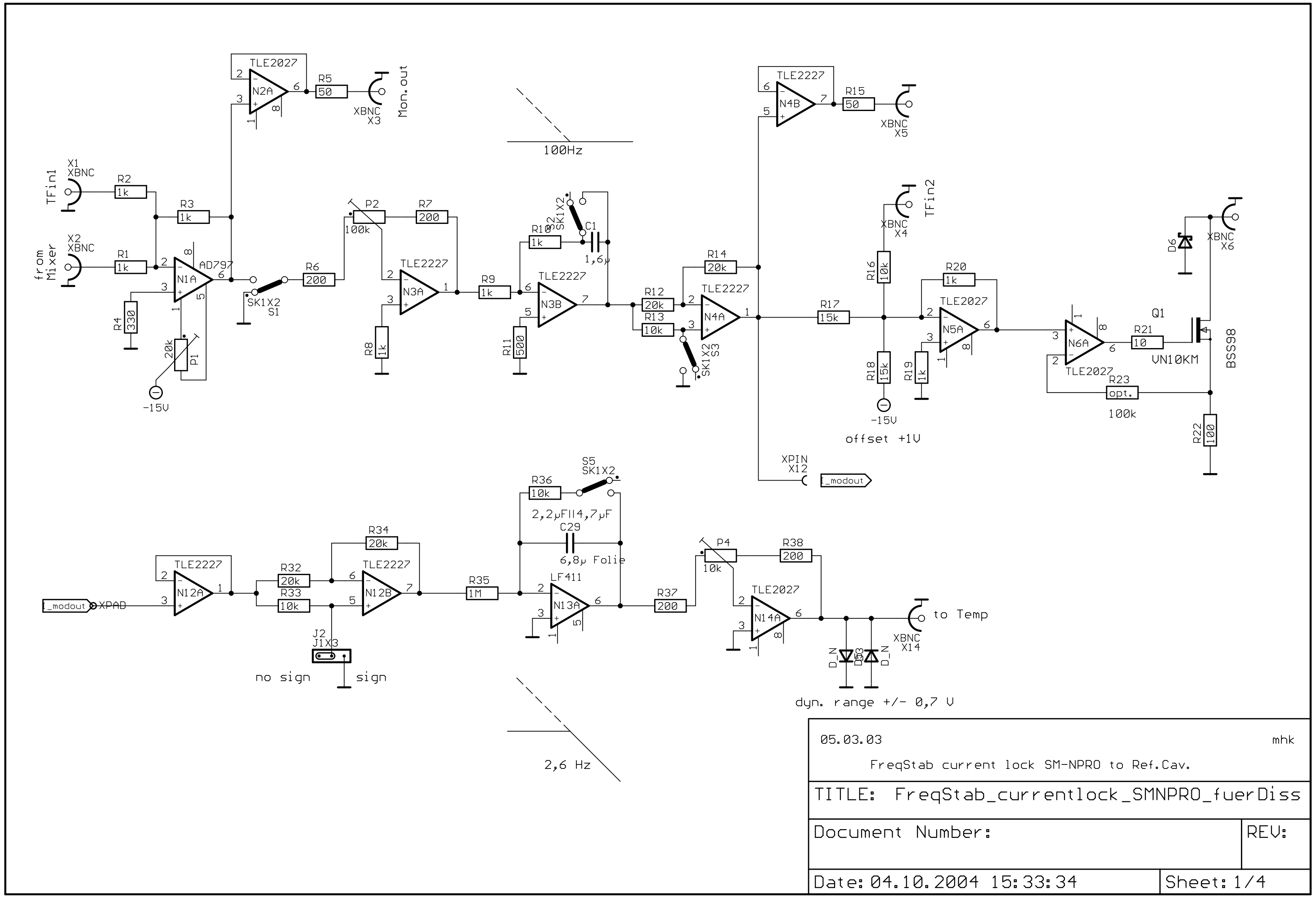

Figure B.11: Schematic of the current lock electronics. With a Pound-Drever-Hall modulation scheme the single-mode NPRO can be stabilised to an optical cavity by means of the current lock technique. Light reflected from an optical cavity is detected by a photodetector. The signal is demodulated by a mixer and passed on to the current lock electronics. The end stage then bypasses the right amount of current past the single-mode laser diode to tune the NPRO frequency to the cavity resonance. This results in frequency noise reduction of the single-mode NPRO (figure 4.32 and 4.33) as well as simultaneous intensity noise suppression (figure 4.34).

C. Appendix: The hard facts on photodetectors

The various laser stabilisations described in this thesis call for specialised photodetectors. Depending on the stabilisation task silicon (Si) or indium-gallium-arsenide (InGaAs) photodiodes are implemented in different electronic circuits. The selection criteria for the photodiodes are described in chapter 2.3.1, whereas the circuits are shown here. The following gives an introduction on the basic function principle of photodiodes as well as a detailed description of the detector circuits.

C.1. The function principle of photodiodes

Photodiodes are semiconductor devices consisting (in the most basic version) of a pn-junction. Figure C.1 shows the p- and n-doped region as if they had just been brought into contact, as well as the carrier free junction zone, the so-called *depletion region*, which forms at the junction due to recombination of electrons from the n-doped and holes from the p-doped zone. Drift of the carriers into the junction removes carriers from the p- respectively n-doped semiconductor, which leads to the build up of an electrical field. Recombination at the junction therefore takes place until the resulting electrical field, referred to as *internal bias*, and the drift of the carriers into the junction are in equilibrium, limiting the width of the depletion region.

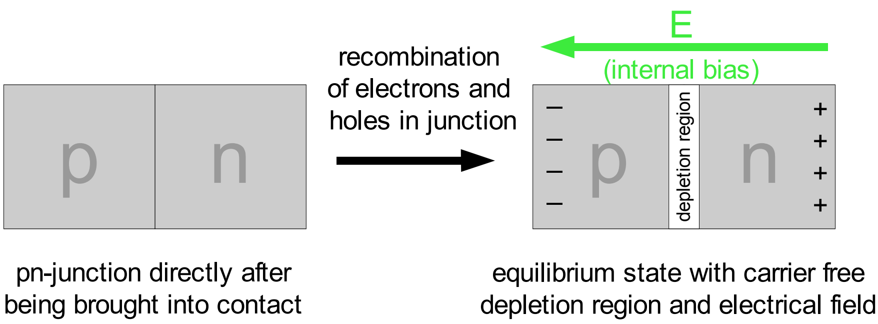

Figure C.1: pn-junction without external bias.

A photon absorbed in the pn-junction creates an electron-hole-pair in the semiconductor. In the depletion region the pairs are immediately seperated and swept across the junction by the natural internal bias. Electron-hole-pairs created outside the depletion region move randomly, many of them eventually entering the depletion region to face the same fate as those above, but others recombining before reaching the depletion region. These carriers are lost for the conversion of light into an electrical signal. For many applications it is therefore desirable to maximise the width of the depletion region, as the device response is faster and the *quantum efficiency* η (the ratio of photocurrent in electrons to incident light intensity in photons) is increased. This can be achieved by *reverse biasing*, shown in figure C.2, which increases the speed (and thereby the bandwidth) of the device significantly. For this reason the photodetectors used in this work are always reverse biased. Reverse biasing is accomplished by applying a voltage of the same polarity as the internal bias (but with larger magnitude) to the pn-junction, thereby increasing the electric field in the device and the junction width. Figure C.2 shows how the created charges are "sucked" towards the applied reverse biasing electrodes, constituting a *photo current*. Unbiased operation of the photodiode is referred to as *photovoltaic operation*, as opposed to *photoconductive operation*, where an external bias is applied. In applications where low dark current and high linearity of the response are of highest priority photovoltaic operation can be preferrable over photoconductive operation.

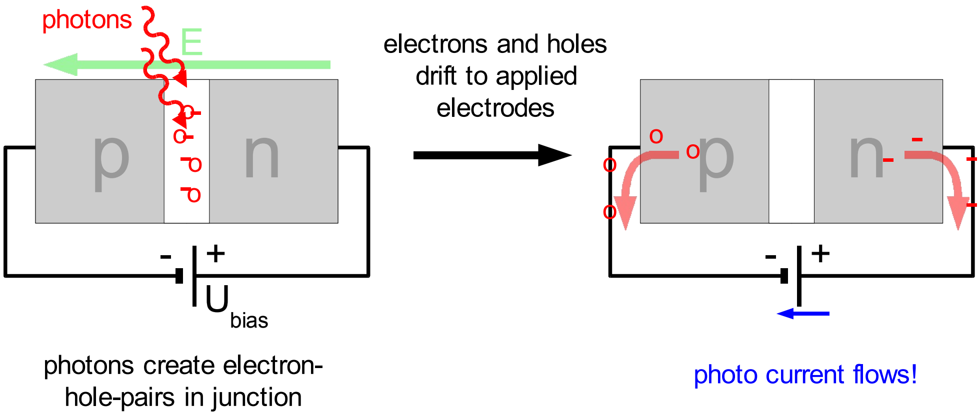

Figure C.2: pn-junction with reverse bias.

The photodiodes used in this work are not simple pn-junctions, but PIN (positive-intrinsic-negative) photodiodes. They possess an undoped (intrinsic) layer between the p- and the n-doped region. This is another method to increase the width of the depletion region, allowing for a more efficient conversion of photons to charge carriers by increasing the quantum efficiency. PIN photodiodes are the most commonly used photodiodes; a schematic design is depicted in figure C.3: Light enters the device through the thin p-doped region. In the semiconductor light intensity decreases exponentially with penetration depth due to absorption of photons. The external bias is applied via the metallised surfaces.

The easiest way to transform the photo current into a voltage would be by means of a simple resistor. This has the disadvantage, though, of very limited bandwidth and results in a noisy photo voltage. Using a transimpedance amplifier for the conversion of photo current to voltage is by far more appealing, as can be seen in the following section.

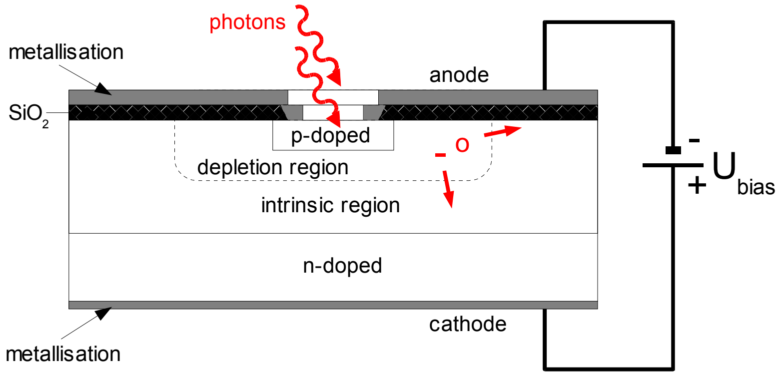

Figure C.3: Schematic design of a PIN photodiode.

C.2. The bandwidth of a transimpedance amplifier photodetector circuit

The basic transimpedance amplifier for (ideally frequency independent) conversion of a photo current into a proportional photo voltage is shown in figure C.6. The photo current produced in the photodiode by absorption of photons and creation of electron-hole-pairs cannot flow into the high impedance input of the operational amplifier. Due to Kirchhoff's law (according to which the sum over all currents in a node is zero) the current cannot just 'sit' at the input of the op amp. The output of the operational amplifier therefore produces a voltage which leads to a current compensating for the photo current. Within the bandwidth of the circuit this output voltage of the operational amplifier is proportional to the photo current.

The bandwidth of a photodetector circuit, however, is mainly determined by the capacitance of the photodiode and the transit frequency of the transimpedance amplifier stage. The cut-off frequency is the geometric mean of the two, shown in the following equation:

$$\nu_{\text{cutoff}} = \sqrt{\left(\frac{1}{2\pi \cdot R \cdot C_{\text{PD}}}\right)^2 + (\nu_{\text{transit}})^2}\ , \tag{C.1}$$

(Heinzel 2002), where R is the transimpedance in the feedback of the transimpedance amplifier, C_{PD} is the photodiode capacitance (which depends on the bias voltage) and ν_{transit} is the transit frequency of the amplifier. In many cases the transit frequency is not given in the datasheet; in this case the full power bandwidth (FPBW) can be used as a (very rough) lower limit:

$$\text{FPBW} = \frac{\text{slewrate}}{2\pi \cdot V_{\text{op}}}\ , \tag{C.2}$$

with V_{op} being the maximum voltage.

Depending on the material photodiodes have a specific capacitance which in effect limits the achievable bandwidth of the resulting photodetector. The InGaAs photodiodes with

1 mm diameter, type C30641 from PerkinElmer (formerly EG&G), have a typical capacitance of $C_{\mathrm{C30641}} = 40\,\mathrm{pF}$ when they are biased with $U_{\mathrm{bias}}15\,\mathrm{V}$ (PerkinElmer Optoelectronics 2001). They are typically used in the photodetector circuit shown in figure C.5. Silicon photodiodes have a capacitance which is approximately a factor of 10 smaller at the same diameter, but their low quantum efficiency at $\lambda = 1064\,\mathrm{nm}$ is a drawback for many applications. The Si photodiodes used in this work are a large area photodiode from Thales Optronics (type IPL10050) (Thales Optoelectronics 2003) and a fast photodiode from Hamamatsu Photonics (type S3399) (Hamamatsu Photonics 2001). The IPL10050 with an active area of $41.3\,\mathrm{mm}^2$ has a capacitance of $C_{\mathrm{IPL10050}} \approx 75\,\mathrm{pF}$ when it is biased with $V_{\mathrm{bias}} = -15\,\mathrm{V}$. It is implemented in the circuit shown in figure C.8. The S3399 photodetector has an effective active area of $7\,\mathrm{mm}^2$ (diameter 3 mm), the resulting capacitance at a bias voltage of $V_{\mathrm{bias}} = -15\,\mathrm{V}$ is $C_{\mathrm{S3399}} = 20\,\mathrm{pF}$.

C.3. Shot noise of a photodetector

An intensity noise measurement basically counts the number of photons arriving at the detector in a defined time interval. The probability distribution $p(N)$ connected to this measurement is a *Poisson distribution*

$$p(N) = \frac{\bar{N}^N e^{-\bar{N}}}{N!} \quad , \tag{C.3}$$

in which N is the actual number of photons and $\bar{N}$ the mean number of photons per counting interval (Saulson 1994).

The *shot noise* of the detected light power stems from this random arrival of photons at the detector. It is a fundamental noise source connected to the nature of laser light. Every photon arriving at the detector is converted into an electron-hole-pair with the quantum efficiency η, which for a laser wavelength of $\lambda = 1064\,\mathrm{nm}$ is typically $\eta \approx 0.15\,\mathrm{A/W}$ for silicon (Hamamatsu Photonics 2001) and $\eta \approx 0.8\,\mathrm{A/W}$ for indium-gallium-arsenide (PerkinElmer Optoelectronics 2001) photodiodes.

The current shot noise is the observable of interest; it is given by equation C.4.

$$I_{\mathrm{SN}} = \sqrt{2\mathrm{q}\left(I_{\mathrm{photo}} + I_{\mathrm{dark}}\right)} \left[\frac{A}{\sqrt{Hz}}\right] \quad . \tag{C.4}$$

Here I_{photo} is the photo current caused by the absorbed photons, I_{dark} is the dark current of the photodiode (which can mostly be neglected), and q is the elementary electric charge. In relative units (and omitting the negligible dark current) this equation becomes

$$I_{\mathrm{rel.SN}} = \sqrt{\frac{2\mathrm{q}}{I_{\mathrm{photo}}}} \left[\frac{1}{\sqrt{Hz}}\right] \quad . \tag{C.5}$$

Obviously the shot noise of the detected light is a lower limit to detection sensitivity, as it is a fundamental noise source. It is our goal to be able to actually measure this level without any spurious noise, such as electronic noise of the detection path.

Following this train of thought, an intensity noise measurement is called *shot noise limited* when the electronic noise of the photodetector does not limit the detection sensitivity, but the 'real' shot noise (equation C.4) of the detected light power level is measured.

According to equation C.4, increasing the detected power level quite intuitively leads to an increase in current shot noise. We commonly present *relative* intensity noise measurements, though, where the spectrum is divided by the DC power level to allow for easy comparability of results. The *relative shot noise* given by equation C.5 in these measurements goes as $1/\sqrt{I_{\text{photo}}}$ (the inverse of the square-root of the photo current $\propto$ detected power). This illustrates why it is easier to perform a shot noise limited relative intensity noise measurement using a low level of detected power, since the *relative* shot noise is then high.

C.4. Implemented photodetector designs

Different stabilisation tasks obviously call for different photodiodes (as explained in section 2.3.1), which differ in quantum efficiency, responsivity homogeneity, geometry, size and noise performance. Consequentially there is also the need for specialised photodetector circuits, depending on the desired detection bandwidth, low noise requirements and the designated photocurrent. The photodetector circuits used in this thesis are described in the following sections.

C.4.1. Photodetector with indium-gallium-arsenide photodiode, high bandwidth and high quantum efficiency

This photodetector circuit is based on a design by Sascha Brozek and established in this form by Sascha Brozek (Brozek 1999) and myself. It was developed to provide an adequate detector for the Pound-Drever-Hall-schemes used for frequency stabilisation and injection locking, where high bandwidth is needed due to the modulation frequencies in the radio frequency band. Usual modulation frequencies in the laser lab are traditionally 12 MHz and 29.02 MHz, which is why the bandwidth of this photodetector is designed for 60 MHz with an InGaAs photodetector with 1 mm diameter respectively 20 MHz with 2 mm diameter.

The transfer function of both the AC and the DC path of a photodetector of this kind can be seen in figure C.4.

In general it is advisable to operate a photodetector at approximately the middle of its dynamic range, usually corresponding to a DC photo voltage of around $P_{\text{DC}} = 5\,\text{V}$. The high quantum efficiency of the InGaAs photodiode is advantageous when only little laser power ($P < 10\,\text{mW}$) is available for the measurement. This is the case when for instance a near-ideally modematched laser is frequency stabilised to a high finesse cavity, or when the frequency stabilised laser itself has very little output power (as is the case for the single-mode NPRO).

The schematic of the fast photodetector with InGaAs photodiode is shown in figure C.5. The DC-output of the photodetector consists of a transimpedance amplifier with a transimpedance of commonly $R = 1\,\text{k}\Omega$ or $R = 500\,\Omega$, the AC-output is equipped with additional gain of 21 for frequencies above 16 kHz. These values can easily be modified by exchanging components such as the transimpedance resistor in the DC path or the high pass capacitor before the AC path.

There also exists a design with resonant enhancement of the photodetector gain. This is not commonly used anymore, though, since phase changes unintentionally introduced by

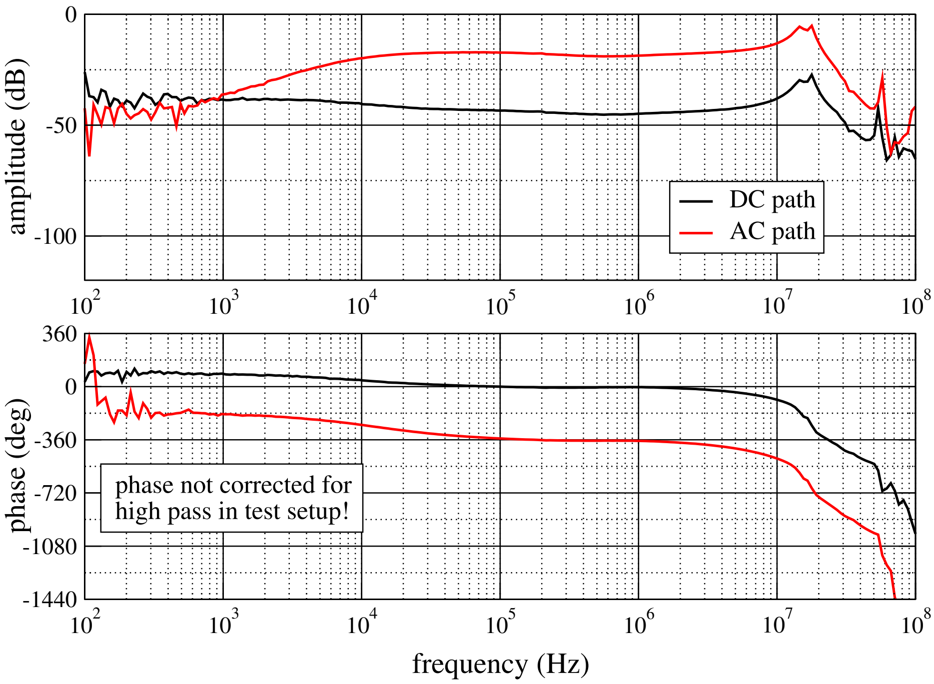

Figure C.4: Transfer function of a photodetector with indium-gallium-arsenide photodiode, high bandwidth and high quantum efficiency, AC and DC path. The transfer function was taken with a test setup consisting of an amplitude modulated laserdiode and a highpass at $\approx$ 1.6 kHz. The effect of the test setup was eliminated in the measured amplitude transfer function by calibration, but not in the phase.

changes of the environmental parameters can and have in the past proved detrimental to the stability of sensitive control loops.

C.4.2. High bandwidth photodetector with indium-gallium-arsenide photodiode, optimised for high photo current

The intensity noise measurements of the injection locked high power laser system in chapter 3 were partially conducted with a modified photodetector design, which is described here. Applications calling for high bandwidth, but at the same time requiring a high detected power level, encounter the following problem: Amplifier stages that have sufficient bandwidth cannot drive the currents needed to compensate for the large photo currents produced by the high detected intensity. The problem can be solved by seperating the amplifier into two stages, where the first has sufficient bandwidth and the second the capability of driving large currents. The bandwidth of the second stage then does not limit the overall bandwidth, but is determined by that of the fast first stage. Additionally the photodetector is actively cooled to evade thermal problems caused by dissipation of heat due to the large currents.

This photodetector was originally developed for implementation of InGaAs photodiodes, type C30641 and C30642. Various other photodiodes have since been tested in this design

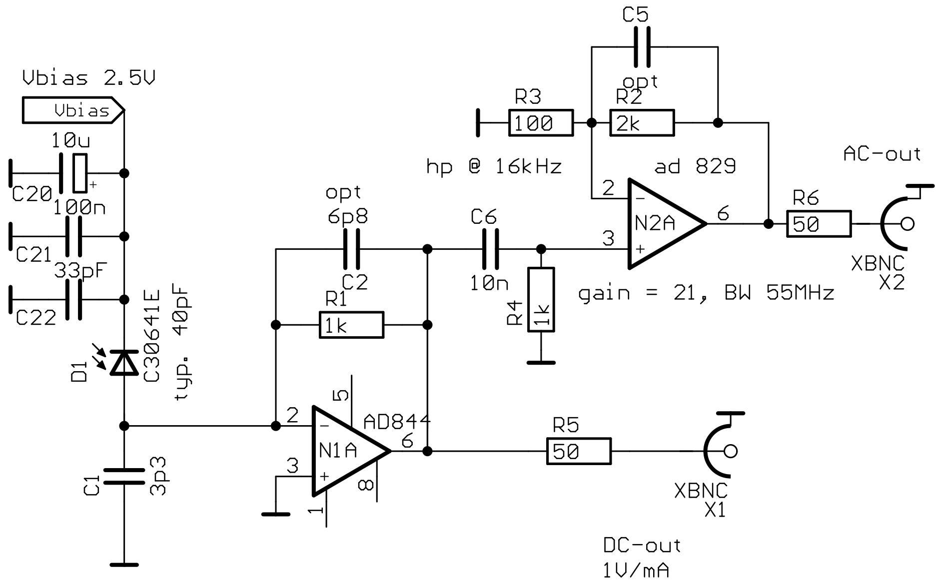

Figure C.5: Schematic of the photodetector with indium-gallium-arsenide photodiode, high bandwidth and high quantum efficiency.

(Seifert 2002), but the above are used in this work for some measurements in chapter 3. With the 2 mm photodiode the bandwidth of the photodetector is typically 20 MHz, with the smaller 1 mm photodiode it reaches 60 MHz.

As slight drawback of this photodetector design is the complicated mechanical assembly and the higher effort that has to be put into the soldering of the SMD circuit. Apart from these technical complications (and the resulting higher production cost) this photodetector is the most versatile of the presented designs. The schematic of this high power photodetector and a more detailed treatment is given in (Seifert 2002).

C.4.3. Photodetector with large area silicon photodiode (type IPL10050)

Many applications do not require extraordinarily high bandwidths (in the tens of MHz region), nor do they need the high quantum efficiency of InGaAs photodiodes, but merely call for a simple, easy to use, reliable and cost efficient photodetector. For these tasks I developed a transimpedance photodetector with a designed bandwidth of approximately ≥ 1 MHz for use with a large area silicon photodiode (type IPL10050). It is used for example for the relative intensity noise measurements of the single-mode NPRO pump source in chapter 4. The photodetector schematic is shown in figure C.6; a typical transfer function of this photodetector is given in figure C.7.

C.4.4. Photodetector with silicon photodiode and high bandwidth

If the requirements posed on the photodetector are the same as described in section C.4.3, but an enhanced bandwidth is needed, then the following photodetector design can be used. It was originally developed for use in the squeezing experiments in our group (Vahlbruch

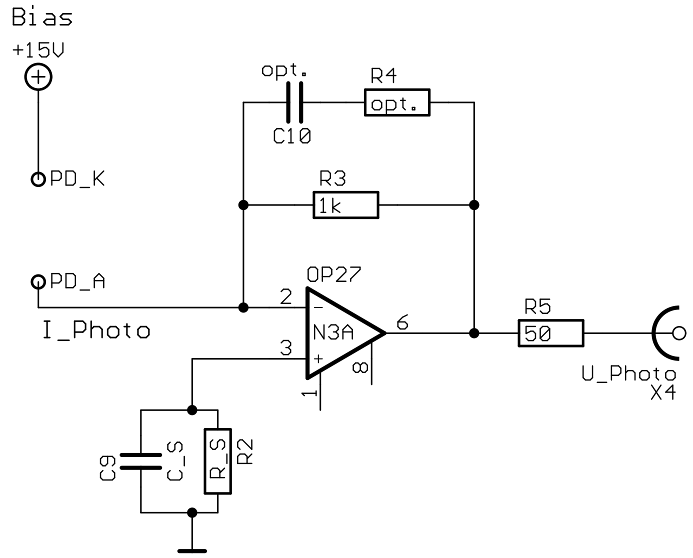

Figure C.6: Schematic of the simple transimpedance photodetector designed for implementation with a large area silicon photodiode (type IPL10050). It is used for instance to measure the relative intensity noise of the single-mode laser diode pump source for the single-mode NPRO (see chapter 4).

2004; Franzen 2004; Hage 2004) by Boris Hage. It is very compact ($5 \times 5 \times 2\,\mathrm{cm}^3$) and versatile, as almost any operational amplifier can be implemented due to the variable voltage supply (± 5 or $\pm$ 15 V). In this thesis it is used as the Pound-Drever-Hall-photodetector for the mode cleaner-lock in chapter 4. Figure C.8 shows the schematic of this photodetector, whereas figure C.9 gives the measured transfer function.

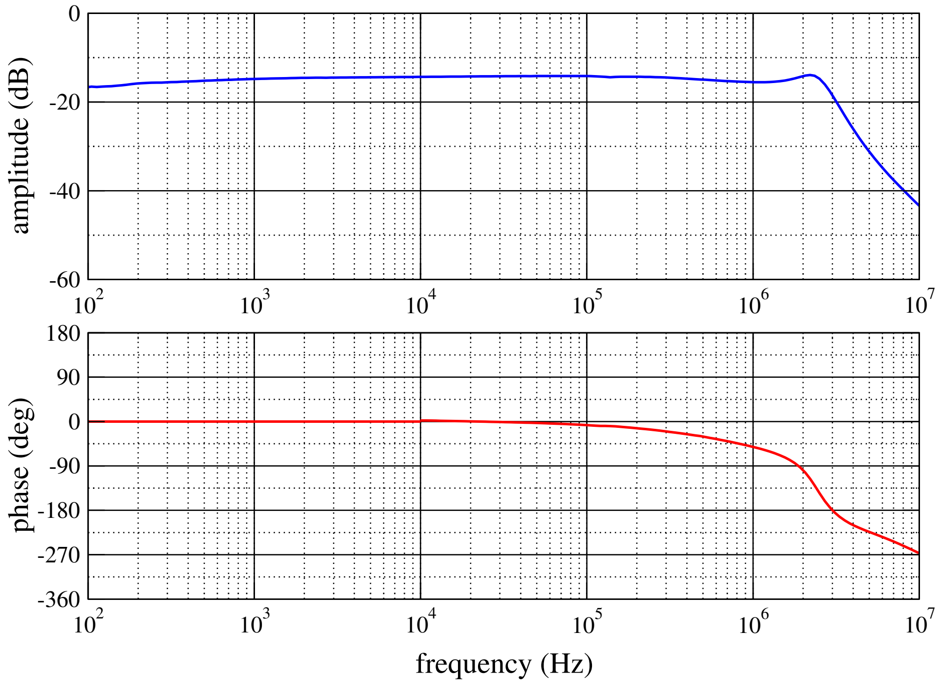

Figure C.7: Transfer function of the transimpedance photodetector with large area silicon photodiode (type IPL10050). The bandwidth can be determined to $f > 1\,\mathrm{MHz}$. The transfer function was taken with a test setup consisting of an amplitude modulated laserdiode and a highpass at $\approx 300\,\mathrm{Hz}$. The effect of the test setup was eliminated in the measured transfer function by calibration.

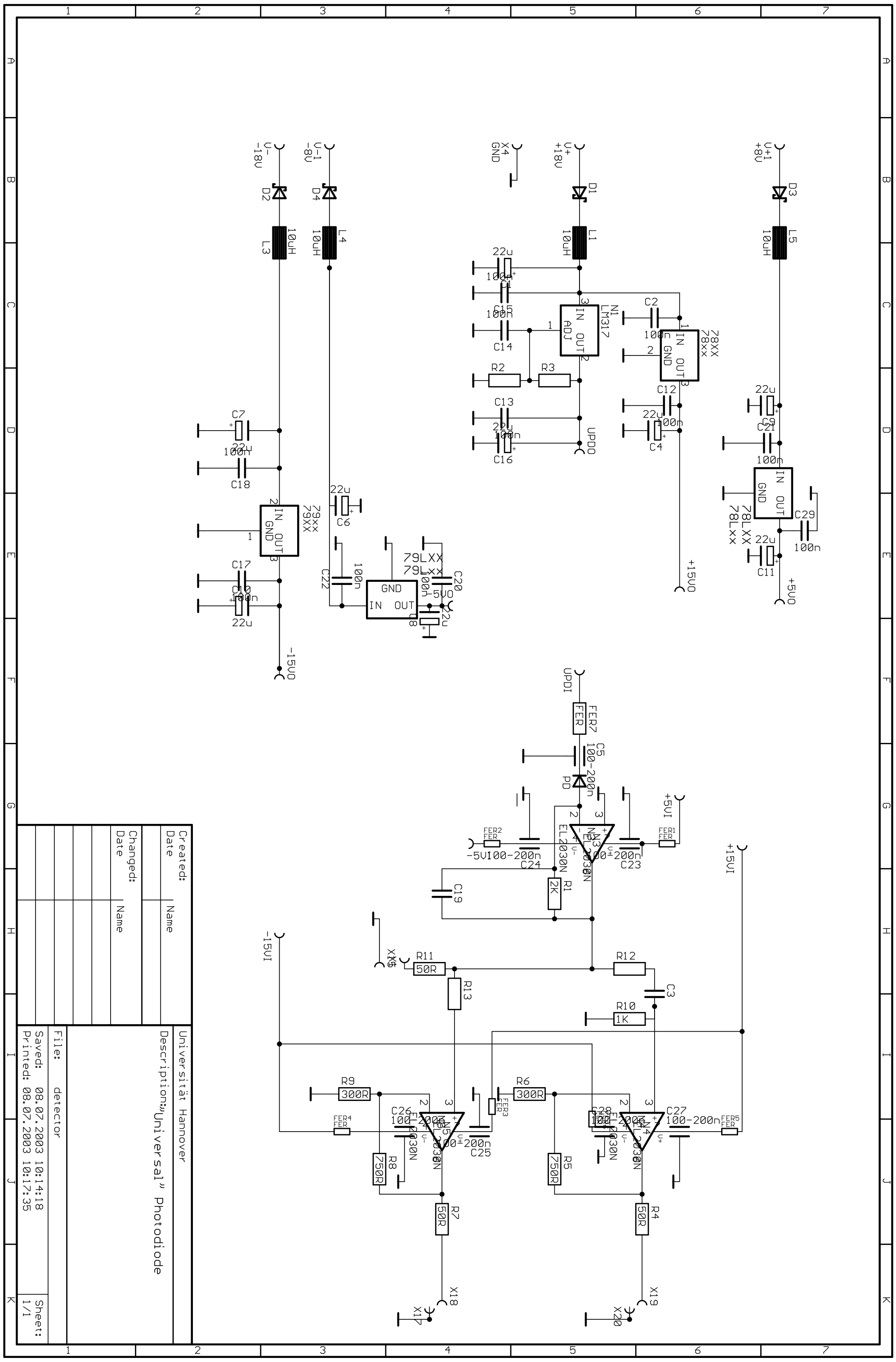

Figure C.8: Schematic of the transimpedance photodetector designed for high bandwidth, with silicon photodiode (type S3399). It is used for the Pound-Drever-Hall detection scheme of the mode cleaner in the optical setup of the single-mode NPRO (see chapter 4). Picture courtesy of Boris Hage.

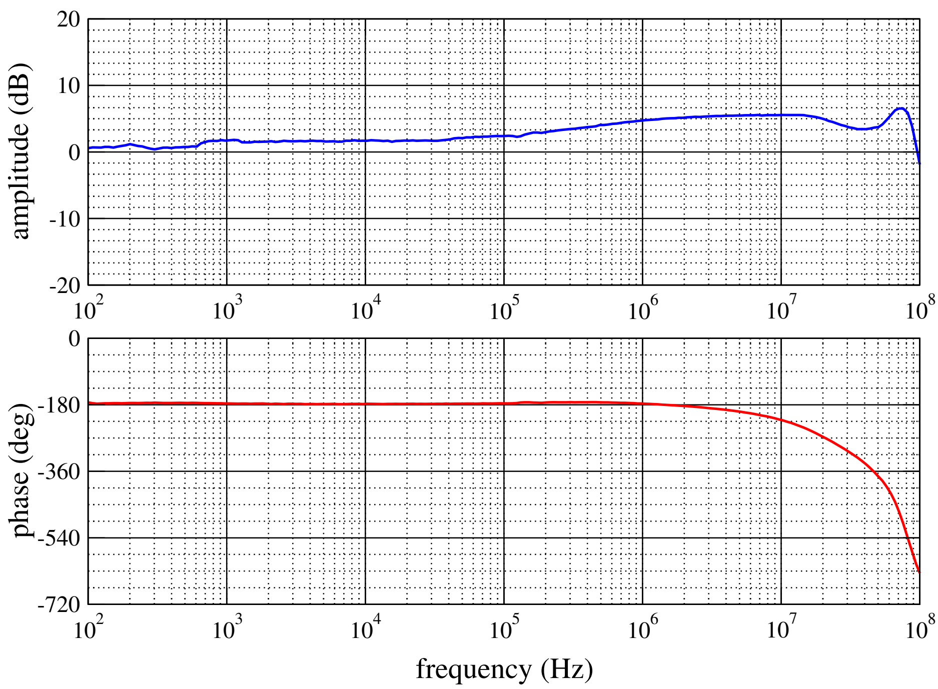

Figure C.9: Transfer function of the high bandwidth photodetector with silicon photodiode (type S3399). The bandwidth is approximately $f \approx 32\,\mathrm{MHz}$.

D. Appendix: Gaussian optics

This thesis deals with the stabilisation of different solid-state laser systems. This appendix is therefore intended to provide an overview of the defining characteristics of laser beams as well as of the special formalism used to describe them, the so-called Gaussian optics. With the help of this knowledge the described optical setups can be understood more easily.

Laser radiation shows four typical characteristics, which are elucidated in the following:

- The *monochromaticity* of laser light arises from the fact that only radiation of a frequency ν, corresponding to an optical transistion, is amplified in the active medium of a laser. A narrowband laser resonator can reduce the bandwidth of this emission even further, often by many orders of magnitude[1].
- The spatial and temporal *coherence* of laser light (each as such independent of one another) stems directly from the lasing process, which is based on stimulated emission.
- The *directionality* of laser radiation is a direct consequence of the fact that the active laser medium is placed in an optical resonator. Divergence of the laser beam is unavoidable, since it experiences at least one aperture (that of the laser resonator) which introduces diffraction. If the divergence of the laser beam is determined by the limiting aperture of the laser resonator, then the beam is said to be *diffraction limited*.
- The *brightness* of a light source can be defined as the light power emitted per unit surface area per unit solid angle. To exemplify the concept of brightness in a laser, compare a light bulb with an output power of 25 W with a laser system with identical output power. The brightness of the light bulb is very limited (one could indeed call it dim), whereas the moderately focussed laser beam with 25 W is sufficient to burn holes in most materials. This difference is mainly caused by the high directionality of the laser beam (Svelto 1998).

Beam optics, or *geometrical* optics, describes the propagation of light (and any other electromagnetic wave) under the assumption that all apertures d and radii of curvature R of all optical elements are much larger than the wavelength of the electromagnetic radiation:

$$d, R \gg \lambda \quad . \tag{D.1}$$

The propagation of laser beams, however, is described by Gaussian or *paraxial optics*. It follows from beam optics, when two boundary conditions are applied:

- All distances r from the optical axis are smaller than the apertures d of all optical elements.

[1]The monochromaticity of a laser is directly connected to its frequency stability. A limit to the achievable frequency stability is the *Schawlow-Townes-limit*.

- The angle between the optical axis and the beam is small ($\leq 10°$), so that the approximation $\sin\theta \approx \tan\theta \approx \theta$ holds.

The propagation of paraxial beams through free space and optical components can conveniently be described by two-dimensional matrices.

Matrix formulation of geometric optics
Let z be the optical axis of a system. Then r_1 is a ray vector given at a point $z = z_1$, given by its radial displacement $r(z_1)$ from the z-axis and its angular displacement θ_1. The ray vector r_2 at $z = z_2$ is defined analogously. Figure D.1 shows the above quantities.

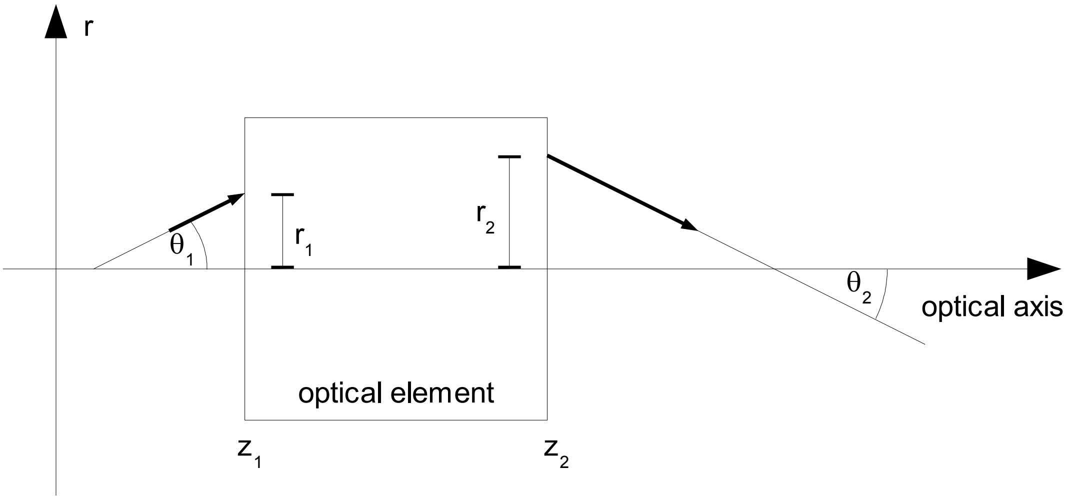

Figure D.1: Visualisation of the matrix formulation in paraxial optics.

The variables of the output beam, r_2 and θ_2,and those of the input beam, r_1 and θ_1, are related by a linear transformation. As the angular displacements θ_i are approximately given by the slope of the beam, $\theta_i = dr_i/dz_i \equiv r'_i$, we can write the transformation in the following form:

$$\begin{aligned} r_2 &= Ar_1 + Br'_1 \ , \\ r'_2 &= Cr_1 + Dr'_1 \ . \end{aligned} \tag{D.2}$$

Instead of writing two equations defining r_2 and r'_2, equations D.2 can be written as a matrix:

$$\begin{pmatrix} r_2 \\ r'_2 \end{pmatrix} = \begin{pmatrix} A & B \\ C & D \end{pmatrix} \begin{pmatrix} r_1 \\ r'_1 \end{pmatrix} \ . \tag{D.3}$$

The ABCD matrix characterises the optical element which produces the transformation between the incoming and the outgoing beam. Two common optical elements, free space and focussing lenses, and their presentation as an ABCD matrix are shown in table D.1.

optical element	pictogramm	ABCD matrix
free space	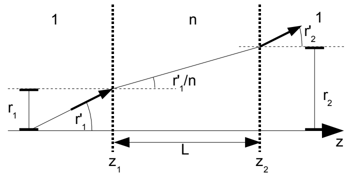	$\begin{pmatrix} 1 & L/n \\ 0 & 1 \end{pmatrix}$
thin lens	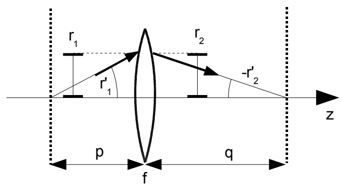	$\begin{pmatrix} 1 & 0 \\ -1/f & 1 \end{pmatrix}$

Table D.1: Free space propagation and propagation through a thin lens as ABCD matrices.

The most striking advantage of the ABCD matrix formalism is the fact that multiple optical elements in the beam path can easily be calculated by multiplying the matrices of the individual elements.

For a more detailed treatment of Gaussian optics and its consequences on resonator design (Kneubühl and Sigrist 1991) and (Svelto 1998) are recommended. The original paper is a classic: ‘Laser Beams and Resonators’ by Kogelnik & Li (Kogelnik and Li 1966).

Important equations
A knowledge of a small row of mathematical expression makes dealing with lowest order Gaussian beams (TEM_{00}, as this is the geometry we most often encounter) very easy. The equations were originally formulated in the above mentioned article by Kogelnik & Li and are only stated here. This little collection is useful when one needs to calculate modematching into an optical cavity, which is necessary frequently.

In a Gaussian beam the decrease of the field amplitude $E(r)$ with radial distance r from the optical axis is given by

$$E(r) = E_0 \cdot exp\left(\frac{-r^2}{w^2}\right) \quad . \tag{D.4}$$

As the intensity $I(r)$ is proportional to the square of the field distribution, the distribution of power density is given by

$$I(r) = I_0 \cdot exp\left(\frac{-2r^2}{w^2}\right) \quad . \tag{D.5}$$

The radius $w(z)$ of a Gaussian beam at position z with waist radius w_0 at $z = 0$ is given by

$$w^2(z) = w_0^2 \left[1 + \left(\frac{\lambda z}{\pi w_0^2}\right)^2\right] \quad . \tag{D.6}$$

The corresponding radius of curvature $R(z)$ at position z is then given by

$$R(z) = z\left[1 + \left(\frac{\pi w_0^2}{\lambda z}\right)^2\right] \quad . \tag{D.7}$$

The radius of curvature of the phasefront of a Gaussian beam is transformed in the following way when the Gaussian beam propagates through a thin lens:

$$\frac{1}{R_2} = \frac{1}{R_1} - \frac{1}{f} \quad , \tag{D.8}$$

where R_1 is the radius of curvatureof the beam before the thin lens with focal length f and R_2 is the radius of curvature of the imaged beam behind the lens. This fact is visualised in figure D.2.

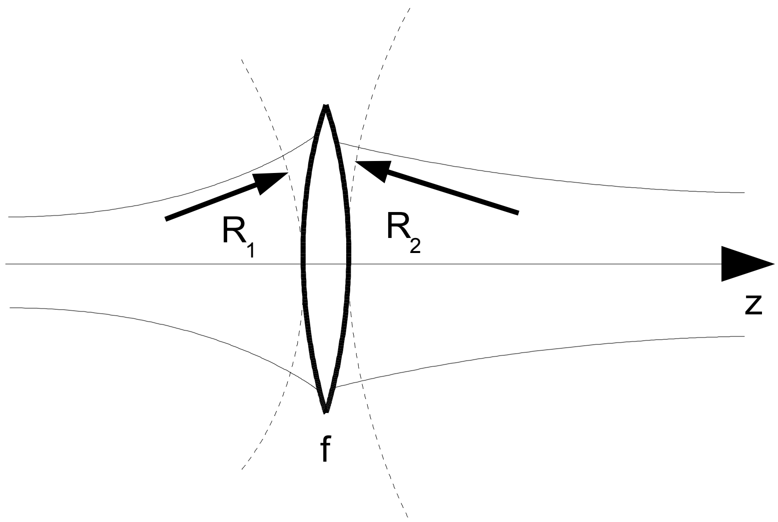

Figure D.2: Transformation of a Gaussian beam by a thin lens.

The *Rayleigh range* z_R is a useful quantity which is defined as the position on the optical axis where the radius of the Gaussian beam is $\sqrt{2}$ times its waist radius w_0. It is also the position where the radius of curvature of the equiphase surfaces is minimal, i.e. the Rayleigh range marks the position with strongest radius of curvature. Another formulation of this fact is that the beam makes a transition from parabolical to spherical waves at $z = z_R$. The Rayleigh range is given by

$$z_R = \frac{\pi w_0^2}{\lambda} \quad . \tag{D.9}$$

In far field (i.e. for $z \gg z_R$) the beam can be considered to be approximately spherical, which is why it is useful to define a far field divergence Θ of the beam:

$$\Theta = \frac{\lambda}{\pi w_0} \quad . \tag{D.10}$$

Curriculum Vitae

name	– Michèle Heurs, née Kirchner
date of birth	– 20.02.1975
place of birth	– Hannover, Germany
citizenship	– German
marital status	– married, no children
1980-1985	– primary school in Eimbeckhausen, Germany
1985-1987	– orientation school in Bad Münder, Germany
1987-1994	– high school Otto-Hahn-Gymnasium in Springe, Germany. Abitur, grade 1.6
1990	– winner of the Bundeswettbewerb Fremdsprachen
1991-1994	– group leader at the International Student Leadership Institute, Department of Defence Dependent Schools
Oct. 1994 - Dec. 1999	– undergraduate physics studies at Hannover University, Germany. Graduation with grade 1.
Sept. 1997	– internship in the VIRGO laser group in Orsay (A. Brillet, C.N. Man), France
Feb. 1998	– internship in the LIGO laser group in Stanford (R. L. Byer), California, USA
Juli-Aug. 1998	– summer work in the LIGO laser group in Stanford (R. L. Byer), California, USA
March 2000 - Dec. 2004	– graduate studies in physics at the institute for atomic- and molecular physics, spectroscopy, Max-Planck-institute for gravitational physics (Albert-Einstein-institute), Hannover, Germany. Graduation summa cum laude.
languages	– German and English (mothertongue), French (fluent)
interests	– horseback riding, ballroom dancing, mountaineering

Publications

M. Kirchner: *Langzeit-Frequenzstabilisierung eines Nd:YAG-Lasersystems für GEO 600*
Diploma thesis, Universität Hannover, 1999

M. Kirchner, V. Quetschke, I. Zawischa, B. Willke, K. Danzmann: *Amplitude stabilization of a 13 W master-slave Nd:YAG laser system for the gravitational wave detector GEO 600*
in: Conference on Lasers and Elektro-Optics Europe, 2000

I. Zawischa, M. Brendel, K. Danzmann, C. Fallnich, M. Kirchner, S. Nagano, V. Quetschke, H. Welling, B. Willke: *The GEO 600 Laser System*
in: Class. Quantum Grav. 19 (2002) p1775-p1781

B. Willke, . . . , M. Heurs, . . . : *The GEO 600 gravitational wave detector*
in: Class. Quantum Grav. 19 (2002) p1377 - p1387

J. Hough, . . . , M. Kirchner, . . . : *GEO 600 – Research, Progress and Prospects*
in: R. T. Jantzen, V. Gurzadyan, R. Ruffini (eds.) Proceedings of the Ninth Marcel Grossmann Meeting on General Relativity. World Scientific, Singapore (2002) p1843 - p1844

S. Goßler, . . . , M. Heurs, . . . : *The mode-cleaning and injection optics of the gravitational wave detector GEO 600*
in: Rev. Sci. Inst. 74 (2003) p3787 - p3796

G. Woan, . . . , M. Heurs, . . . : *The GEO 600 Gravitational Wave Detector – Pulsar Prospects*
in: M. Bailes, D. Nice, S. Thorsett (eds.) Radio Pulsars. ASP Conference Series, Vol CS-302, (2003) 351 - 355

M. Hewitson, . . . , M. Heurs, . . . : *A report on the status of the GEO 600 gravitational wave detector*
in: Class. Quantum Grav. 20 (2003) p581 - p592

A.M. Sintes, . . . , M. Heurs, . . . : *Detector characterization in GEO 600*
in: Class. Quantum Grav. 20 (2003) p731 - p740

B. Willke, . . . M. Heurs, . . . : *Status of GEO 600*
in: Class. Quantum Grav. 21 (2004) p417 - p423

M. Heurs: *Research Highlight: Laser research for gravitational wave detectors*
in: Annual report of the Max-Planck-Society (2004)

M. Heurs, V. M. Quetschke, B. Willke, K. Danzmann, I. Freitag: *Simultaneously suppressing frequency and intensity noise in a Nd:YAG nonplanar ring oscillator by means of the current-lock technique*
in: Opt. Lett. 29 (2004), No. 18, p2148 - p2150

M. Heurs, V. M. Quetschke, B. Willke, I. Freitag, K. Danzmann: *Intensity and frequency noise reduction of a Nd:YAG NPRO via pump light stabilisation*
to be submitted to Applied Physics B

Acknowledgements

This work was supported by a range of people whom I would like to thank at this point.

First and foremost I thank my boss, Prof. Karsten Danzmann, for the opportunity to work in his group and for his neverending enthusiasm about science. His amazingly broad knowledge and his personability are always inspiring to me. Prof. Manfred Kock I thank greatly for the many discussions over a cup of tea, his valuable corrections to this work and especially for his friendship over all the years.

Working in the Max-Planck-Institute for gravitational physics with so many talented and dedicated scientists has been an honour to me. I wish to thank all the great people, too numerous to mention, I have been blessed to work with over the years, be it in Hannover or in Ruthe. I thank Benno Willke for proof reading this work and his advice over the years we have been working together. I also thank Gerhard Heinzel for correcting parts of this thesis. My four diploma students Thomas Wildhagen, Sven Herden, Frank Seifert and Tobias Meier were - each in his own way - very important for my personal development as well as in building my abilities as a teacher. Special thanks goes to Boris Hage, my 'adoptee' diploma student with a bright mind and a great personality. Warmest thanks go to Volker Quetschke, who was so much fun working with in the laser lab, besides being a source of knowledge and a very good friend.

Heiko zur Mühlen I would like to thank for building the major part of the electronics used in this thesis. Jan Diedrich and Hans Melching would always find a clever solution to my mechanical problems. I thank all of them for being of so much help! Andreas Weidner is not only a guru on electronics and especially Eagle, but also someone who can always make me laugh with a funny poem, for which I want to thank him very much.

A heartfelt thanks goes to the 'tea drinkers' for the physics discussions and the direly needed breaks. My friend Carlo Nicola Colacino corrected parts of this thesis and gave me an insight on cosmology, for both I thank him dearly.

I thank all the people from InnoLight GmbH for their help on questions concerning their NPROs and for the friendly atmosphere. Thanks, guys! Especially Ingo Freitag is always a source of productive criticism and has played an important role in my academic development. Ivo Zawischa was always great to work with and gave me many answers concerning his slave laser, amongst other things.

The team from the Weihnachtsvorlesung I thank for the wonderful team spirit and the nights and days spent together having physics fun in preparation for the show. Working with Sascha Skorupka, Boris Hage, Frank Seifert, Frank Steier, Ulf Gottschalk, Jan Diedrich, Jens Reiche and Aiko Samblowski always reminded me that what I do is the right thing for me.

I have known Gerrit Kühn for ages, and I thank him very much for our deep friendship and for the many fruitful discussions we have had. He is also to thank for correcting parts of this thesis and for his wonderful patience in helping me find my way in the computer world. My friends Stella and Tobias have been extremely supportive, I thank them both so much!

My family has supported me throughout my studies and I wish to thank my wonderful Mother for her undying love and support, my amazing Uncle for being my best friend and role model (not only as a scientist) and my inlaws for their warmth, love and help in so many ways. My husband Daniel is the person I thank most, for his help and support, but mostly for all the things that are left unsaid.

Parts of this work were funded by the Sonderforschungsbereich 407 'Quantenlimitierte Meßprozesse mit Atomen, Molekülen und Photonen'.

Bibliography

1 **Abbott and the LIGO Science Collaboration 2004** ABBOTT, B. ; LIGO SCIENCE COLLABORATION the: Detector Description and Performance for the First Coincidence Observations between LIGO and GEO. In: *Nuclear Instruments and Methods in Physics Research A* 517 (2004), p. 154–179

2 **Arie et al. 1992** ARIE, A. ; SCHILLER, S. ; GUSTAFSON, E. K. ; BYER, R. L.: Absolute frequency stabilization of diode-laser-pumped Nd:YAG lasers to hyperfine transitions in molecular iodine. In: *Optics Letters* 17 (1992), No. 17, p. 1204–1206

3 **Bock 1994** BOCK, P. H.: *Using and understanding decibels*. 1994. – Tutorial

4 **Bode 2004** BODE, M.: *personal communications*. 2004

5 **Bondu et al. 2002** BONDU, F. ; BRILLET, A. ; CLEVA, F. ; HEITMANN, H. ; LOUPIAS, M. ; MAN, C. N. ; TRINQUET, H. ; VIRGO COLLABORATION the: The VIRGO injection system. In: *Classical and Quantum Gravity* 19 (2002), p. 1829–1833

6 **Bronstein and Semendjajew 1993** BRONSTEIN, I. N. ; SEMENDJAJEW, K. A.: *Taschenbuch der Mathematik*. Verlag Harri Deutsch, 1993

7 **Brozek 1999** BROZEK, O. S.: *Frequenzstabilisierung eines Nd:YAG-Hochleistungs-Laser-Systems für den Gravitationswellendetektor GEO 600*, Universität Hannover, PhD thesis, 1999

8 **Day 1990** DAY, T.: *Frequency stabilized solid state lasers for coherent optical communications*, Stanford University, PhD thesis, 1990

9 **Drever et al. 1983** DREVER, R. W. P. ; HALL, J. L. ; KOWALSKI, F. V. ; HOUGH, J. ; FORD, G. M. ; MUNLEY, A. J. ; WARD, H.: Laser Phase and Frequency Stabilization Using an Optical Resonator. In: *Applied Physics B* 31 (1983), p. 97–105

10 **Franzen 2004** FRANZEN, A.: *Erzeugung von gequetschtem Licht für die Gravitationswellen-Astronomie*, Universität Hannover, diploma thesis, 2004

11 **Freise 2003** FREISE, A.: *The Next Generation of Interferometry: Multi-Frequency Optical Modelling, Control Concepts and Implementation*, Universität Hannover, PhD thesis, 2003

12 **Freitag 1994** FREITAG, I.: *Entwicklung und Charakterisierung einer Laserstrahlquelle für den interferometrischen Nachweis von Gravitationswellen*, Universität Hannover, PhD thesis, 1994

13 **Freitag et al. 1995** FREITAG, I. ; TÜNNERMANN, A. ; WELLING, H.: Power scaling of diode-pumped monolithic Nd:YAG lasers to output powers of several watts. In: *Optics Communications* 115 (1995), p. 511–515

14 Gea-Banacloche and Leuchs 1987 GEA-BANACLOCHE, J. ; LEUCHS, G.: Squeezed states for interferometric gravitational-wave detectors. In: *Journal of Modern Optics* 34 (1987), No. 6/7, p. 793–811

15 Gossler 1999 GOSSLER, S.: *Aufbau und Charakterisierung des Modencleanersystems für GEO 600*, Universität Hannover, diploma thesis, 1999

16 Gossler 2004 GOSSLER, S.: *The GEO 600 suspension system*, Universität Hannover, PhD thesis, 2004

17 Grote 2003 GROTE, H.: *Making it Work: Second Generation Interferometry in GEO 600!*, Universität Hannover, PhD thesis, 2003

18 Hage 2004 HAGE, B.: *Quantentomographische Charakterisierung gequetschter Zustände*, Universität Hannover, diploma thesis, 2004

19 Harb et al. 1997 HARB, C. C. ; RALPH, T. C. ; HUNTINGTON, E. H. ; MCCLELLAND, D. E. ; FREITAG, I. ; BACHOR, H.-A.: Intensity-noise dependence of Nd:YAG lasers on their diode-laser pump source. In: *Journal of the Optical Society of America B* 14 (1997), No. 11, p. 2936–2945

20 He et al. 1990 HE, L. ; LIN, Y. ; RHEENEN, A. D. van ; ZIEL, A. van der ; YOUNG, A. ; ZIEL, J. P. van der: Low-frequency noise in small InGaAs/InP p-i-n diodes under different bias and illumination conditions. In: *Journal of Applied Physics* 68 (1990), No. 10, p. 5200–5204

21 Heilmann and Wandernoth 1992 HEILMANN, R. ; WANDERNOTH, B.: Active light induced thermal frequency stabilisation of monolithic integrated twisted-mode-cavity Nd:YAG laser. In: *Electronics Letters* 28 (1992), p. 1367–1368

22 Heinzel 2002 HEINZEL, G.: *personal communications*. 2002

23 Heurs et al. 2004 HEURS, M. ; QUETSCHKE, V. M. ; WILLKE, B. ; DANZMANN, K. ; FREITAG, I.: Simultaneously suppressing frequency and intensity noise in a Nd:YAG nonplanar ring oscillator by means of the current-lock technique. In: *Optics Letters* 29 (2004), No. 18, p. 2148–2150

24 Heurs et al. HEURS, M. ; QUETSCHKE, V. M. ; WILLKE, B. ; FREITAG, I. ; DANZMANN, K.: Intensity and frequency noise reduction of a Nd:YAG NPRO via pump light stabilisation. . – to be submitted to Applied Physics B

25 Kane and Byer 1985 KANE, T. J. ; BYER, R. L.: Monolithic, unidirectional single-mode Nd:YAG ring laser. In: *Optics Letters* 10 (1985), No. 2, p. 65–67

26 Kirchner KIRCHNER, M.: *Langzeit-Frequenzstabilisierung eines Nd:YAG-Lasersystems für GEO 600*, Universität Hannover, diploma thesis

27 Kneubühl and Sigrist 1991 KNEUBÜHL, F. K. ; SIGRIST, M. W.: *Laser*. 3rd. Teubner Studienbücher Physik, 1991

28 Koechner 1996 KOECHNER, W.: *Solid-State Laser Engineering*. 4th. Springer-Verlag Berlin Heidelberg New York, 1996 (Optical Sciences)

29 **Kogelnik and Li 1966** KOGELNIK, H. ; LI, T.: Laser Beams and Resonators. In: *Applied Optics* 5 (1966), No. 10, p. 1550–1567

30 **Larason and Bruce 1998** LARASON, T. C. ; BRUCE, S. S.: Spatial uniformity of responsivity for silicon, gallium nitride, germanium, and indium gallium arsenide photodiodes. In: *Metrologia* 35 (1998), p. 491–496

31 **Lipson et al. 1997** LIPSON, S. G. ; LIPSON, H. S. ; TANNHAUSER, D. S.: *Optik*. 1st. Springer, 1997

32 **Mao et al. 2002** MAO, Y. ; DENG, P. ; ZHANG, Y. ; GUO, J. ; GAN, F.: High Efficient Laser Operation of the High-Doped Nd:YAG Crystal Grown by Temperature Gradient Technology. In: *Chinese Physics Letters* 19 (2002), No. 9, p. 1293–1295

33 **Hamamatsu Photonics 2001** HAMAMATSU PHOTONICS: *Large area, high-speed Si PIN photodiodes*. 2001. – Datasheet for silicon photodiode S3399

34 **InnoLight GmbH 2004** INNOLIGHT GMBH: *Mephisto Product Line*. 2004

35 **Judson Technologies 2000** JUDSON TECHNOLOGIES: *J16 series germanium photodiodes*. 2000. – Datasheet for germanium photodiode J16

36 **Osram Opto Semiconductors 2003** OSRAM OPTO SEMICONDUCTORS: *Laser Diode in TO-220 Package 2.0 W cw*. 2003. – Datasheet laser diode SPL 2Yxx

37 **PerkinElmer Optoelectronics 2001** PERKINELMER OPTOELECTRONICS: *Large Area InGaAs Photodiodes*. 2001. – Datasheet for InGaAs photodiode C30641 and C30642

38 **SDL / JDS Uniphase 2002** SDL / JDS UNIPHASE: *Product Bulletin SDL-5400 Series*. 2002. – Datasheet laser diode SDL 5422-H1-810

39 **Thales Optoelectronics 2003** THALES OPTOELECTRONICS: *PIN Photodiodes*. 2003. – Datasheet for silicon photodiode IPL10050

40 **Verlag Stahleisen mbH 1991** VERLAG STAHLEISEN MBH: *Eisenlegierungen mit besonderer Wärmeausdehnung. Nummer 385 in STAHL-EISEN-Werkstoffblätter*. 1991

41 **Pound 1946** POUND, R. V.: Electronic Frequency Stabilization of Microwave Oscillators. In: *Review of Scientific Instruments* 17 (1946), No. 11, p. 490–505

42 **Quetschke 2003** QUETSCHKE, V.: *Korrelationen von Rauschquellen bei Nd:YAG Lasersystemen*, Universität Hannover, PhD thesis, 2003

43 **Saulson 1994** SAULSON, P. R.: *Fundamentals of interferometric gravitational wave detectors*. World Scientific Publishing, 1994

44 **Schmitt 2004** SCHMITT, A.: *personal communications*. 2004. – Osram Semiconductors

45 **Seifert 2002** SEIFERT, F.: *Entwicklung einer quantenrauschbegrenzten Leistungsstabilisierung für ein Präzisionslasersystem*, Universität Hannover, diploma thesis, 2002

46 Siegman 1986 SIEGMAN, A.: *Lasers*. University Science Books, Mill Valley, California, 1986

47 Slusher et al. 1985 SLUSHER, R. E. ; HOLLBERG, L. W. ; YURKE, B. ; MERTZ, J. C. ; VALLEY, J. F.: Observation of Squeezed States Generated by Four-Wave Mixing in an Optical Cavity. In: *Physical Review Letters* 55 (1985), No. 22, p. 2409–2412

48 Svelto 1998 SVELTO, O.: *Principles of Lasers*. Plenum Press, New York and London, 1998

49 Thorne et al. 1999 THORNE, A. ; LITZÉN, U. ; JOHANSSON, S.: *Spectrophysics - Principles and Applications*. 1st revised. Springer Verlag, 1999

50 Tröbs et al. 2004 TRÖBS, M. ; WESSELS, P. ; FALLNICH, C.: *Phase-noise properties of an Yb-doped fiber amplifier for LISA*. 2004. – submitted to Optics Letters

51 Vahlbruch 2004 VAHLBRUCH, H.: *Squeezing bei kleinen Seitenbandfrequenzen*, Universität Hannover, diploma thesis, 2004

52 Willke et al. 2000a WILLKE, B. ; BROZEK, O. S. ; DANZMANN, K. ; FALLNICH, C. ; GOSSLER, S. ; LÜCK, H. ; MOSSAVI, K. ; QUETSCHKE, V. ; WELLING, H. ; ZAWISCHA, I.: The GEO 600 Stabilized Laser System and the Current-Lock Technique. In: *Gravitational Waves, Third Eduardo Amaldi Conference, Pasadena, California 12-16 July 1999, AIP Conference Proceedings* (2000), p. 215

53 Willke et al. 2000b WILLKE, B. ; BROZEK, S. ; QUETSCHKE, V. ; GOSSLER, S. ; DANZMANN, K.: Frequency stabilization of a monolithic Nd:YAG ring laser by controlling the power of the laser-diode pump source. In: *Optics Letters* 25 (2000), No. 14, p. 1019–1021

54 Willke and the GEO 600 team 2004 WILLKE, B. F. ; GEO 600 TEAM the: Status of GEO 600. In: *Classcal and Quantum Gravity* 21 (2004), p. 417–423

55 Winkler 2002 WINKLER, W.: *Fluctuating light pressure in recycled interferometers*. November 2002. – draft available on the GEO documentation server

56 Yang et al. 1996 YANG, S. T. ; IMAI, Y. ; OKA, M. ; EGUCHI, N. ; KUBOTA, S.: Frequency-stabilized, 10-W continuous-wave, laser-diode end-pumped, injection-locked Nd:YAG laser. In: *Optics Letters* 21 (1996), No. 20, p. 1676–1678

57 Yariv 1989 YARIV, A.: *Quantum Electronics*. 3rd. John Wiley & Sons, Inc., 1989

58 Zawischa 2003 ZAWISCHA, I.: *Injektionsgekoppelte diodengepumpte Nd:YAG- und Nd:YVO$_4$-Laser für terrestrische interferometrische Gravitationswellendetektoren*, Universität Hannover, PhD thesis, 2003

59 Zawischa et al. 2002 ZAWISCHA, I. ; BRENDEL, M. ; DANZMANN, K. ; FALLNICH, C. ; KIRCHNER, M. ; NAGANO, S. ; QUETSCHKE, V. ; WELLING, H. ; WILLKE, B.: The GEO 600 Laser System. In: *Classical and Quantum Gravity* 19 (2002), p. 1775–1781